Biological response to episodic wind events in Massachusetts Bay

A dissertation presented

by

Patricia Alejandra Moreno Arancibia

to

The Department of Earth and Planetary Sciences

in partial fulfillment of the requirements

for the degree of

Doctor of Philosophy

in the subject of

Earth and Planetary Sciences

Harvard University

Cambridge, Massachusetts

May 2007

Thesis advisors

Allan R. Robinson

James J. McCarthy

Author

Patricia Alejandra Moreno Arancibia

Biological response to episodic wind events in Massachusetts Bay

Abstract

In this dissertation the biological response to wind-induced upwelling events in Massachusetts Bay is studied. Massachusetts Bay is a semi-enclosed embayment adjacent to a large shallow shelf-sea and is characterized by winds that vary frequently in magnitude and direction.

To determine the biological response to episodic wind events 3-dimensional physical-biological simulations are carried out for June 6-26, 2001. During this time the ASCOT-01 combined physical and biological experiment took place in Massachusetts Bay and the Gulf of Maine and a large data set was collected for initialization, assimilation, and determination of biological parameters.

Three wind forcings are used: 1) real winds from June 2001, 2) feature-model wind events of strong storms during 1985-2005, and 3) historical summer winds from the same period. During June 2001 the winds were unusually weak and hence caused very little upwelling. By modeling strong feature wind events we are able to amplify the biological responses.

The physical response to strong southerly wind events in Massachusetts Bay is characterized by three processes: 1) Upwelling along the mainland coast, 2) large off-

shore currents near the surface, and 3) on-shore currents deeper in the water column. The deep on-shore current plays a crucial role as it advects nitrate from the Gulf of Maine into Massachusetts Bay, recharging the aphotic zone. After the upwelling event has subsided this nitrate can continue to enhance primary production in the overlying euphotic zone.

The biological response to the wind event happens on two time scales. During the wind event the nutrients and biomass are redistributed mainly by advection and the only biological process of importance is ammonium uptake. After the wind event there is a phytoplankton bloom. Advective processes are weak and interactive biological processes dominate changes in nutrients and biomass.

Contents

List of Figures

Acknowledgments

First and foremost I would like to thank my two advisors, Prof. Allan R. Robinson and Prof. James J McCarthy. Throughout the years they have provided guidance, encouragement and enthusiasm without end. They have been wonderful mentors generously sharing their knowledge and experiences. They have taught me to be a better scientist in many ways.

I would also like to thank the members of the oceanography group: Prof. Pierre Lermusiaux for many interesting discussions about physical-biological modeling all along the way; Dr. Patrick Haley who taught me the Harvard Ocean Prediction System (and answered millions of questions); Mr. Wayne Leslie for endless computer help throughout the years and for editing help during the last weeks of the thesis writing; Dr. Oleg Logutov, a great office mate; Ms. Gioia Sweetland for administrative support; and Ms. Peggy Zaldivar for practical support and kindness. Dr. John Nevins from the biological oceanography group provided me with information about the biological sampling methods.

Many individuals were involved in collecting the data used in this work. I enjoyed working at sea with the captain of the University of Massachusetts - Dartmouth R/V Lucky Lady and JF Bertrand collecting the biological data for this project. Prof. Avijit Gangopadhyay supervised the R/V Lucky Lady logistics. Dr. Jurgen Sellschopp of the NATO Undersea Research Centre organized the ASCOT-01 experiment. Dr. Michael Mickelson of the Massachusetts Water Resources Authority provided me with both biological data and supporting information. This work was funded by the National Science Foundation (grant No. 5710001319), the Office of Naval Research (grants N00014-95-0-0371 and N00014-02-1-0989 and the Persistent

Littoral Undersea Surveillance Network project, No. S05-06), and the Committee on Oceanography.

I am very grateful to my family and friends for the love, support, and encouragement that they have provided through the years. A special thank you to Luis, Nancy, Andrea, David, Alejandra, Daniela, Cecilia, Gloria, and Lina.

Dedicated to Luis and Nancy.

Chapter 1

Introduction

The subject of this thesis is the effects of advection and upwelling events on the biological processes in the coastal ocean in the early summer.

1.1 Description of upwelling

Description of coastal upwelling

Advection and upwelling are important physical processes in the ocean for biology as they redistribute nutrients and plankton leading to changes in the rate of biological processes, in particular primary production. The basic principles of upwelling theory were first derived by Ekman in 1905 [12]. He reasoned that in the uppermost part of the ocean, the flow is driven by a balance between the Coriolis force and friction. Solving for the velocity shows that the surface current is 45° to the right of the wind on the northern hemisphere (to the left on the southern hemisphere). This angle increases with depth while the magnitude of the velocity decreases with depth. The

resulting flow is described by the Ekman spiral (see Figure 1.1). Notice that at a certain depth the wind induced current is in the opposite direction of the wind.

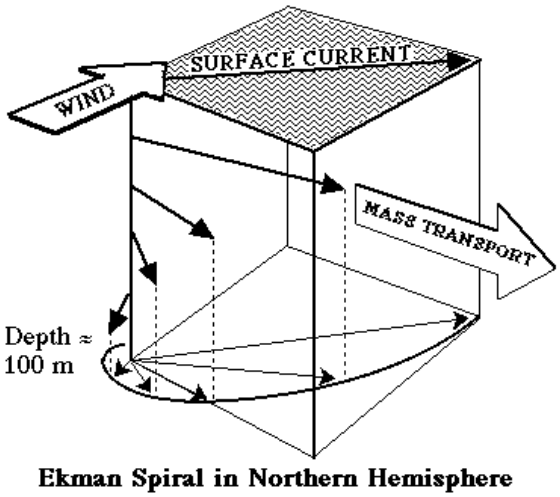

Figure 1.1: Ekman Spiral and Ekman Transport. Source: Don Garlick (http://www.humboldt.edu/ gdg1/); adapted from Thurman, Harold V., Essentials of Oceanography.

The mass transport, the so called Ekman transport, is obtained by integrating the horizontal velocity with respect to the vertical coordinate. The resulting Ekman transport is 90^o to the right of the wind in the northern hemisphere (to the left on the southern hemisphere). Thus a wind that blows along the coast will give rise to an Ekman transport that is perpendicular to the coast, and the Ekman transport is either on-shore or off-shore depending on the direction of the wind (see Figure 1.1). An off-shore Ekman transport causes displacement of water from the top layer of the ocean. To conserve mass, the water that is removed by the Ekman transport has to be replaced by water upwelled from below.

The importance of upwelling for biological activity in the ocean

To understand the importance of upwelling on biological activity in the ocean we need to take a closer look at the light and nutrient distribution in the water column. Primary production, the fixation of inorganic carbon into organic matter, is produced through either photosynthesis or chemosynthesis. Both these processes use an external source of energy. In the case of photosynthesis it is light and in chemosynthesis the energy comes from inorganic chemical compounds. Photosynthesis by phytoplankton is responsible for the largest portion of marine primary production [49].

As sunlight penetrates the ocean it is absorbed by water, plankton and other particulate and dissolved materials in the water. The upper layer where there is enough light for photosynthesis is referred to as the euphotic zone. The thickness of the euphotic zone depends primarily on the amount of plankton and other material in the water and ranges from a few meters in turbid coastal waters to more than 100 m in tropical oceanic water. The region below the euphotic zone is called the aphotic zone.

Photosynthesis also requires inorganic nutrients such as nitrogen, phosphorus, silica, and micronutrients. A typical nutrient profile shows low concentrations near the surface and increasing nutrient concentrations with depth. Nutrients at great depth are not utilized for primary production as there is insufficient light.

Generally speaking, any vertical motion in the ocean has an impact on biology as it can move phytoplankton and nutrients into and out of the euphotic zone. As water is upwelled nutrients are brought into the euphotic zone where they can be utilized by phytoplankton in the photosynthetic process.

Coastal upwelling plays an important role in global primary production and fisheries. In the coastal ocean, regions of intense upwelling are associated with some of the most productive fisheries, such as the west coasts of South America and United States, and southern Africa. In these locations wind forced upwelling results in seasonable persistent periods of high biological production.

Sustained upwelling vs episodic events

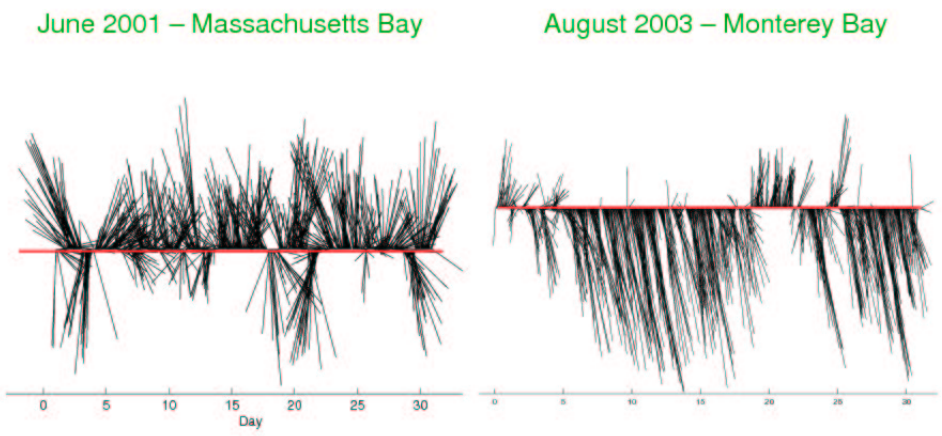

Figure 1.2: Stickplot of winds in Massachusetts Bay and and Monterey Bay. Figure courtesy of Prof. Allan R. Robinson.

The regions in the coastal ocean where wind induced upwelling leads to high primary production are characterized by sustained upwelling. Here the winds blow in the same direction for long periods of time, with occasional changes in direction for short periods. Figure 1.2 shows stickplots of winds vectors during the summer in Monterey Bay (California) and Massachusetts Bay. The wind vectors point away from the baseline and indicate the direction in which the wind is blowing towards. In Monterey Bay the winds can sustained for over 10 days giving rise to substantial

upwelling. In Massachusetts Bay on the other hand, the winds quickly change both direction and magnitude. In this latter case the upwelling is episodic, lasting only a few days.

Many different taxonomic groups of phytoplankton respond to upwelling events, but diatoms are prevalent among these in most regions of persistent upwelling. Since diatoms have a silicious encasement (frustule) and tend to be large (single and multiple cell groups or "chains") their success in upwelling systems may, in part, result from vertical motion that helps to keep them in suspension within the euphotic zone.

1.2 Description of Massachusetts Bay

Geographical location and geometry

Massachusetts Bay (see Figure 1.3) is located west of the Gulf of Maine and is surrounded by land on three of its four boundaries. Its boundaries are made up, on the north by Cape Ann, to the south by Cape Cod, and by Stellwagen Bank towards the Atlantic Ocean. To the west it is bounded by the coast of Massachusetts, which includes Boston Harbor. Topographical features of particular interest are Stellwagen Bank and Stellwagen Basin. The Bank is located on the eastern part of Massachusetts Bay and rises to 30 meters below the sea surface. Just west of the Bank, is Stellwagen Basin, where the greatest depths in Massachusetts Bay are found (up to 100 m). The North and South Passage are two sills north and south of Stellwagen Bank with depths of 50 and 60 m, respectively. On average, the depth of Massachusetts Bay is 35 m. The southern part of the bay is referred to as Cape Cod Bay.

Physical and biological characteristics

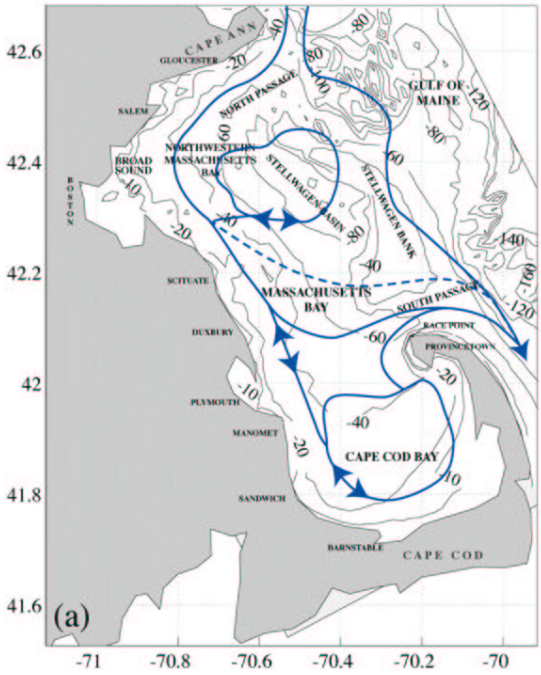

Figure 1.3: Bottom topography and coastal currents in Massachusetts Bay [25] and [43].

The circulation in Massachusetts Bay depends on the history of the wind and is characterized by a high level of variability [4]. Figure 1.3 shows the coastal currents and the bottom topography in Massachusetts Bay. The main coastal current can have three branches starting from the northern part of the Bay. One branch does not enter the Bay at all and passes east of Stellwagen Bank. The current can also enter Massachusetts Bay and exit through the South Passage (between Cape Cod and the southern tip of Stellwagen bank). The third path is one in which the coastal current extends from Massachusetts Bay into Cape Cod Bay and exits through South Passage. The circulation in Cape Cod Bay may be either cyclonic or anticyclonic.

In addition to the general circulation described above, tidal flow, wind mixing

and wind induced upwelling and downwelling play a central role in the circulation of the Bay. All these physical processes influence the biological activity of the Bay. More specifically, in Massachusetts Bay there is tidal mixing over Stellwagen Bank which is believed to be an important process in making nutrients available to the phytoplankton. Boston Harbor water, which contains anthropogenic nutrients, is advected into Massachusetts Bay. Nutrients are also advected in from the Gulf of Maine with the coastal current. Also, along the coast wind driven upwelling can give rise to enhanced primary productivity.

The Massachusetts Water Resource Authority (MWRA) monitors the water quality in the Bay [27]. The emphasis of the monitoring program is on the sewage outfall. Nutrients, biomass, and primary production rates are measured on a regular basis throughout the year. The timing and strength of seasonal events such as the winter/spring bloom and summer stratification vary annually [22]. Spring 2001 was unusual in that the typical large spring bloom was absent [27]. Primary production rates and chlorophyll remained below average throughout the spring. Maximum nutrient concentrations were the highest in February and declined through April and reached depleted levels before June. Zooplankton biomass was also low during spring 2001, most probably due to the low chlorophyll levels.

Figure 1.4 shows the upwelling situations in Massachusetts Bay and Monterey Bay. Not only do the different wind patterns give rise to different upwelling situations but the geometry of each bay also matters. Monterey Bay is essentially a straight coast line and only one direction of the wind gives rise to upwelling. In contrast, Massachusetts Bay has a box-like geometry. Almost any wind direction induces upwelling somewhere

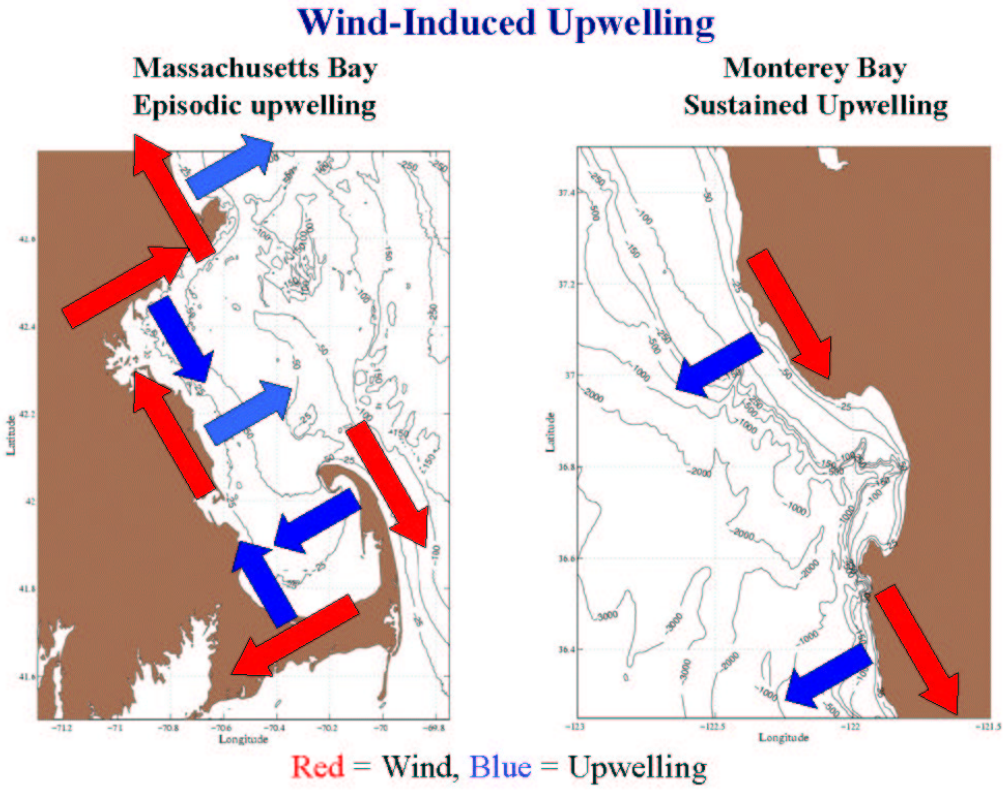

Figure 1.4: Wind induced upwelling off the coast off California and in Massachusetts Bay. Red arrows indicate the wind direction and the blue arrows the resulting Ekman transport. Figure courtesy of Prof. Allan R. Robinson.

along a coast.

1.3 ASCOT-01 experiment

The Assessment of Skill for Coastal Ocean Transients 2001 (ASCOT-01) experiment was carried out in Massachusetts Bay/Gulf of Maine in June 2001. This experiment was part of a series of real-time Coastal Predictive Skill Experimentation (CPSE)/Rapid Environmental Assessment (REA) experiments and simulations focused on quantitative skill evaluation and cost-effective forecast system development.

The overall purpose of ASCOT was to enhance efficiency, improve accuracy and extend the scope of nowcasting and forecasting of oceanic fields for CPSE and for REA in the coastal ocean and to quantify such CPSE and REA capabilities. The general objectives of ASCOT were to: i) obtain data sets adequate for - 1) definitive real-time verification of regional coastal ocean predictive skills, with and without REA constraints; 2) CPSE and REA Observational System Simulation Experiments (OSSEs), both for ASCOT design and more generally; and, 3) definitive knowledge of dynamics; ii) define useful skill metrics and real-time forecast validation and verification procedures for REA; and, iii) assemble, calibrate, exercise in real-time, evaluate and improve a generic, portable, scalable advanced ocean forecast system (dynamical models and data analysis, management and assimilation schemes) applicable for CPSE in general and NATO REA in particular.

The specific objectives of ASCOT-01 were to: i) carry out and quantitatively evaluate in Massachusetts Bay (MB) and the Gulf of Maine (GOM) a coupled multiscale interdisciplinary real-time forecast experiment; ii) obtain an intensive data set adequate for definitive quantitative skill assessment and suitable for the design of minimal data requirements for both REA and for an efficient regional monitoring and prediction system; iii) obtain a data set: adequate to define multiscale physical dynamical processes (sub-meso-, meso-, bay-, gulf- scales) that govern the formation and evolution of structures and events, including generic processes and the coupling of wind-forced events and buoyancy currents; and capable of providing a context for interdisciplinary forecasting and process studies; and, iv) maintain, via surveys and adaptive sampling, a continuous synoptic description of Massachusetts

Bay with mesoscale resolution throughout and sub-mesoscale resolution as dynamically required

The goal of the biological component of ASCOT-01 was to test hypotheses that link the physical and biological event scales in the coastal ocean and provide the basis for coupled forecasting. The biological objectives of ASCOT-01 were to: i) obtain a companion suite of data for biological state variables, and fully embed these in the real-time forecast experiment; ii) using forecasts for the evolution of physical processes and events, and for the biological responses to them, strategically assess these biological reaction rates for the further refinement of models.

The physical dimensions of the ASCOT-01 region allowed for an interdisciplinary endeavor with a comprehensiveness that would have been unattainable in a larger domain. The physical processes of the area strongly influence the rates and fates of biological productivity in Massachusetts Bay. The response of biological processes to pulses of upwelling or tidal mixing are generally brief, only a day or two (the generation time for the phytoplankton). Given typical rates of biological activity and advective and diffusive dissipation, a local record of the primary features of such events, e.g. the elevation of nutrients, would presumably be diminished only a few days after the event.

1.4 Scope and objectives of this research

Coastal upwelling and the resulting primary production are well studied topics ([39], [52], [6], [7], [35]). Few studies though have focused on episodic (1-2 days) winds events (storms) and the biological response these upwelling events. This thesis

aims at answering the question as to whether storms play an important role in the circulation and biological processes in Massachusetts Bay. If so, on what spatial and temporal scale. This work focuses on wind events that give rise to upwelling along the mainland coast in Massachusetts Bay in early summer. The size and box-like geometry of Massachusetts Bay makes it a suitable place to conduct a study of the physical processes and their influence on biological processes.

During upwelling events nutrients are advected upward into the euphotic zone where they can be utilized by phytoplankton. The resultant increase in primary production depends on the strength and duration of the wind event. The stronger the wind event the deeper the source depth of the upwelled nutrients and the stronger the biological response to the upwelling event.

Horizontal advection is also important during an upwelling event because of its role in the horizontal redistribution nutrients and biomass. Near the surface the currents are off-shore and deeper in the water column on-shore. This deep on-shore current plays a crucial role as it advects nitrate from the Gulf of Maine into Massachusetts Bay, recharging the aphotic zone. Thus a strong upwelling event can result in an increase of nitrate in the aphotic zone and continue to enhance primary production in the overlying euphotic zone after the upwelling has subsided.

To determine the biological response to wind-induced upwelling events 3-dimensional physical-biological simulations are carried out. The domain includes Massachusetts Bay and the western Gulf of Maine. The timeperiod of the simulation is June 6-26, 2001 which corresponds to the time of the ASCOT-01 experiment when the data used for initialization and assimilation were collected. Three different wind forcings are

used: 1) real wind forcing from June 2001, 2) modeled wind events of strong storms, and 3) historical summer winds. During June 2001 the winds were unusually weak and hence responsible for very little upwelling. By modeling strong feature wind events we are able to amplify the biological responses. Simulations with historical dynamically interesting winds allowed examination of more typical conditions.

The outline of this dissertation is as follow. In Chapter 2 the governing physical and biological equations are described. The physical and biological data collected during the ASCOT-01 experiment are presented in Chapter 3. In Chapter 4 the initialization procedure and dynamical adjustment is discussed. The determination of the biological parameters is carried out in Chapter 5. The results of the data-based simulation using real wind are discussed in Chapter 6. In Chapter the simulations with feature modeled strong wind events and real historical winds arer analyzed. The conclusions of the dissertation are found in Chapter 8.

Chapter 2

Governing equations

We are interested in how the state variables that describe the physical, biological, and chemical ocean evolve in space and time. We want to identify the physical processes that can influence the biology and study how the biology and chemistry react to these processes.

Physical processes in the ocean occur on a multitude of time and space scales. These scales are set either by the external forcing or internal processes. The time scales of biological processes occur on time scales given by biological processes, physical processes, and the interaction of the two [20]. It is obvious that not all spatial and time scales can be represented in a single model. The spatial scales are determined by the computational grid being used, with the largest scales determined by the computational domain and the smallest one by the grid resolution. The integration time step gives the time scale of the processes that can be resolved. The total integration time is the time scale of the processes we are interested in. Scales that are too small to be resolved have to be parameterized while scales that are too big enter the model

through initial and boundary conditions [34].

We use an Eulerian approach to describe the physical and biological state of the ocean. The independent variables are time and the three space coordinates. The dependent variables, e.g. velocity, density, pressure, temperature, phytoplankton concentration, etc. are expressed as functions of space and time, e.g. $\phi(\vec{r}, t) = \phi(x, y, z, t)$. Such a function, of space and time, is referred to as a field.

This chapter discusses the physical and biological equations. The numerical methods used to solve these equations are the same as in [4].

2.1 Physical equations

The general dynamics of a flow is governed by the conservation equations for momentum (Navier-Stokes), mass, and energy. These equations are derived under the assumption that the fluid is a continuum [10]. The principle behind each equation is the same, the net flux into a fluid box equals the sources and sinks within the box. The set of equations that describe the flow in the ocean are called Primitive Equations (PE). These are given below, followed by a short discussion of some of ocean specific aspects. In oceanography, the motion occurs on a thin fluid shell on a rotating sphere. For more details about the PE see for example [40].

In the equations that follow $\vec{u} = (u, v, w)$ are the current velocities in the (x, y, z) directions, p is the pressure, ρ is the density, T is the temperature and S is the salinity.

Horizontal momentum equations

$$\frac{\partial u}{\partial t} + \vec{u} \cdot \nabla u = -\frac{1}{\rho}\frac{\partial p}{\partial x} + fv + \frac{\partial}{\partial x}\left(k_h \frac{\partial u}{\partial x}\right) + \frac{\partial}{\partial y}\left(k_h \frac{\partial u}{\partial y}\right) + \frac{\partial}{\partial z}\left(k_v \frac{\partial u}{\partial z}\right) \tag{2.1}$$

$$\frac{\partial v}{\partial t} + \vec{u} \cdot \nabla v = -\frac{1}{\rho}\frac{\partial p}{\partial y} - fu + \frac{\partial}{\partial x}\left(k_h \frac{\partial v}{\partial x}\right) + \frac{\partial}{\partial y}\left(k_h \frac{\partial v}{\partial y}\right) + \frac{\partial}{\partial z}\left(k_v \frac{\partial v}{\partial z}\right) \tag{2.2}$$

Vertical momentum equation

$$0 = -\frac{1}{\rho}\frac{\partial p}{\partial z} - g \tag{2.3}$$

Continuity equation

$$\frac{\partial u}{\partial x} + \frac{\partial v}{\partial y} + \frac{\partial w}{\partial z} = 0 \tag{2.4}$$

Temperature equation

$$\frac{\partial T}{\partial t} + u\frac{\partial T}{\partial x} + v\frac{\partial T}{\partial y} + w\frac{\partial T}{\partial z} = \nabla_h(K_h \nabla_h T) + \frac{\partial}{\partial z}\left(K_v \frac{\partial T}{\partial z}\right) \tag{2.5}$$

Salinity equation

$$\frac{\partial S}{\partial t} + u\frac{\partial S}{\partial x} + v\frac{\partial S}{\partial y} + w\frac{\partial S}{\partial z} = \nabla_h(K_h \nabla_h S) + \frac{\partial}{\partial z}\left(K_v \frac{\partial S}{\partial z}\right) \tag{2.6}$$

Equation of state

$$\rho = \rho(T, S, p) \tag{2.7}$$

Coriolis parameter

$$f = f_0 + \beta(y - y_0) \quad \text{where} \quad f_0 = 2\Omega \sin\phi_0 \quad \text{and} \quad \beta = \frac{2\Omega \cos\phi_0}{R} \tag{2.8}$$

R is the earth's radius, Ω is the rotation rate of the earth, $7.29 \cdot 10^{-5}$ s^{-1}, and ϕ_0 is the reference latitude.

Rotation Newton's second law is valid in a non-accelerating coordinate frame. As the Earth is rotating our reference frame is accelerating. This has to be taken into account in the momentum equations. The rotation of the coordinate frame is taken into account through the Coriolis force and the centrifugal force. The latter is negligible for ocean problems. The Coriolis force is

$$F_{Co} = \hat{k} \times \vec{v} \tag{2.9}$$

This is a force that only deflects the flow and does not do any work as it is perpendicular to the velocity. It can be shown that the vertical component of the Coriolis force can be neglected. In the x-direction the Coriolis force is fv, and in the y-direction $-fu$.

Thinness Although the oceans may seem deep, they are very shallow on a global perspective. The average depth of the ocean is about 5 km which compared to

the Earth's radius of 6370 km gives a minute aspect ratio. Thinness implies that the main motion occurs in the horizontal and that the vertical accelerations can be neglected. The vertical momentum equation is then reduced to only 2.3.

Sphericity As the flow in the ocean is on an sphere the coordinate system should be spherical. Instead we use a local Cartesian coordinate where the sphericity is taken into account by the latitude dependence of the Coriolis parameter. In this coordinate system x denotes the eastward direction, y the northward direction and z is the vertical coordinate. This approximation is referred to as the β-plane approximation.

Turbulence The molecular dissipation processes are important in the ocean but not on the scales of the numerical grid. Turbulence mixing can be modeled as a dissipation process. Fourier-Fick Law for molecular fluxes can only be used if the molecular motion is random and dissipation of kinetic energy happens towards smaller scales. These conditions are not always satisfied in geophysical fluid dynamics. Processes can be both up- and down-gradient. It is common to make a distinction between processes in the vertical and horizontal direction. For small scales the vertical and horizontal scales are of the same order of magnitude. For larger scales, there are orders of magnitude difference between the horizontal scale, given by the width of the ocean basin, and the vertical scale given by the mixed-layer depth (or the shallow depth of the basin).

Continuity equation The continuity equation expresses conservation of mass within a fluid box. In its full format it is given by

$$\frac{\mathrm{D}\rho}{\mathrm{D}t} + \rho\nabla \cdot \vec{u} = 0 \tag{2.10}$$

For an incompressible fluid the density following the fluid does not change, i.e.,

$$\frac{\mathrm{D}\rho}{\mathrm{D}t} = 0 \tag{2.11}$$

For an almost incompressible fluid the lowest approximation to 2.10 takes the form 2.4.

Primitive equation By introducing the thinness approximation, adding the effects of rotation, and introducing the beta-plane approximation the so called primitive equations on the beta-plane are obtained which are used to describe the state of the ocean.

2.2 Biological equations

Conceptual equations, like the conservation of mass, momentum, and energy equations used in fluid dynamics, are not readily available to describe the dynamics of ocean biology ([18] and [32]). An advective-diffusive-reactive (ADR) equation is used to describe the dynamics of the biology in the presence of a flow. It is derived in a similar manner as the physical equations and is based on conservation of the state variables. Following the derivation by Robinson [45], let ϕ be a biological state variable affected by advection and diffusion. The governing equation is then

$$\frac{\partial \phi}{\partial t} + \nabla \cdot (\vec{v}\phi) - \nabla \cdot (k \nabla \phi) = R \tag{2.12}$$

where the first term on the left-hand side is the local time rate of change of ϕ. The second term is the change in ϕ due to advection where $\vec{v}$ is the velocity vector. The third term on the left-hand side is the diffusive term where k is the molecular diffusivity, or with turbulence, the eddy diffusivity. It is common to differentiate between vertical and horizontal eddy diffusivity as was done for the momentum equations in the previous section. R represents the biological activity of state variables ϕ and includes all sources and sinks of ϕ such as reproduction, mortality, predation, life-stage transition, or progression of developmental stages.

The equations governing the dynamics of a general n-component biological system is given by

$$\frac{\partial \phi_i}{\partial t} + \nabla \cdot (\vec{v}\phi_i) - \nabla \cdot (k \nabla \phi_i) = R_i(\phi_1, \ldots, \phi_i, \ldots \phi_n), \quad i = 1, \ldots, n \tag{2.13}$$

where R_i now describes the biological activity between the state variables. No fixed mathematical formulation exists for R and many expressions have been used ([6], [4], [17], [2], [15], [53], [30]).

ϕ is commonly expressed as concentration of nutrient or biomass.

The choice of biological state variables and formulation of reaction terms is based on [4]. In this model the chosen biological state variables are: nitrate (N), ammonium (A), phytoplankton (P), zooplankton (Z), detritus (D), and chlorophyll (Chl). They are expressed in terms of nitrogen concentration mmol N m^{-3}, except for chlorophyll which has units mg Chl m^{-3}.

Two nitrogen based nutrients (nitrate and ammonium) are used. This allows for tracking new (nitrate based) and recycled (ammonium based) primary production [13]. This distinction is not possible with the other macronutrients, carbon and phosphorous. The phytoplankton state variable includes all species that are capable of photosynthesis regardless of taxonomic grouping and size. When determining the biological parameters the size of phytoplankton is taken into account.

The main role of zooplankton in this biological model is phytoplankton grazing. No attempt is made to model actual animal behavior such as daily vertical migration and daily variations in grazing patters. Zooplankton are assumed to be grazing throughout the day and night. The detritus state variable includes, in addition to detrital matter, bacteria and dissolved organic material. The detrital processes represent recycling of phytoplankton and zooplankton to ammonium. The model [4] allows for an independent chlorophyll equation with varying carbon-to-chlorophyll ratio. In this work a fixed carbon-to-chlorophyll ratio is used. For more details on

the chlorophyll equation see [4].

Figure 2.2 shows an overview of the biological model. The arrows between the boxes indicate biological processes that transfer nitrogen from one reservoir to another. Below follows a description of the biological sources and sinks for each biological state variable.

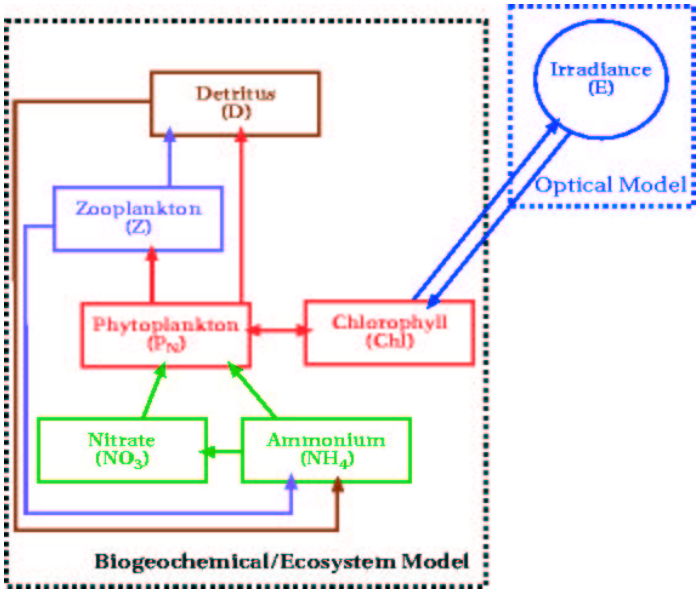

Figure 2.1: Overview of the biological model.

2.2.1 Phytoplankton

The phytoplankton reaction term, R_P, is expressed as

$$R_P = L(Q_1 + Q_2)P - gZ - n_3 P - \nu_P \frac{\mathrm{d}P}{\mathrm{d}z} \tag{2.14}$$

where the first term, LQP, is primary production (nutrient uptake) where L (day^{-1}) is the effective photosynthesis rate taking into account the photosynthesis

response to available light energy. Q_1 and Q_2 are nutrient uptake limitation terms for nitrate and ammonium respectively. Primary production is described in more detail below. The second term in the equation, gZ, represents phytoplankton losses due to zooplankton grazing (see zooplankton reaction term below). Phytoplankton mortality is expressed as a linear function, $n_3 P$, where n_3 (day^{-1}) is the phytoplankton mortality rate. The last term represents phytoplankton loss due to sinking where ν_P (m day^{-1}) is the phytoplankton sinking rate.

The effective photosynthesis is given by

$$L = P_m(1 - e^{-\alpha I/P_m})e^{-\beta I/P_m} \tag{2.15}$$

where P_m (day^{-1}) is the maximum photosynthesis rate, α is the initial slope of the photosynthesis vs light curve, β is the photoinhibition parameter, and I is the irradiance (Wm^{-2}). The depth dependence of irradiance is given by

$$I = I_0 e^{-\left(k_w z + k_c \int_0^z [Chl] dz\right)} \tag{2.16}$$

where $I_0 = I(x, y, z = 0, t)$ is the irradiance at the surface, k_w is the light attenuation coefficient due to water, and k_c the light attenuation due to chlorophyll.

The Michaelis-Menten formulation is used to describe the nitrate and ammonium uptake by phytoplankton. The nitrate uptake (new production) limitation term is expressed as

$$Q_1 = \frac{N}{k_1 + N} e^{-\psi A} \tag{2.17}$$

where k_1 (mmol N m^{-3}) is the half-saturation constant for nitrate uptake. In the

presence of ammonium the uptake of nitrate is inhibited. An ammonium inhibition term is often included in the form of an exponential function [53] where ψ is the ammonium inhibition parameter with unit (mmol N m^{-3})$^{-1}$.

The ammonium uptake (regenerated production) is expressed as

$$Q_2 = \frac{A}{k_2 + A} \tag{2.18}$$

where k_2 (mmol N m^{-3}) is the half-saturation constant for ammonium uptake.

2.2.2 Zooplankton

The zooplankton reaction term, R_Z, is given by

$$R_Z = (1 - \gamma_1 - \gamma_2)gZ - n_1 Z - n_2 Z^2 \tag{2.19}$$

Zooplankton grazing, gZ, is modeled with Ivlev's formulation [21]

$$g = R_m(1 - e^{-\Lambda P}) \tag{2.20}$$

where R_m (day^{-1}) is the maximum grazing rate and λ is the Ivlev constant ((mmol N m^{-3})$^{-1}$). This expression is commonly used where zooplankton graze on phytoplankton only. In models where zooplankton graze on bacteria and detritus as well, the Michaelis-Menten formulation is weighted with preference factors for each food group. The Ivlev formulation is similar to the Michaelis-Menten formulation for nutrient uptake in that the grazing rate varies linearly for low phytoplankton concentrations and becomes saturated for high phytoplankton concentration.

Grazing losses are expressed as a grazing specific process. γ_1 is the fraction of grazing losses that goes to ammonium and γ_2 the fraction that goes to detritus.

Zooplankton losses are parameterized as linear and quadratic. The linear loss term, $n_1 Z$, models natural mortality and the quadratic loss term, $n_2 Z^2$, models losses to higher trophic levels. n_1 (day^{-1}) is the natural mortality rate and n_2 ((mmol N m^{-3})$^{-1}$ day^{-1}) is the rate of losses to higher trophic levels.

A fraction, ϵ_1, of the linear mortality terms goes to detritus. The remaining fraction, $(1-\epsilon_1)$, goes to ammonium. Similarly, a fraction ϵ_2 of the quadratic mortality term goes to detritus and the rest to ammonium.

2.2.3 Detritus

The detritus reaction term, R_D, is given by

$$R_D = -k_D D + \gamma_2 g Z + \epsilon_1 n_1 Z + \epsilon_2 n_2 Z^2 + n_3 P - \nu_D \frac{\mathrm{d}D}{\mathrm{d}z} \tag{2.21}$$

The first term, $k_D D$ is the remineralization of detritus to ammonium where k_D is the remineralization rate (day^{-1}). This term represent all recycling processes that convert detritus to ammonium. The last term is the loss of detritus due to sinking, where ν_D is the sinking rate (m day^{-1}).

2.2.4 Ammonium

Ammonium (A)

$$R_A = -LQ_2 P + \gamma_1 g Z + (1-\epsilon_1) n_1 Z + (1-\epsilon_2) n_2 Z^2 + k_D D \tag{2.22}$$

2.2.5 Nitrate

Nitrate (N)

$$R_N = -LQ_2P \tag{2.23}$$

The only biological term in the nitrate equation is the loss term due to nitrate uptake by phytoplankton. The source terms are all physical; advection and diffusion from beyond the domain that bring nitrate into Massachusetts Bay.

2.3 Coupled physical-biological equations

The coupled physical-biological equations used in this research are a component of the Harvard Ocean Prediction System (HOPS). HOPS is a regional interdisciplinary nowcasting and forecasting system (see Figure 2.3). It is portable and can be deployed in any open, closed or semi-enclosed region of the world ocean. The physical version was first initiated by Robinson and Leslie [42] and a full overview is provided in Robinson and Waldstad [44]. A comprehensive review of the interdisciplinary aspects is presented in Robinson [40] and the present version of HOPS with data assimilation is reviewed by Robinson and Lermusiaux [41]. HOPS was first applied in Massachusetts Bay for a physical-biological study in Besiktepe *et al.* [4] which provides the starting point of the modeling research carried out in this thesis.

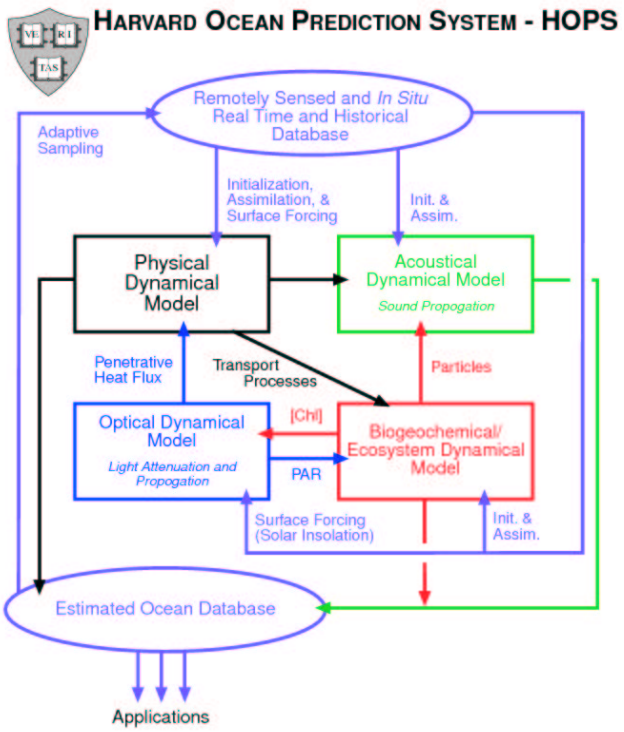

Figure 2.2: HOPS components

Chapter 3

Data

3.1 Physical data

The ASCOT-01 experiment utilized three research vessels throughout the June 2001 field exercise. These vessels were: the NRV Alliance (NATO SACLANT Undersea Research Centre), the RV Lucky Lady (University of Massachusetts - Dartmouth), and the RV Neritic (University of Massachusetts - Boston). Each of these vessels collected vertical profiles of temperature, salinity, and fluorescence using a Seabird SBE 911 CTD system. Calibration stations (stations nearly simultaneous in space and time) were carried out. Table 3.1 shows the region covered by each ship and the number of CTD profiles obtained.

Plotted below are the locations of the CTD stations for each of the individual vessels collected during the period 6-25 June 2001 and the composite profiles of temperature and salinity versus depth. Measured mixed layer depths were generally in the 5-10m depth range with a main thermocline depth of 40-50m.

Research vessel	Regions covered	Nr. of stations
Alliance	Massachusetts Bay	286
	Gulf of Maine	
Lucky Lady	Massachusetts Bay	118
	Cape Cod Bay	
	North Passage	
Neritic	Northern Massachusetts Bay	52

Table 3.1: Location and number of stations collected by the three main research vessels during the ASCOT-01 experiment, June 2001.

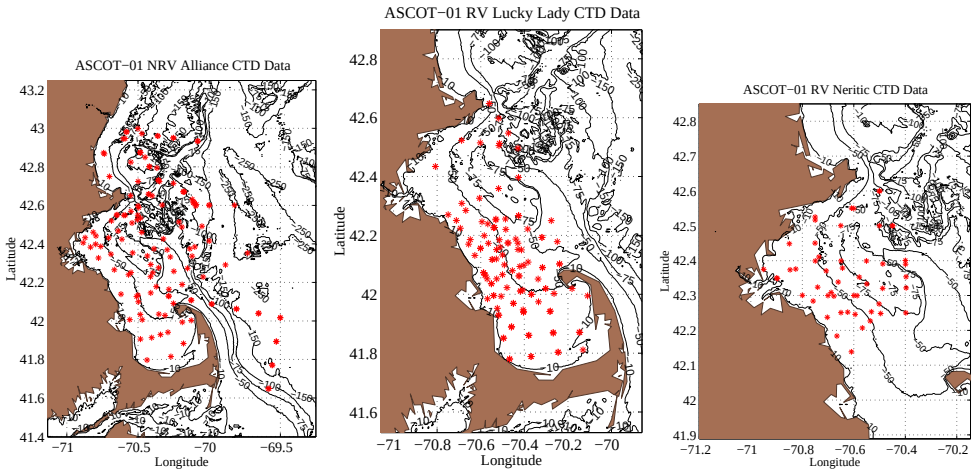

Figure 3.1: NRV Alliance, RV Lucky Lady and RV Neritic CTD Positions.

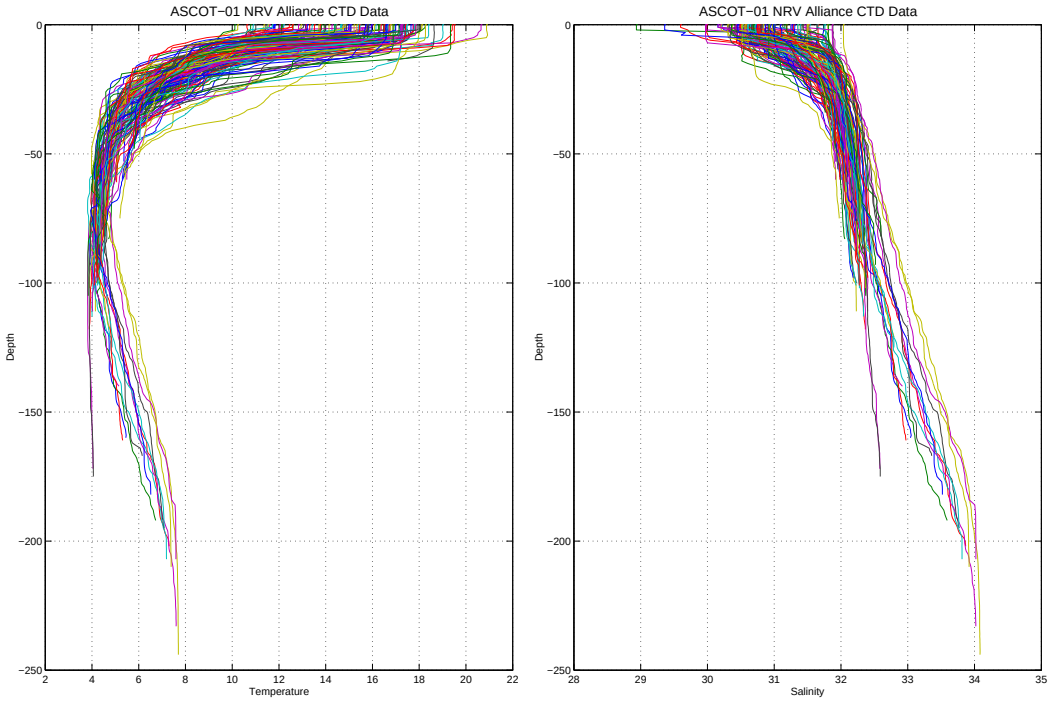

Figure 3.2: NRV Alliance CTD Temperature and Salinity Profiles.

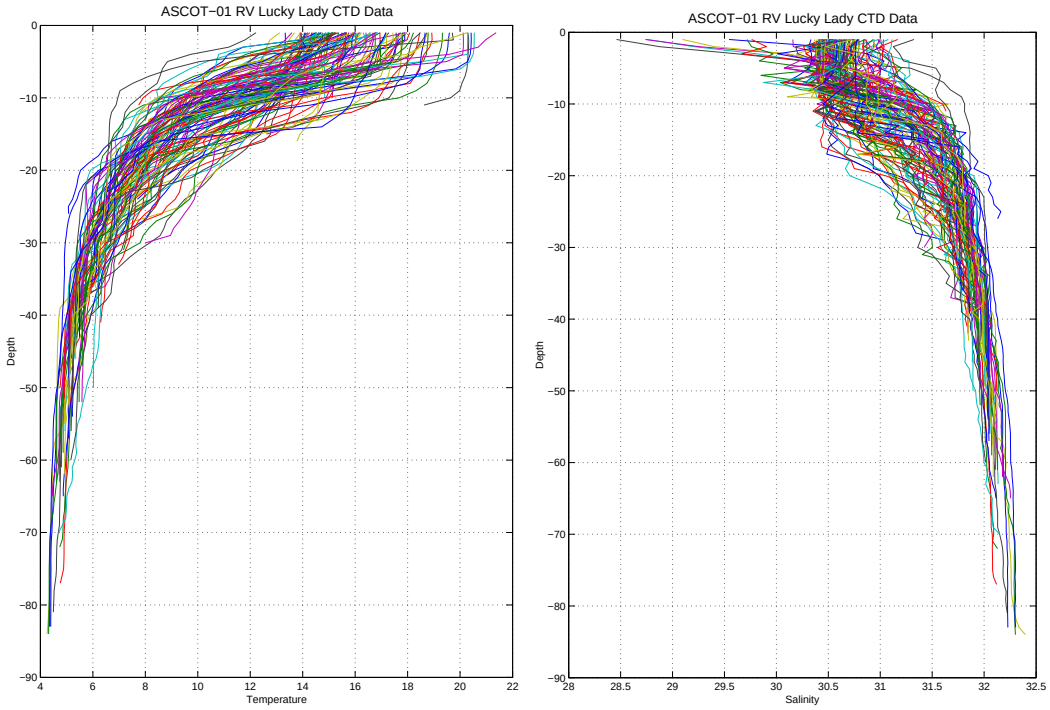

Figure 3.3: RV Lucky Lady CTD Temperature and Salinity Profiles.

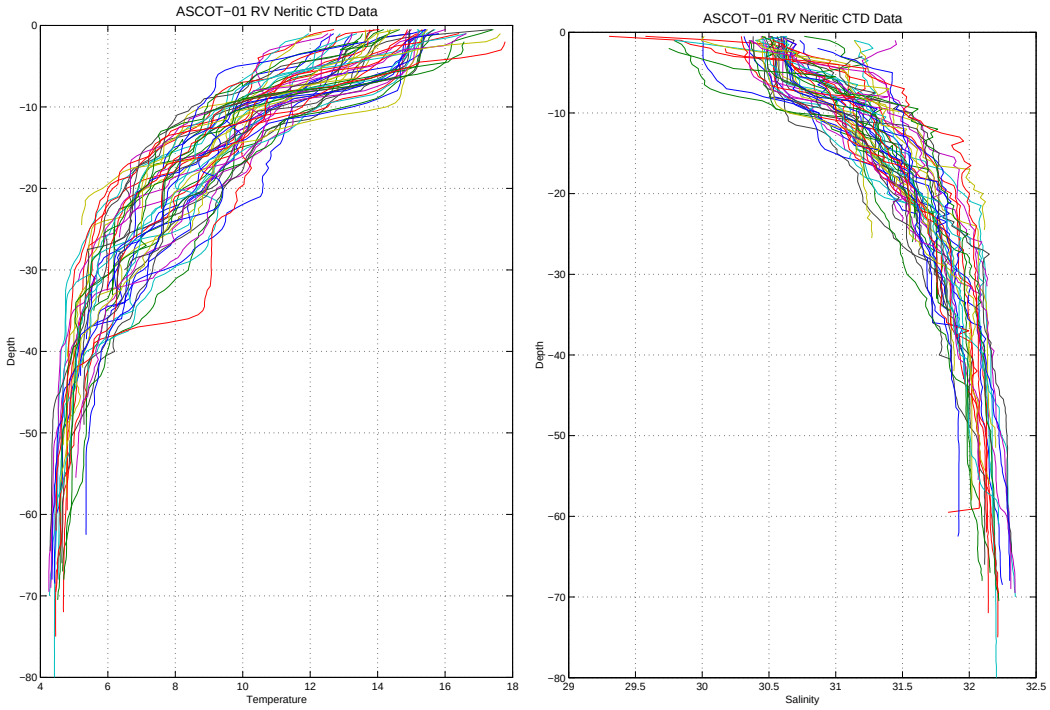

Figure 3.4: RV Neritic CTD Temperature and Salinity Profiles

3.2 Biological data

In addition to CTDs and fluorometry, basic measurements of biological and chemical fields from the RV Lucky Lady and RV Neritic included nutrients, chlorophyll and a full suite of plant pigments on selected stations, samples collected but not immediately processed for phytoplankton microscopic counts, zooplankton net collections and microscopic counts, and nitrogen turn-over times. The biological data is used to create initialization fields of the biological state variables and is used as an aid in determining the biological parameters.

3.2.1 Nutrient bottle data

Samples of dissolved inorganic nutrients NO_3, NO_2, SiO_4, and NH_4 were collected at a subset of CTD stations (see Figure 3.5). Typically 3 bottle samples per station were collected. The 'shallow' samples were collected from within the mixed-layer, the 'mid-depth' samples from around the thermocline, and the 'deep' samples from close to the bottom. The analysis of dissolved inorganic nutrients was based on EPA methods [26] under the direction of C. Oviatt, University of Rhode Island, Graduate School of Oceanography (GSO). Samples were passed through 0.4 μm pore size membrane filters in the field, stored in ice-filled coolers and transferred to GSO within 12 h for immediate analysis. The concentrations of ammonium, nitrate, and nitrite were measured colorimetrically on a Skalar Autoanalyzer. The ammonium analysis is based on the technique of Solorzano [47] whereby absorbance of an indophenol blue complex is measured at 660 nm. Nitrite is measured by the method of Bendschneider and Robinson [3]. The total of nitrate and nitrite is determined by reducing nitrate in

the sample to nitrite and analyzing for nitrite as above. The concentration of nitrate is obtained by difference. The reduction is accomplished using a cadmium column [33].

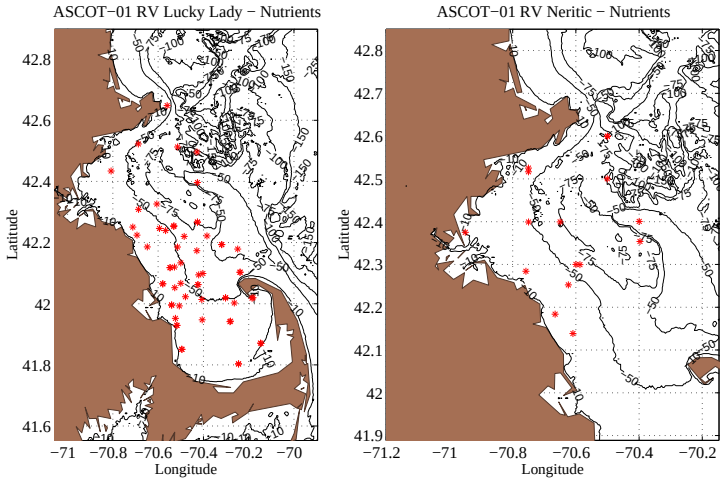

Figure 3.5: Station locations for dissolved nutrients; Lucky Lady (left), Neritic (right)

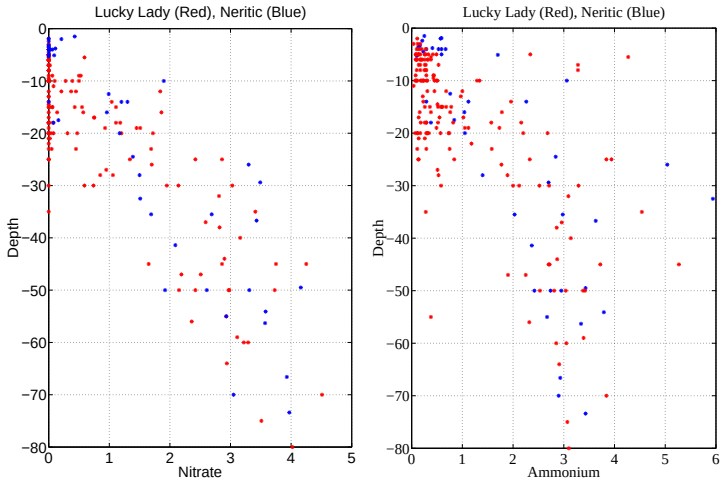

Figure 3.6: Left: Nitrate concentration (mmmol N m^{-3}) versus depth (m). Right: Ammonium concentration (mmol N m^{-3}) versus depth (m).

Figure 3.6 shows the nitrate and ammonium concentration data. The distribution is typical for summer conditions in a stratified coastal ocean. Near the surface both

nutrients show low concentrations with nitrate depleted in most of Massachusetts Bay. Deeper in the water column the nitrate and ammonium concentrations are high.

3.2.2 Chlorophyll and fluorescence

Chlorophyll

At a subset of the CTD stations chlorophyll bottle samples were collected (see Figure 3.5). On average 2 chlorophyll samples per station were collected. One sample was from near the surface and the other one from around the subsurface chlorophyll maximum (as determined from the fluorescence profiles).

Samples for chlorophyll a/phaeophytin were processed according to EPA methods ([26], [37]) under the direction of C. Oviatt (URI/GSO). Samples were collected by filtration onto Whatman GF/F glass fiber filters in the field, stored in dry ice, and transferred to GSO within 12 h for immediate analysis. All handling steps were performed in subdued light. The chlorophyll a/phaeophytin was extracted from the cells retained on the GF/F filter by mechanical grinding followed by a 2-24 hour steep in 90% buffered acetone at 4 ^{o}C. The samples were then centrifuged and the extract analyzed using a Sequoia Turner Fluorometer, Model 450-003. 150 μL of 0.1 N HCl was added to the extract and the extract re-measured after 90 seconds to determine phaeophytin concentrations.

Diatom Chl a was determined by the protocols of Bidigare & Ondrusek [5] using HPLC pigment analyses provided by L. Van Heukelem, Horn Point Environmental Lab (HPEL), Cambridge, MD. Samples were collected by filtration onto Whatman GF/F glass fiber filters in the field, stored in liquid nitrogen, and transferred to HEPL

for HPLC analysis.

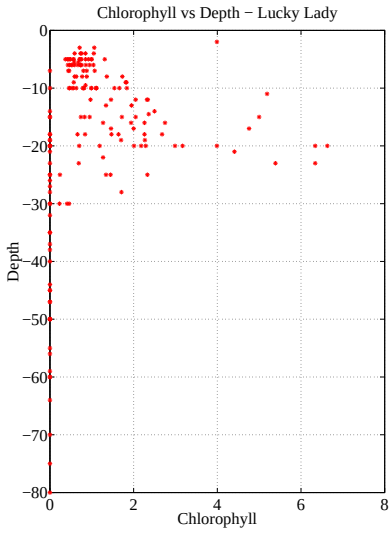

Figure 3.7: Lucky Lady Chlorophyll bottle sample vs depth

Fluorescence

A fluorometer was mounted on the CTD of the Lucky Lady (June 6-25) and the Alliance (June 10-24). Fluorescence was measured at all CTD stations within the time period indicated. The vertical resolution of the fluorescence profiles is the same as for temperature and salinity profiles, 1 m.

At each station where chlorophyll bottle samples were collected a fluorescence profile is available. Using the chlorophyll sample data the fluorescence data can be converted to chlorophyll concentration.

No chlorophyll samples were collected by the Alliance so contemporary Lucky Lady fluorescence profiles are used for the calibration. The Alliance sailed during day and night near the coast and off-shore while the Lucky Lady sailed only during

the day near the coast. As the fluorescence response depends on the light history we compare only profiles collected during the day and near the coast.

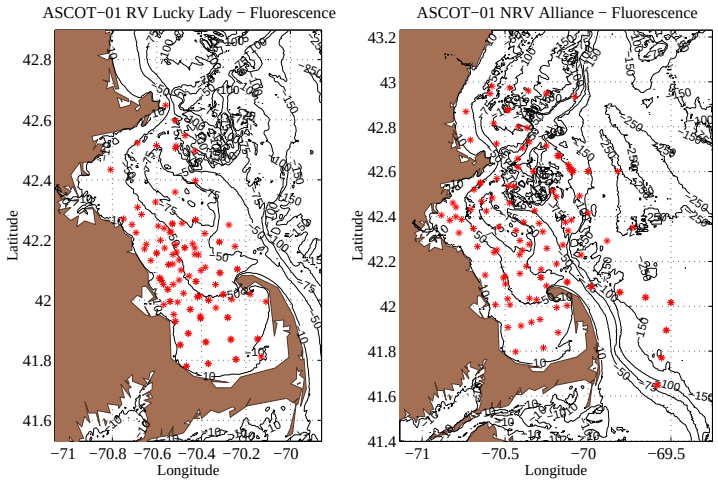

Figure 3.8: Location of biological stations; Lucky Lady (left), Alliance (right)

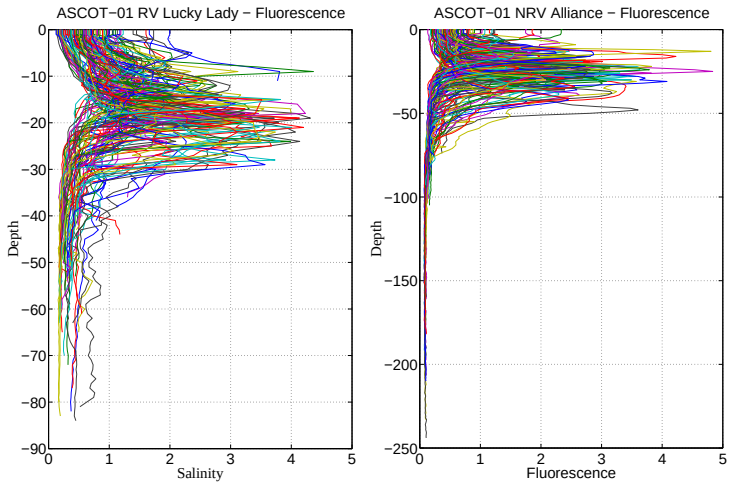

Figure 3.9: Fluorescence profiles; Lucky Lady, (left), Alliance (right)

The fluorescence subsurface maxima is located between 10 and 30 m with values ranging between 1.5 to almost 5 mg Chl m^{-3}.

3.2.3 Plankton sampling

The initial NAFC Plankton Sorting and Identification Data Coding Form for the plankton samples were completed for identification and collection locality data using the format from the NAFC - Plankton Sorting and Identification Format for Marine Plankton. The samples were taken out of formalin and diluted with water. Large objects were removed, rinsed carefully through a 0.202 mm or smaller mesh dip net, examined for target organisms, and discarded. Prior to subsampling large organisms greater than 1 cm were removed, identified measured and wet weighed and then preserved anew.

Subsequently, the sample was split into halves using a Folsom splitter, one half being used for biomass determination, the other half to determine taxonomic composition and abundance. For biomass estimation, the sample aliquot was passed through a 1 mm screen and the two resulting fractions collected onto fine mesh 20 micron Nitex screen, dried at 60 degrees C for 48 hrs. and weighed (three decimals). The proper aliquot was used for taxonomic identification and enumeration by visual inspection to determine if subsampling was necessary. Subsampling was performed on the sample: 1) if it was dominated by one or two taxa or when numbers appeared to exceed 200 of a given taxon, and/or 2) if it appeared to contain more than 200 of the target invertebrate organisms. The HMSC beaker technique ([50], in line with methods defined by [46]) was used for subsampling the sample for ichthyoplankton and zooplankton prior to sorting. Species data was coded following Foy and Anderson [16].

3.2.4 Zooplankton

One zooplankton tow was carried out on each biological stations. A subset of those samples was analyzed (see Figure 3.10 for location of these samples). Vertical tows with a 0.5 m diameter 100 m mesh net were conducted from a depth of 20 m. Samples were placed in 500 ml Glass jars and preserved with 10% formalin. J. Turner, University of Massachusetts at Dartmouth, provided sampling equipment and tow volume calibration data. Copepod species enumeration and zooplankton dry weight biomass determinations were carried out under the direction of G. Pohl, Atlantic Reference Center, St. Andrews, NB, Canada.

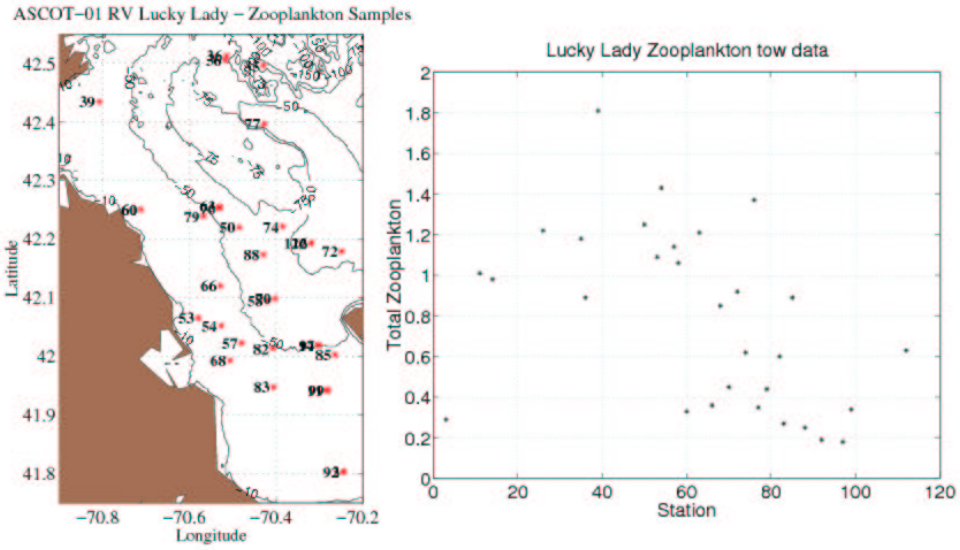

Figure 3.10: Station IDs for zooplankton sampling (left). Some station pairs are co-located: (11,99), (14,97), (26,112), (58,70) and (63,76). Zooplankton tow data vs Station ID (right).

3.2.5 Particular Organic Nitrogen (PON) and Nutrient uptake rates

Rates of NO3-and NH4+ uptake were determined with 15N tracer techniques ([29], [28]). Samples collected from the water column were stored in 250 ml polycarbonate bottles, stored in ice filled coolers and transported to the laboratory of J.J. McCarthy, Harvard University, Cambridge, MA, where 15N labeled substrates (99 atom-%) were added to the samples. Euphotic zone samples were incubated in an environmental chamber at near ambient temperature under banks of "GroLux" fluorescent lamps providing approximately 60% of cloud-free PAR. Sub-euphotic zone samples were incubated in opaque boxes placed in the environmental chamber. The 15N incubations were terminated after a period of 6 hours by filtration onto pre-combusted (1 hr @ 450^{o}C) 25 mm Whatman GF/F glass fiber filters. The filters were dried at 60^{o}C and stored in a desiccator .15N enrichment and elemental N and C concentration in particulate material from these tracer experiments were determined with a Europa Scientific 20/20 mass spectrometer equipped with an automated Dumas combustion sample preparation system (ANCA nt) in a continuous flow configuration [28].

3.2.6 Secchi depth

The Secchi depth was measured at all CTD stations. The depth of the euphotic zone (defined as the depth where downward irradiance is 1% of its surface value) can be estimated from the Secchi depth.

From the Secchi depth it is possible to calculate the euphotic depth by assuming that at the Secchi depth we have 16% of the surface irradiance [38]. The mean

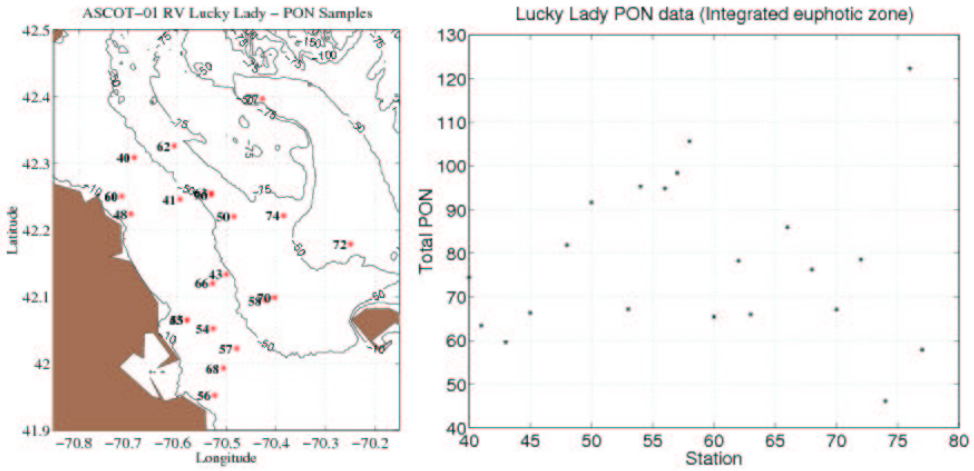

Figure 3.11: Station IDs for Particular Organic Nitrogen (PON) sampling (left). Some station pairs are co-located: (45,53) and (63,76). Integrated PON in the euphotic zone vs Station ID (right).

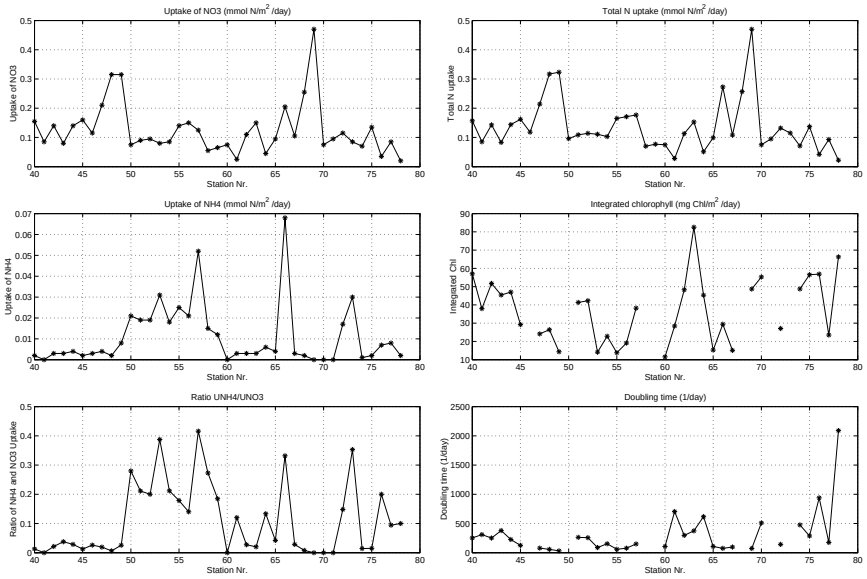

Figure 3.12: Nutrient uptake rates vs station ID.

euphotic depth measured during the ASCOT01 experiment is 23.5 m.

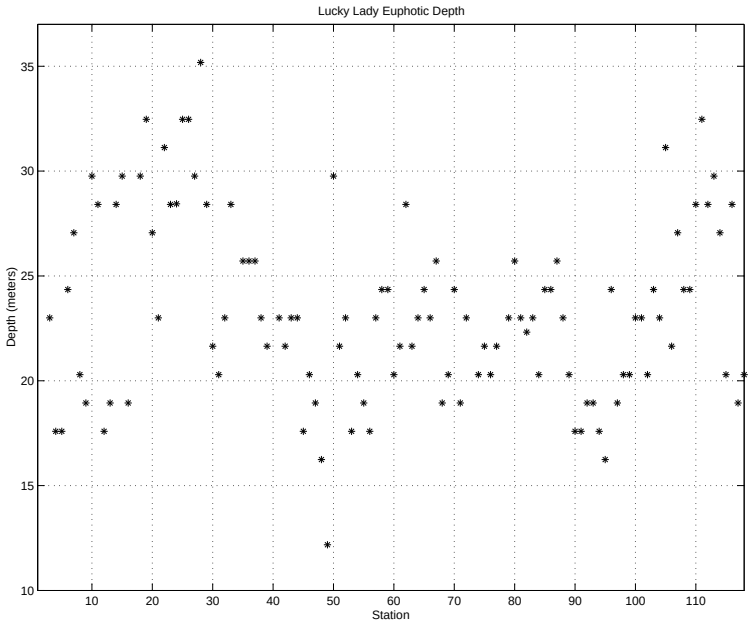

Figure 3.13: Euphotic depth (m) based on Secchi depths measurements at hydrological stations during the ASCOT01 experiment.

Chapter 4

Initialization and dynamical adjustment

To initialize the physical-biological simulation 3-dimensional fields of all state variables in the model are needed. Three considerations must be taken into account when producing the initial fields. First, the physical and biological data available are irregularly spaced in space and time, and of limited coverage within the computational domain. Secondly, data are not available for all the state variables. Initial fields still need to be created for the non-observable physical (e.g.vertical velocity) and biological variables (phytoplankton, zooplankton, and detritus). Lastly, ideally, all the state variables should be dynamically adjusted to each other. In the first Section (4.1) the observable physical (temperature and salinity) and biological (nitrate, ammonium and chlorophyll) variables are objectively analyzed. In Section 4.2 the initialization of non-observable variables is discussed and in Section 4.3 the dynamical adjustment procedure is discussed.

4.1 Objective analysis of observable variables

The objective analysis (OA) interpolates and extrapolates the irregularly spaced data onto the computational grid ([8], [11], [40], [4]). First the data is linearly interpolated to flat levels (OA levels). The data is then extrapolated horizontally so that it covers the entire computational domain. At each OA level, the horizontal extrapolation is carried out in threee steps. First, using all the data a constant average value is calculated for each OA level. Spatial variation is then introduced to this mean value by making large-scale corrections using the observed data set. The decorrelation scale used for the correction is referred as as "mean" scale. Corrections are then made to this spatially varying field using the synoptic data set. For this correction the decorrelation scale is smaller that the "mean" scale. This resulting field includes the mesoscale features.

The synoptic fields are designed for a particular date. Usually the data set used to create the initial fields include data from days other than the actual initialization date. A time decorrelation scale is used to allow for the data closest in time to the initialization data to have the heaviest weight.

The same OA parameters are used for the physical (temperature and salinity) and biological (chlorophyll, nitrate, and ammonium) data. Table 4.1 shows the time and spatial scales for the OA. The decay scale indicates the exponential decay scale for the correlation function and the zero-crossing scale the distance at which the correlation function becomes zero.

Scales	Time decorrelation (days)	Decay scale (km)	Zero-crossing scale (km)
Synoptic	10000	10	40
Mean	10000	25	60

Table 4.1: Decorrelation scales for the objective analysis of the initial physical and biological data.

Data coverage

To create the initialization fields for temperature and salinity data from the NRV Alliance and RV Lucky Lady and Neritic are used. The initialization fields are created for June 6 and only the subset of the data that is close in time is used.

The R/V Alliance completed 286 CTD casts but only 136 of them are used in these simulations. The rest are considered to be located too far away from the computational grid relative to the objective analysis scales used. Including them would slow down the objective analysis calculations with no added benefit.

The synoptic fields are complemented with climatological data to improve the coverage in the eastern part of the domain.

Figure 4.1 shows the OA of the temperature at 2 m.

Temperature and salinity assimilation

Temperature and salinity is assimilated throughtout the simulation. Table 4.2 shows the dates on which temperature and salinity fields are assimilated and in what region the particular data was collected. The temperature and salinity fields that are assimilated are created in the same manner as the initialization fields. The objective analysis for the assimilation fields uses the same spatial scale as for the initial fields

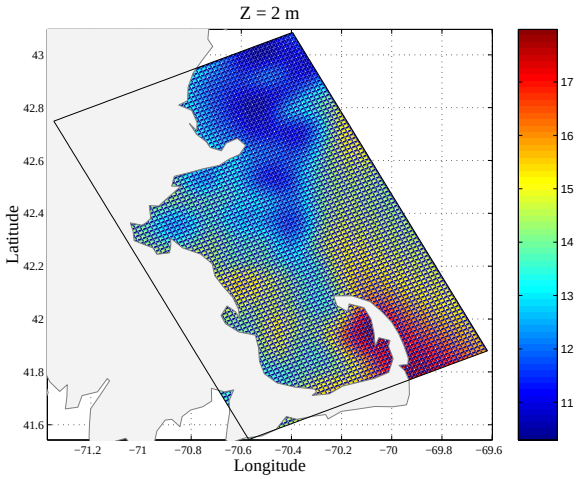

Figure 4.1: Objective analysis of temperature at 2 m.

but the time decorrelation scale is set to 1 day.

Biological data

Only the chlorophyll (based on fluorescence), nitrate and ammonium data are considered to have high enough resolution to make an objective analysis.

Chlorophyll

The objective analysis of the chlorophyll is based on fluorescence profiles. These are of much higher resolution than the chlorophyll bottle samples (see Section 3.2.2). The fluorescence was measured at each CTD stations with a vertical resolution of 1 meter. Only RV Lucky Lady fluorescence measurements are used as the RV Neritic fluorometer failed during the experiment.

June	Region covered	Nr. of stations
06	West of Cape Ann	30
	Cape Cod Bay	
07	Massachusetts Bay	27
	North Passage	
08	Western Massachusetts Bay	22
	West of Cape Ann	
11	Cape Ann	15
12	Western Massachusetts Bay	34
	Mass bay	
	Gulf of Maine	
13	Along the Scituate-	22
	Nanomet coast	
15	Gulf of Maine	10
17	West of Cape Ann	6
19	Along Boston coast	15
	Cape Cod Bay	
20	Western Massachusetts Bay	35
	Massachusetts Bay	
	West of Cape Ann	
21	Stellwagen Bank	8
22	Massachusetts Bay	11
23	Stellwagen Bank	18
	South Passage	
24	Cape Cod Bay	27
	North Passage	
25	Cape Cod Bay	20
	North Passage	

Table 4.2: Daily coverage of ASCOT01 synoptic data.

Nitrate and ammonium

The objective analysis of nitrate and ammonium is based on bottle samples of these nutrients. We use both Lucky Lady and Neritic data.

4.2 Initialization of non-observable variables

4.2.1 Physical variables

The initialization of the physical variables requires primitive equation consistent velocities. The initial velocities are given in terms of an internal (baroclinic) and an external (barotropic) component. The first step is to assume geostrophic balance and calculate the total horizontal velocities. This one is vertically averaged to obtain the external component. The internal comonent is calculated as the difference between the depth-dependent geostrophic velocity and the barotropic component.

4.2.2 Biological variables

To initialize the model 3-dimensional fields are also needed for phytoplankton, zooplankton, and detritus. Zooplankton and detritus data are available but are not of high enough resolution to use directly for initialization. Instead it is used as a guide for determining relationships between the observable and non-observable biological variables. One common approach is to use the observed variable to deduce the non-observed ones. Here we use the chlorophyll data to initialize phytoplankton, zooplankton and detritus.

Phytoplankton

With a fixed carbon to chlorophyll ratio the phytoplankton can easily be calculated,

$$P = \theta^C_{Chl} \times \theta^N_C \times \frac{1}{M_C} \times [Chl] \tag{4.1}$$

where θ^C_{Chl} is the carbon to chlorophyll ratio, θ^N_C is the nitrogen to carbon ratio according to the Redfield ratio, and M_C is the molecular mass of carbon (12 g/mol). Introducing the values for the conversion factors results in

$$P = 1 \times [Chl] \tag{4.2}$$

Zooplankton

The zooplankton distribution is initialized as being proportional to the phytoplankton distribution. The proportionality factor is determined by comparing the zooplankton tow data and average phytoplankton concentration in the euphotic zone. The zooplankton tow data is interpreted as being the average value of zooplankton in the euphotic zone. On average the ratio between the zooplankton and phytoplankton is 1 thus

$$Z = 1 \times P \tag{4.3}$$

To only use the zooplankton data for initialization is not considered a good alternative due to the low spatial resolution. Another alternative would be to combine zooplakton tow data with zooplankton based on phytoplankton profiles but this could create issues at the blending regions. The present initialization is considered good enough as the main role of zooplankton is to graze on the phytoplankton.

Detritus

Detritus is the most difficult biological variable to initialize. In this model detritus is not only simple detritus, but also includes bacteria and dissolved organic matter. A limited set of particulate organic nitrogen (PON) data set is available for the ASCOT-01 experiment from which detritus can be estimated. This data set is of low spatial resolution and can therefore not be used to initialize the entire domain. Similarly to zooplankton, the detritus is initialized as a fraction of the phytoplankton distribution. The proportionality factor, 2, is obtained from the ratio of the average detritus (from PON) and phytoplankton in the euphotic zone so that

$$D = 2 \times P \tag{4.4}$$

The main role of detritus in this model is to supply ammonium to balance the losses due to uptake by phytoplankton. For this purpose the initialization of detritus according to Equation 4.4 is sufficient.

A more refined initialization would take into account the role of bacteria that convert detritus to ammonium. For a more realistic detritus distribution zooplankton daily vertical migration (DVM) can be taken into account. A consequence of DVM is that the zooplankton produce detritus throughout the water column.

If the same OA correlation scales are used for all biological variables the order between calculating the non-observed variables and the OA fields can be switched. The non-observable can first be calculated from the observable variables and then OA'ed or directly from the OA fields of the observable variables. The result in both cases is the same.

4.3 Dynamical Adjustment Procedure

The purpose of dynamical adjustment procedure is to obtain dynamically consistent 3-dimensional physical and biological fields to initialize the simulation for a specific date [4]. Due to the fact that some of the biological variables are of low spatial resolution, the nutrients, and that the zooplankton and detritus are initialized as proportional to the phytoplankton it is important for the biological variables to have time to adjust to each other before the start of the forecast simulation. Generally, when initializing a physics-only simulation it is acceptable to start with vertical velocities that are not accurate. This is not the case for a physical-biological simulation, as the vertical velocity plays a crucial role in determining the distribution of nutrients and biomass relative to the euphotic zone and therefore affecting the primary production rate.

Physical adjustment

The physical variables are adjusted in two consecutive runs. In the first run the velocities are adjusted while keeping temperature and salinity fixed. This is motivated by the high resolution of the temperature and salinity data. No forcing is used for this part of the adjustment which lasts 4 days. In the second run, temperature and salinity are allowed to vary and atmospheric forcing is introduced. This run lasts two days. The purpose is to give the vertical velocities additional time to adjust and the physical fields time to get used to atmospheric forcing. The output of this last run is used as initial physical fields for the physical-biological simulation. This is the procedure followed in [4].

Biological adjustment

The biological fields are adjusted in an 8-day long run [4]. For the biological adjustment the only physical process allowed is vertical diffusion and horizontal Shapiro filter. This adjustment is essentially a zero- dimensional biological model at each grid point as the diffusion parameters are very low. The biological equations are forced with frozen light fields (June 5, 2001), this means that the light forcing varies over the day and is repeated for each day of the run. Except for (phytoplankton and detritus) sinking, all biological source/sinks terms in the equations are kept.

Results

Comparison of simulations with and without the dynamical adjustment procedure shows that for Massachusetts Bay in the early summer, a 8-day dynamical adjustment is not critical for physical-biological simulations. Within a day of physical-biological simulation the vertical velocities are well-developed and the biological variables are adjusted to each other. The simulations in this work are therefore started without the dynamical adjustment procedure. Instead, the first day of the simulation is considered as dynamical adjustment and it not included in the analysis.

Chapter 5

Determination of biological parameters

It is not a trivial task to determine the biological model parameters. Measurements of biological processes in the ocean are not abundant. The biological processes also depend on the history of their environment. The parameters are determined through literature survey, measurements (ASCOT-01 experiment and MWRA) and model tuning.

Measurements of nutrient, chlorophyll and zooplankton concentrations during the ASCOT-01 experiment show that they are stable to a first approximation. There are variations and peaks but no steady gradients. The biological model parameters should therefore be chosen such that the modeled nutrients and biomass remain stable throughout the simulation.

This means that for these variables the biological processes nearly balance each other. Based on the phytoplankton equation this implies that nutrient uptake is bal-

anced by losses due to zooplankton grazing. Phytoplankton mortality is not included in this model and phytoplankton sinking is assumed to be a small loss term compared to zooplankton grazing. The zooplankton equation indicates that zooplankton growth is balanced by zooplankton mortality. The ammonium equation implies that uptake by plankton is balanced by the recycling processes.

The nutrient uptake rate was measured for 4 days over a period of 10 days during the ASCOT-01 experiment. Except for a few extreme values the nutrient uptake rate remains stable. Photosynthesis parameters, determined from Carbon-14 measurement are available from MWRA for northern Massachusetts Bay for the end of June. These two data sets, aided by a literature review, allows the determination of the nutrient uptake parameters. Once these have been fixed the rest of the model parameters can be determined by requiring that the biological variables and processes are stable throughout the simulation.

Generally, the physical parameters may be tuned one parameter at a time. This is not possible for the biological parameters as some of the processes are balanced. For example, increasing the maximum photosynthesis rate requires that the grazing rate be increased to maintain stable phytoplankton. If the grazing rate is higher the mortality rates must be adjusted accordingly. An increase in grazing and mortality rates leads to a change in recycling rates so the detritus remineralization rate must be adjusted to maintain stable total ammonium. This make the tuning of the biological parameters a difficult task. Over 500 simulations were carried out tuning the biological parameters.

5.1 Phytoplankton parameters

5.1.1 Photosynthesis response to light

In this section the parameters for the photosynthesis light response curve, initial slope of the photosynthesis versus light curve (α), the photoinhibition (β), and maximum photosynthesis (P_m), are discussed.

Initial slope of photosynthesis versus light curve

During the MWRA WF017 cruise photosynthesis versus light curves were determined from carbon-14 uptake experiments at 5 depths within the water column. Using these curves the initial slope of the photosynthesis curve, α and the photoinhibition parameter, β, can be calculated. The parameters are determined graphically and only the top 3 (out of 5) sampling depths are used. The top value ('surface') is within 3 m of the surface and the middle one ('middle') at the Chl maximum or pycnocline, and the 'mid-surface' sample from in between these two. The deeper samples are not used as the low primary production rates makes it difficult to determine α and β with accuracy. The values obtained for α are shown in Table 5.1.

Depth	Station N04	Station N18
Surface	0.022	0.031
Mid-surface	0.007	0.019
Middle	0.013	0.011
Mean	0.014	0.021

Table 5.1: Initial slope of photosynthesis vs light curve, α measured at MWRA station N04 and N18 at the 3 top sampling depths. Unit: $(\mathrm{Wm}^{-2})^{-1}$ day^{-1}

The initial slope of the PI-curve, α, is a very sensitive parameter [FASHAM,1990].

Rather than just selecting the mean value a sensitivity study is carried out with α ranging from 0.010 to 0.035 $(\mathrm{Wm}^{-2})^{-1}$ day^{-1}. The α value that gives the most stable phytoplankton and primary production rate was selected. The most stable simulation is obtained for $\alpha = 0.020$ $(\mathrm{Wm}^{-2})^{-1}$ day^{-1}. Higher α values lead to initially high primary production rates that could not be sustained due to depletion of nutrients. Lower values result in too low of a primary production rate to maintain the phytoplankton stock.

Photoinhibition parameter

Based on the photosynthesis versus light curve for station N04 and N18 photoinhibition is present in Massachusetts Bay. The values are determined graphically for the 3 top depths. Table 5.2 shows the values for β at the two stations.

Depth	Station N04	Station N18
Surface	0.0014	0.0008
Mid-surface	0.0006	0.0005
Middle	0.0007	0.0017
Mean	0.0009	0.0010

Table 5.2: Photoinhibition parameter, β measured at MWRA station N04 and N18 at the 3 top sampling depths. Unit: $(\mathrm{Wm}^{-2})^{-1}$ day^{-1}

A value of $\beta = 0.0010$ $(\mathrm{Wm}^{-2})^{-1}$ day^{-1} is used for the simulations. The photoinhibition parameter is not a sensitive parameter. Where phytoplankton concentrations are high the light levels are too low for photoinhibition to occur. Only at noon near the surface are the light levels high enough for photoinhibition.

Reference	α	β
Besiktepe *et al.* [4]	0.03	0.0119
Olivieri and Chavez [36]	0.03	-
Fasham *et al.* [15]	0.025	-
McGillicuddy *et al.* [31]	0.0392	0.0

Table 5.3: Parameters for the PI-curve

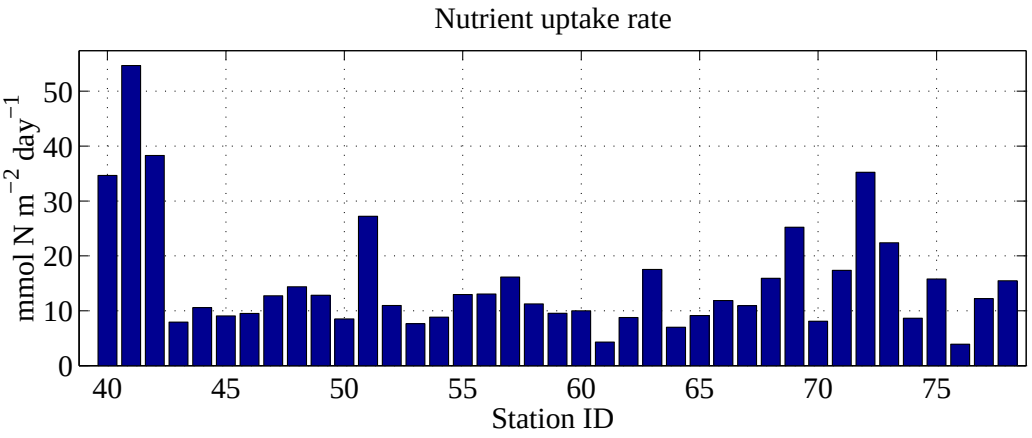

Figure 5.1: Total nitrogen (nitrate and ammonium) uptake (mmol N m^{-2} day^{-1}) in the euphotic zone.

Maximum primary production rate

The choice of maximum production rate is guided by literature values, MWRA data and ASCOT-01 nutrient uptake data. Figure 5.1 shows the areal nutrient uptake rate (mmol N m^{-2} day^{-1}) in the euphotic zone as measured during the ASCOT-01 experiment. These values are obtained by integrating the depth dependent nutrient uptake data over the euphotic zone. The ASCOT-01 nutrient uptake rate was determined in terms of hours. For the conversion to day, which is the unit used in the biological model, it is assumed that the phytoplankton only take up nitrogen during the day when light is available. The mean areal nitrogen uptake rate in the euphotic

zone is 12.9 mmol N m^{-2} day^{-1}.

MWRA collects on regular intervals physical (temperature, salinity), chemical (nutrients, dissolved oxygen) and biological (chlorophyll, production, respiration, phytoplankton and zooplankton species) data for water quality monitoring. One such experiment took place June 19-21,25 2001 (Cruise WF017) where, among other things, primary production was measured at three locations: Station N18 at the outfall, Station F23 in Boston Harbor and Station N04 northeast of the outfall and furthest away from Boston Harbor. The primary production pattern in Boston Harbor during spring-summer differs from the rest of Massachusetts Bay. The ASCOT-01 data is therefore compared with stations N04 and N18 only. The areal production at N04 is 9.9 N m^{-2} day^{-1} and at N18 16.6 N m^{-2} day^{-1}. (The original MWRA primary productivity data is in terms of carbon, the conversion to nitrogen uses the Redfield ratio: 6.7 mol C: 1 mol N.)

The areal production rate divided by the depth of the euphotic zone gives the average nutrient uptake rate in the euphotic zone, 0.56 mmol N m^{-3} day^{-1}. This value corresponds to the term LQP in the biological model. With an average phytoplankton concentration in the euphotic zone of $P = 1.3$ mmol N m^{-3} this results in $LQ = 0.44$ day^{-1}. This value is to be interpreted as the average effective photosynthesis rate in the euphotic zone.

To determine the maximum photosynthesis rate the nutrient (Q) and light (L) limitation terms must be taken into account.

$$LQ = P_m(1 - e^{-\alpha I/P_m})e^{-\beta I/P_m}(Q_1 + Q_2) \tag{5.1}$$

The maximum photosynthesis rate was tuned to reproduce the average photosynthesis rate in in the euphotic zone. The best fit was obtained for $P_m = 3.0$ day^{-1} which is within ranges cited in the literature (see Table 5.4).

Literature values

Reference	P_m
Anderson and Robinson [1]	1.5
Besiktepe *et al.* [4]	1.0
Chai *et al.* [9]	
Olivieri and Chavez [36]	1.9
Fasham and Evans [14]	1.51
	1.17
Fasham *et al.* [15]	2.9
Spitz *et al.* [48]	3.67
McGillicuddy *et al.* [31]	0.66
Wroblewski *et al.* [54]	1.92

Table 5.4: Maximum photosynthesis rate, P_m (day^{-1}), from literature a study.

Figure 5.2 shows the resulting photosynthesis curve for the selected parameters.

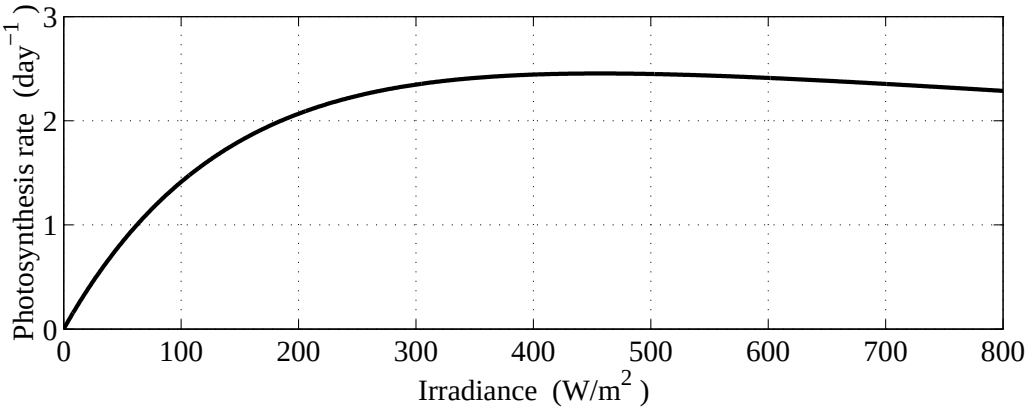

Figure 5.2: Photosynthesis rate versus light curve.

5.1.2 Light attenuation coefficients for water and chlorophyll

In the ocean, light is absorbed by water, chlorophyll, detritus and dissolved organic material. Light is assumed to be exponentially attenuated like in the biological model used in this work. The most simple and common models include only the effects of water and chlorophyll. The light attenuation coefficients, k_w and k_c, determine how quickly light is absorbed with depth. To still account for the fact that detritus and dissolved material absorb light, the light attenuation coefficient for water is slightly redefined to be the absorption of water and all material except for chlorophyll. Light as a function of depth is given by

$$I(z) = I_0 e^{-\left[k_w z + k_c \int_0^z [Chl] dz\right]} \tag{5.2}$$

where I_0 is the light (irridiance) at the surface. Mathematically the euphotic depth, z_e, is defined as the depth at which only 1% of the surface light remains, $I(z_e) = 0.01 \times I_0$ which introduced into Eq. 5.2 gives

$$\ln 100 = k_w z_e + k_c \int_0^{z_e} [Chl] dz \tag{5.3}$$

The light extinction coefficients k_w and k_c can be determined using Eq. 5.3 combined with data for integrated chlorophyl concentration in the euphotic zone and the euphotic depth (from the Secchi depth) both of which are available for the ASCOT-01 experiment.

Equation 5.3 can be rearranged to

$$\frac{\ln 100}{z_e} = k_w + k_c \bar{[Chl]} \tag{5.4}$$

where $[\bar{Chl}]$ is the integrated chlorophyll concentration in the euphotic zone. This is a linear equation for k_w and k_c which can be solved with linear regression.

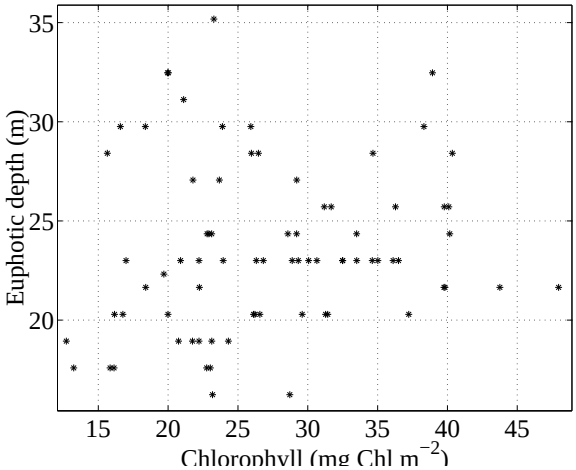

Figure 5.3: Euphotic depth as a function of averaged chlorophyll in the euphotic zone. Chlorophyll data based on fluorescence profiles.

Figure 5.3 shows the euphotic depth against the integrated chlorophyll concentration in the euphotic zone plotted against each. There is substantial scatter in the data. The euphotic depth ranges from 16 to 35 m while the integrated chlorophyll concentration ranges from 13 to 47 mg Chl m^{-3}. The large scattering makes it impossible to use linear regression. Instead a fixed value for k_c is used based on [23]. Typical coastal ocean chlorophyll have a light attenuation of $k_c = 0.016$ m^{-1} (mg Chl m^{-3})$^{-1}$. We use equation 5.3 with mean values for the euphotic depth and integrated chlorophyll and obtain $k_w = 0.18$ m^{-1}.

5.1.3 Nutrient uptake limitation terms

Half-saturation constants

Nitrate uptake by phytoplankton is parameterized using the Menten-Michealis formulation where k_1 and k_2 are the half-saturation constants for nitrate and ammonium uptake respectively. Table 5.5 shows half-saturation constants for a set of biological modeling work.

Reference	k_1	k_2
Besiktepe *et al.* [4]	0.7	0.6
Olivieri and Chavez [36]	0.75	0.5
Fasham *et al.* [15]	0.5	0.5
Spitz *et al.* [48]	0.59	0.04
McGillicuddy *et al.* [31]	0.2	0.05
Wroblewski *et al.* [54]	1.0	1.0

Table 5.5: Half-saturation constant for nitrate k_1 (mmol N m^{-3}) and ammonium k_2 (mmol N m^{-3}).

The half-saturation constant tends to be low for low nutrient conditions and for small phytoplankton. Both of those conditions are satisfied during the summer in Massachusetts Bay. The parameter tuning is therefore carried out for values ranging from 0.1 to 0.6 mmol N m^{-3}. To be able to reproduce the relative high nitrogen uptake rates near the surface the half-saturation constant was set to 0.1 mmol N m^{-3} for both nitrate and ammonium.

5.1.4 Ammonium inhibition parameters

Ammonium inhibition on nitrate uptake is parameterized by an exponential function with the inhibition parameter ψ indicating the strength of this inhibtion [54].

The ASCOT-01 nitrogen uptake data show a clear preference for ammonium. On average the ammonium uptake is approximately 4 times larges than for nitrate. A literature survey shows a large range of values from $\psi = 0.0$ (mmol N m^{-3})$^{-1}$ in Monterey Bay [36] to $\psi = 27.2$ (mmol N m^{-3})$^{-1}$ for the North Atlantic bloom [31] (see Table 5.6). Work at the Bermuda Station "S" uses values around $\psi = 1.5$ (mmol N m^{-3})$^{-1}$ while on the Gulf Stream a value of $\psi = 3.5$ (mmol N m^{-3})$^{-1}$ is used.

Reference	Region	Value	Reference for value
McGillicuddy *et al.* [31]	North Atlantic, spring bloom	27.2	Data
Chai *et al.* [9]	Equatorial Pacific	5.59	Hofmann and Ambler [19]
Anderson *et al.* [2]	The Gulf Stream	3.5	Tuned
Wroblewski [53]	Oregon coast, upwelling	1.462	Walsh and Dugdale [51] (Data)
Fasham *et al.* [15]	Station "S"	1.5 (0.75-3)	Wroblewski [53]
Spitz *et al.* [48]	Bermuda (BATS)	1.48	Tuned
Olivieri and Chavez [36]	Monterey Bay, upwelling	0.0	Kudela [24]

Table 5.6: Ammonium inhibition parameter ψ (mmol N m^{-3})$^{-1}$.

A sensitivity analysis is carried for these values. The ammonium inhibition turns out to have only a small influence on the results. Near the surface where the ammonium concentration is low the nitrate concentration is low as well thus the primary production rates are low regardless of the ammonium inhibition parameter. Deeper in the water column, where nitrate concentrations are high, the light level is low, resulting in low primary production regardless of the ammonium inhibition parameter. Figure 5.4 shows the strength of the ammonium inhibition, $e^{-\psi A}$, for $\psi = 3.5$ mmol N m^{-3})$^{-1}$ which is the value is used for all simulations. Only for ammonium

concentrations below 0.5 mmol N m^3. is there significant nitrate uptake.

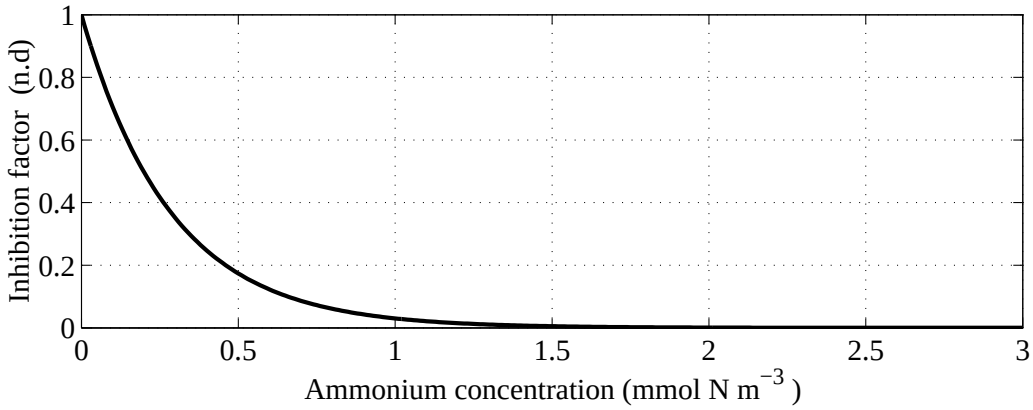

Figure 5.4: Ammonium inhibition parameter as a function ammonium concentration.

5.1.5 Phytoplankton sinking

No measurement of the phytoplankton sinking rate were made during the ASCOT-01 experiment. This parameter is therefore based on literature review only. Typical values cited range from 1.0 m/day for coastal diatoms under nutrient saturated conditions to 0.2-0.4 m/day for dinoflagellates and small diatoms [36]. During the month of June the phytoplankton in Massachusetts Bay are dominated by small species and a sinking rate of 0.3 m/day is used.

5.1.6 Phytoplankton mortality

Phytoplankton mortality rate data are very scarce. For this reason it is not uncommon in ocean biological modeling to not include phytoplankton mortality and instead assume that phytoplankton are lost to grazing only. In these simulations the phytoplankton mortality is not included and $n_3 = 0.0\ ^{-1}$.

5.2 Zooplankton parameters

5.2.1 Zooplankton grazing

Maximum grazing parameter

The zooplankton grazing rate depends on the the size of the zooplankton. Larger zooplankton tend to have a lower grazing rate Table 5.7 shows maximum zooplankton grazing rates for a number of biological modeling studies.

Reference	Rm
Besiktepe *et al.* [4]	0.47
Olivieri and Chavez [36]	0.6
Fasham *et al.* [15]	1.0
Spitz *et al.* [48] (nano/micro)	2.06
Spitz *et al.* [48] (mesozoo)	0.78
McGillicuddy *et al.* [31]	0.69
Wroblewski *et al.* [54]	0.48

Table 5.7: Maximum grazing rate from literature survey.

The maximum zooplankton grazing rate was tuned so that it would balance the nutrient uptake rate and maintain the phytoplankton stock stable. Based on literature surveys the tuning was carried out for maximum grazing rate ranging from from 0.5 to 1 day^{-1}. The lowest value, 0.5 day^{-1}, is used as any higher grazing rate leads to a decline in the phytoplankton stock.

Ivlev constant

The Ivlev constant was left as a free parameter and tuned so that the effective grazing rate, determined by the maximum grazing rate and Ivlev constant, balances

the primary production rate and that the phytoplankton biomass remains stable throughout the simulation. The optimal value is $\lambda = 0.14$ (mmol N m^{-3})$^{-1}$. The phytoplankton concentration at which the grazing rate if half the maximum value is $P = \ln(2)/\lambda = 4.95$ mmol N m^{-3}. Figure 5.5 shows the effective grazing rate for $R_m = 0.5$ day^{-1} and $\lambda = 0.14$ (mmol N m^{-3})$^{-1}$. Based on the chlorophyll data collected during the ASCOT-01 experiment the phytoplankton concentration is below 5 mmol N m^{-3} and the effective grazing rate depends linearly on the phytoplankton concentration.

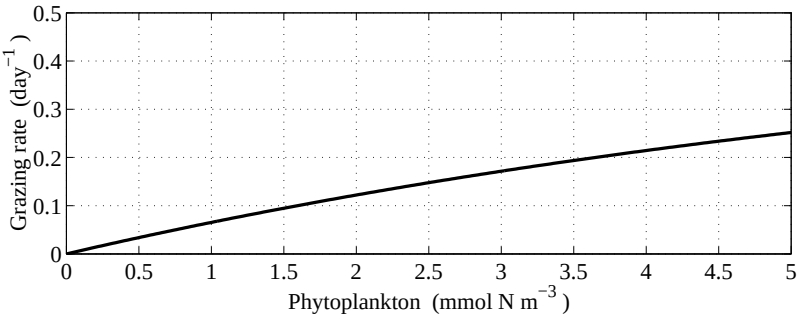

Figure 5.5: Zooplankton grazing rate as a function phytoplankton concentration for $R_m = 0.5$ day^{-1} and $\lambda = 0.14$ (mmol N m^{-3})$^{-1}$.

5.2.2 Zooplankton mortality

Once an estimate of the zooplankton grazing rate has been determined the zooplankton mortality terms were tuned so that the zooplankton biomass is maintained.

5.3 Detritus parameters

The model parameters for detritus, sinking rate and remineralization, are difficult to determine as detritus does not only include detritus but also bacteria and dissolved

organic material. Even for "real" detritus the model parameters can be difficult to determine as detritus is made up of components of varying size and composition.

Detritus sinking rate

Typical sinking rates for (real) detritus range from 1 to 10 m/day. The detrital sinking rate can be difficult to determine even for real detritus as it is made up for components of varying size and sinking rate. In this model detritus includes material that does not sink, a lower detritus sinking velocity of 0.5 m/day is choosen.

Remineralization

The remineralization rate is left as a free parameter and tuned so that remineralization, together with zooplankton losses to ammonium, maintain the ammonium concentration throughout the simulation.

Symbol	Description	Value	Units
P_m	Maximum photosynthesis rate	3.0	day^{-1}
α	Initial slope of photosynthesis vs light curve	0.020	$(\text{Wm}^{-2})^{-1}\ \text{day}^{-1}$
β	Photoinhibition parameter	0.001	$(\text{Wm}^{-2})^{-1}\ \text{day}^{-1}$
k_w	Light attenuation due to water	0.18	m^{-1}
k_c	Light attenuation due to chlorophyll	0.016	$\text{m}^{-1}\ (\text{mg Chl m}^{-3})^{-1}$
ν_P	Phytoplankton sinking rate	0.3	m/day
n_3	Phytoplankton mortality rate	0.0	day^{-1}
k_1	Half-saturation constant for nitrate uptake	0.1	mmol N m^{-3}
k_2	Half-saturation constant for ammonium uptake	0.1	mmol N m^{-3}
ψ	Ammonium inhibition parameter	3.5	$(\text{mmol N m}^{-3})^{-1}$
R_m	Maximum grazing rate	0.50	day^{-1}
λ	Ivlev constant	0.14	$(\text{mmol N m}^{-3})^{-1}$
γ_1	Fraction of grazing losses to ammonium	0.33	n.d.
γ_2	Fraction of grazing losses to detritus	0.33	n.d.
n_1	Linear (natural) zooplankton mortality rate	0.010	day^{-1}
n_2	Quadratic (predation) zooplankton losses	0.010	$(\text{mmol N m}^{-3})^{-1}\text{day}^{-1}$
ϵ_1	Fraction linear zooplankton mortality to detritus	0.30	n.d.
ϵ_2	Fraction quadratic zooplankton mortality to detritus	0.20	n.d
ν_D	Detritus sinking rate	0.5	m/day
k_D	Remineralization rate	0.02	day^{-1}

Table 5.8: Notation and values for biological parameters. n.d. = no dimension

Chapter 6

Data-based physical-biological simulation

The following chapter describes a coupled physical-biological simulation carried out in Massachusetts Bay for June 6-26, 2001. This simulations corresponds to the ASCOT-01 experiment time period. The data collected during the experiment is used for two purposes. A subset of the data, from the first days, is used to initialized the simulation. Throughout the simulation temperature and salinity data is assimilated. The large spatial and temporal coverage of the data allows for almost daily assimilation. The simulation is forced with winds from the National Oceanographic Data Center (NODC) buoy located in northern Massachusetts Bay. The other atmospheric forcing terms are from the Fleet Numerical and Meteorology and Oceanographic Center (FNMOC).

First the wind forcing is analyzed to determine when and where to expect up- and downwelling. On dynamically interesting days the horizontal and vertical velocities

as well as the temperature are analyzed. The purpose is to determine the advective patterns which are later used to determine the redistribution of biological variables during upwelling events.

During June 2001 the winds in Massachusetts Bay were weak with no strong long-lasting upwelling event. The biological variables and processes are integrated over the domain volume to determine as a function of time the total amount of nitrogen in each biological reservoir (mmol N) and the rate at which the biological processes move nitrogen between the different biological reservoirs (mmol N day^{-1}). The volume integration is limited to Massachusetts Bay. The computational grid extends into the western Gulf of Maine but this area is not taken into account in the analysis as there is no biological data outside Massachusetts Bay to verify the results. These timeseries of the volume integrated variables are a first step in analyzing the bulk biological response to wind events.

The analysis focused on the strongest of these weak wind events, that on June 19-20. The biological variables are plotted along a west to east central Massachusetts Bay cross-section.

Figure 6.1 shows the computational grid. The on-shore/off-shore line in central Massachusetts Bay indicates the cross-section along which physical and biological variables are plotted. The line connecting Cape Ann with Cape Cod indicates the region over which the biological variables are integrated. The first day of the simulations is considered dynamical adjustment of the biological variables and is not shown in the figures.

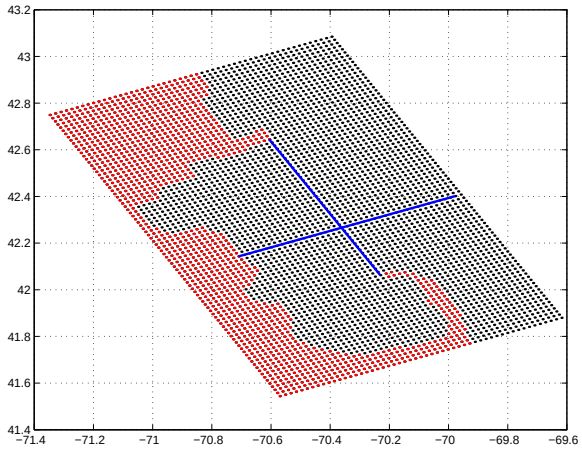

Figure 6.1: Computational grid.

6.1 Description of physical response to wind forcing

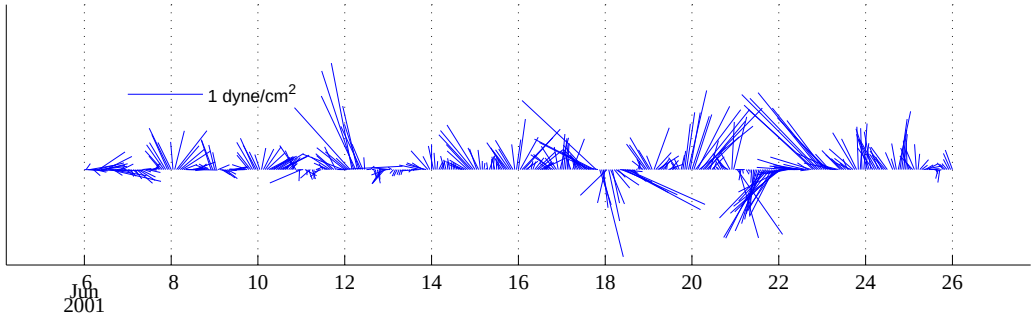

Figure 6.2: Wind vectors measured by the NODC buoy in Massachusetts Bay June 6-26, 2001.

Wind forcing is based on wind data collected by the NODC buoy which is located in northern Massachusetts Bay (at 42.35 N and 70.69 W). This wind is assumed to be representative for all of Massachusetts Bay and is used to force the entire domain. Figure 6.2 shows the wind vectors for the buoy from June 6 to 26, 2001.

The sticklines point away from the baseline in the compass direction towards which the wind is blowing. For example, on June 12 we have southeasterly winds. In the text the standard convention of referring to the winds according to the direction from which they originate is used.

During the time period June 6 to 26, 2001 the winds are fairly weak, occasionally reaching a magnitude above 1.0 dyn/cm^2. For most of June the winds are southerly or southeasterly. The second half of the time period is more dynamic, with 4 successive wind events. In Massachusetts Bay, southerly winds give rise to upwelling along the mainland coast. Two of these wind events have strong southerly components and give rise to upwelling and two have strong northerly components giving rise to downwelling. A description of the wind forcing and the physical (velocities and temperature) response follows below.

First 6 days - weak winds

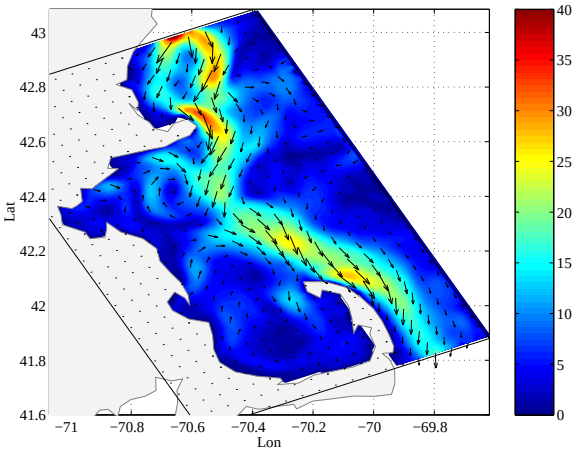

Figure 6.3: Horizontal velocity (cm/s) at 2 m in Massachusetts Bay on June 10 (noon).

During the first 6 days, June 6 to 11, the winds are predominantly southerly and weak. The southerly component of the wind, the one that gives rise to upwelling along the mainland coast of Massachusetts Bay, remains below 0.5 dyn/cm^2. The surface circulation is dominated by a western Gulf of Maine current that does not enter Massachusetts Bay (see Figure 6.3). The current comes in from the north and flows southward along the New Hampshire-Massachusetts coast with an average speed of 23 cm/s. It flows around Cape Ann and turns into Massachusetts Bay without reaching the coast. The coastal current continues southward across Stellwagen Bank and along the eastern (oceanic) coast of Cape Cod. Inside Massachusetts Bay the currents are on average very weak (< 10 cm/s). Two features can be identified inside Massachusetts Bay. The first feature is a clockwise gyre in northern Massachusetts Bay, which is generally present when the winds are weak. The second is is a "half" clockwise gyre in central Massachusetts Bay that brings coastal water into Western Gulf of Maine.

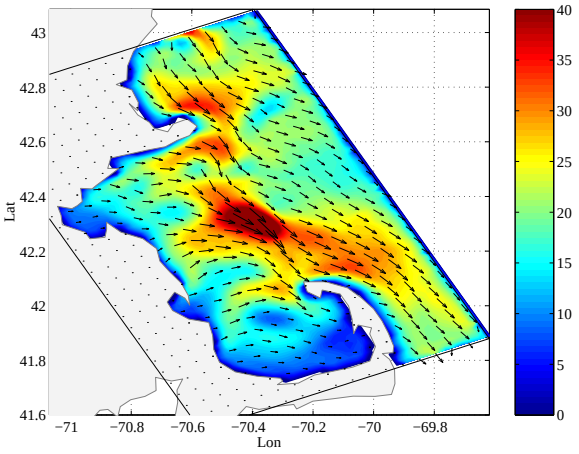

Figure 6.4: Horizontal velocity (cm/s) at 2 m in Massachusetts Bay on June 8.

Despite the weak winds there is some variability in the currents in response to small variations in wind. For example, on June 8 the wind, which is southerly, reaches 0.5 dyn/cm^2 for half a day and we immediately observe a stronger surface current (see Figure 6.4). Near the coast the velocities are off-shore and become southeastward away from the coast. Most of Massachusetts Bay has currents above 20 cm/s with top values of 40 cm/s. There are few traces left of the previously described coastal current.

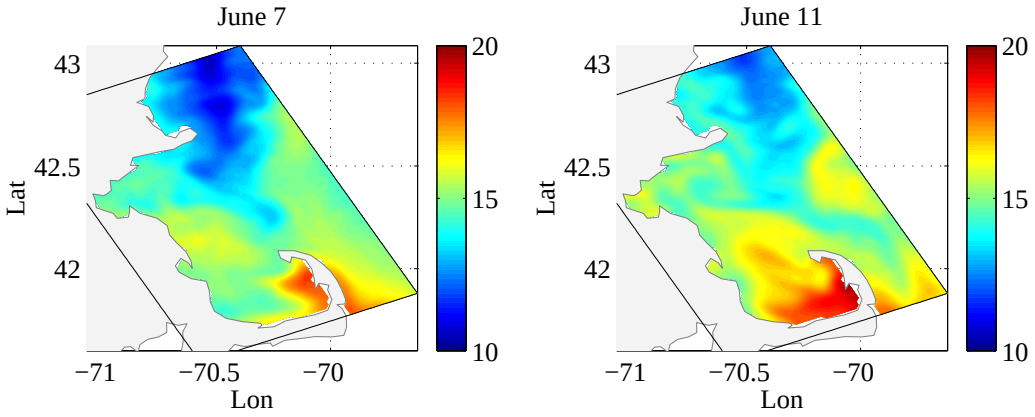

Figure 6.5: Temperature (°C) at 2 m in Massachusetts Bay on June 7 (right) and 11 (left).

During the first days of the simulation the circulation does not play a major role in the evolution of the temperature of Massachusetts Bay. Figure 6.5 shows the temperature at 2 m in Massachusetts Bay on June 7 and June 11. During this time period there is a positive net heat flux leading to warming of the surface water. This is especially noticeable in the shallow regions of Cape Cod Bay. Here the water warms, reaching > 20°C. It is also advected northward into central Massachusetts Bay where over a period of 4 days the surface temperature increases from 15°C to 17°C.

June 12 - weak wind event

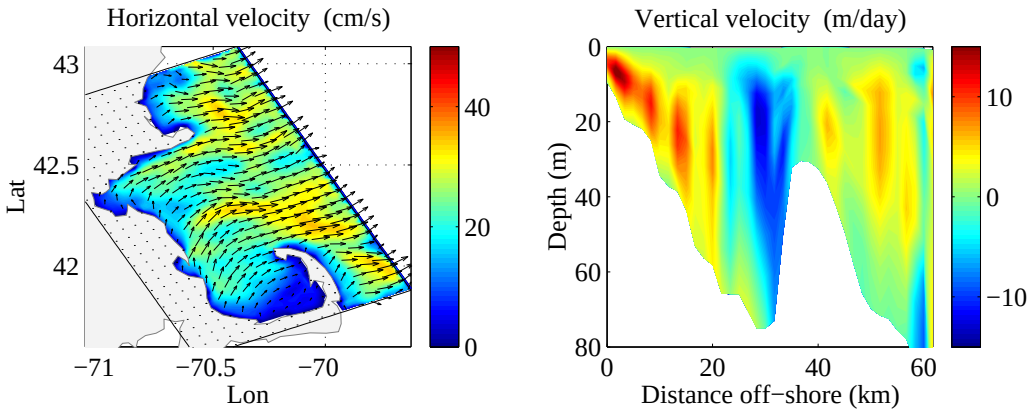

Figure 6.6: The left panel show the horizontal velocity (cm/s) at 2 m in Massachusetts Bay on June 12 (6 am). The right panel shows the vertical velocity (m/day) across central Massachusetts Bay on the same day.

On June 12 the winds are stronger. For half a day there is a southeasterly wind with a peak magnitude of 1.4 dyn/cm^2. Figure 6.6 shows the surface currents (cm/s) at 2 m and the vertical velocity (m/day) across central Massachusetts Bay. During the peak of the wind event the surface currents are mostly off-shore in Massachusetts Bay and reach values as high as 30 cm/s. Along the coast the velocities are northeastward.

The region of high positive vertical velocities extend 20 km off shore. The highest values are found close to shore (10 km) within the top 20 m. Here the vertical velocities are 5 to 10 m/day with peak values of 15 m/day. Further off-shore the vertical velocities are 5 to 8 m/day, which, because of their brevity, have no lasting major effect on the distribution of nutrients or biomass in the water column. In Stellwagen Basin we have strong downwelling with values of about 10 m/day.

Although the peak magnitude of this wind event is moderately strong, the resulting upwelling is weak due to the short duration (0.5 day) of the strong winds. This is

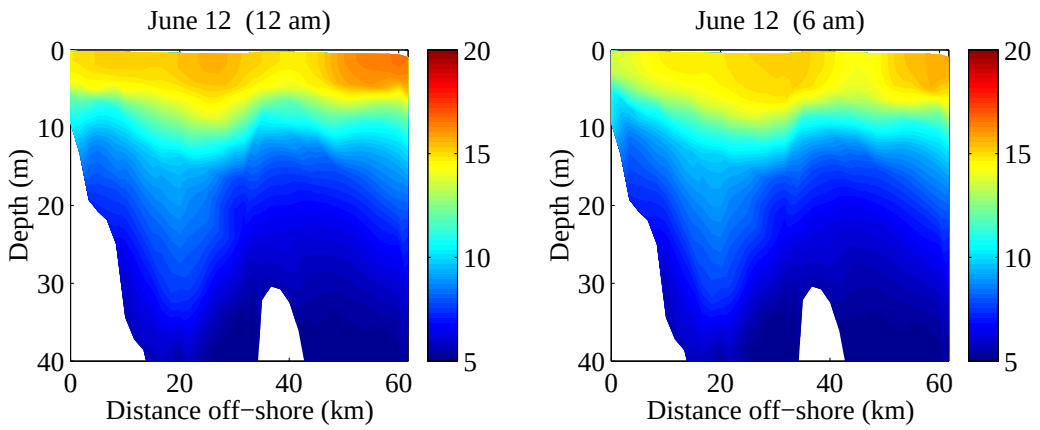

Figure 6.7: Temperature (°C) cross-section in central Massachusetts Bay on June 12 at midnight (left) and 6 am (right).

evident when looking a temperature cross section. Figure 6.7 shows the temperature along central Massachusetts Bay right before the start of the wind event (June 12, 12 am) and at the peak (June 12, 6 am). As seen from Figure 6.7 only water in the top 10 m closest (10 km) to the coast is upwelled. Below 10 m there is no sign of upwelling. The water is upwelled in total 5 m during the event. At the surface the off-shore currents advect cold water 15 km away from the coast and the temperature at the coast decreases from 15°C to 13.5°C.

June 15-17 - three wind events

Starting June 15 there are 3 consecutive wind events with a southerly wind component of varying magnitudes. Each event lasts a day or slightly less and the maximum magnitude ranges from 0.5 dyn/cm^2 to 0.7 dyn/cm^2. None of these events are, in themselves, strong. Thus, although independently they would not give rise to pronounced upwelling, their integrated effect over time does.

Due to the variation in wind strength and duration the velocities vary considerably

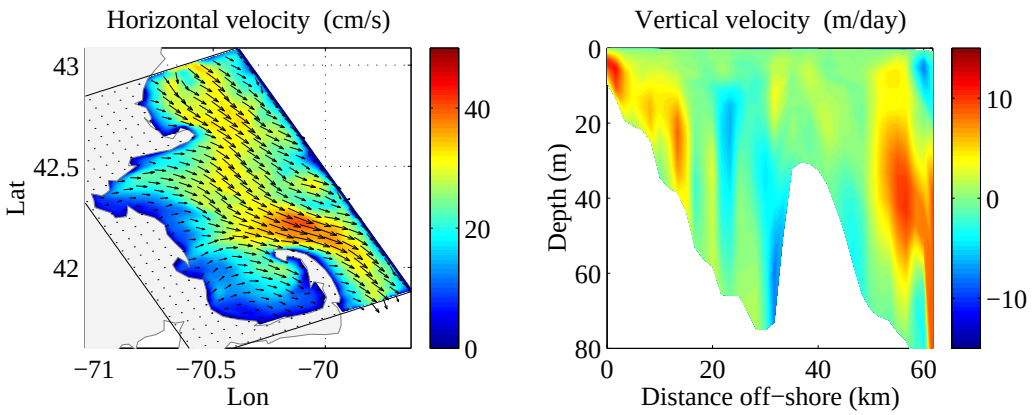

Figure 6.8: The left panel shows the total velocity (cm/s) at 2 m in Massachusetts Bay on June 16. The right panel shows the vertical velocity (m/day) along a cross-section in central Massachusetts Bay on the same date.

between June 15 and 17. Figure 6.8 shows the velocity at 2 m and a cross-section of the vertical velocity along central Massachusetts Bay on June 16 which is when we have the strongest response in the velocity fields. The general aspect of the surface current is very similar to the coastal current observed at the beginning of the simulation when the winds were weak. On June 16 the current is the strongest in eastern Massachusetts Bay with values above 20 cm/s and peak values of 35 cm/s. The general direction of the flow is southeastward. The surface velocity is off-shore in most of Massachusetts Bay except along the coast where the flow is along-shore (but very weak) and in northern Cape Cod Bay where we see the previously described "half" clockwise gyre.

This is a weak but longer-lasting upwelling event. On June 16 to 17 we have a clear upwelling signal in the temperature. Figure 6.9 shows the temperature along a cross-section in central Massachusetts Bay before the start of the wind events (June 14, 6 pm) and at the peak on June 17 at 6 am. Only water within 3 to 5 km off the

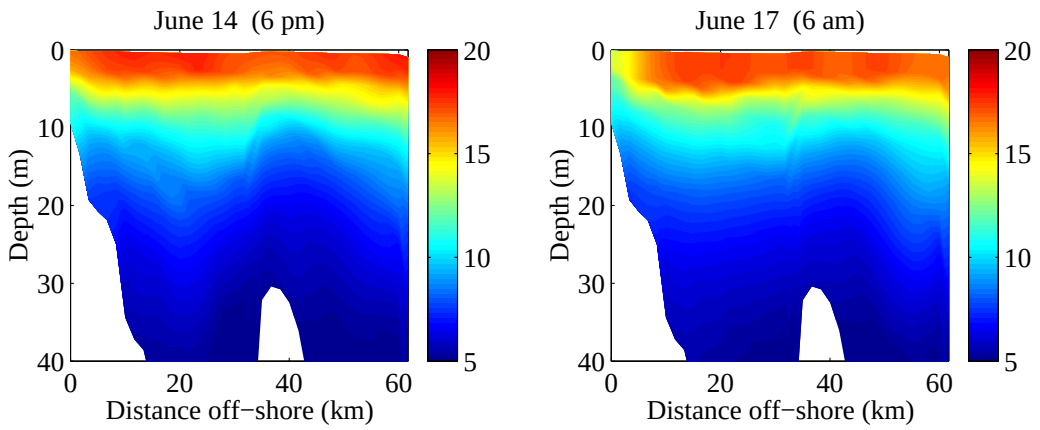

Figure 6.9: Temperature (°C) cross-section in central Massachusetts Bay on June 14 at 6 pm (left) and June 17 at 6 am (right).

coast and in the top 12 m is affected by the wind. The water is upwelled about 5 m over the course of the wind events. The strongest upwelling happens in the top 5 m of the water column; this is the water which reaches the surface. At the surface the water has been advected 8-10 km off-shore. Along the coast the temperature has decreased from 16°C to 13.5°C.

June 18 - short downwelling event

On June 18 there is a brief northerly/northwesterly wind event with a peak magnitude of 1.2 dyn/cm^2 which results in an on-shore flow and downwelling along the coast. Figure 6.10 shows the temperature along central Massachusetts Bay right before the start of the wind event (June 18 at 12 am) and at the peak of the event. Notice that at the start of this event we still have cold temperatures along the coast left from the previous upwelling event. The horizontal velocities are large and on-shore in the entire domain, accumulating warm water near the coast. During this brief wind event the surface water is downwelled 10 m. See, for example, the 14°C

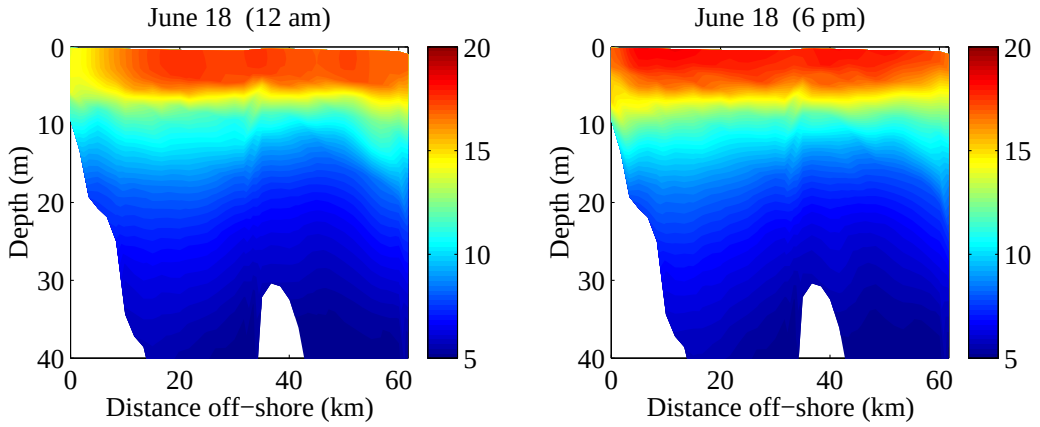

Figure 6.10: Temperature (°C) cross-section in central Massachusetts Bay on June 18 (6 pm).

isotherm which is at the surface near the coast at the start of the event and ends up 10 m below the surface.

June 19-20 - upwelling event

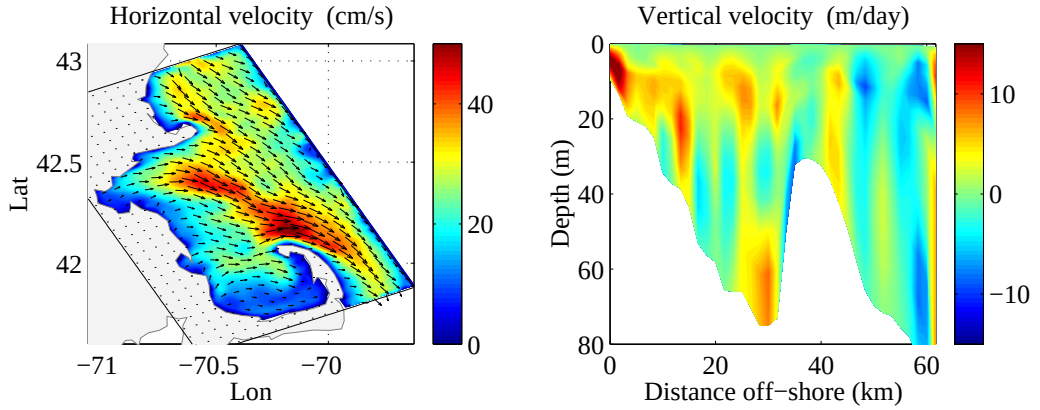

Figure 6.11: The left panel shows the total velocity (cm/s) at 2 m in Massachusetts Bay on June 20. The right panel shows the vertical velocity (m/day) along a cross-section in central Massachusetts Bay on the same date.

On June 19 the winds are southerly again and have a magnitude less than 0.5 dyn/cm^2. This is followed by a stronger south/southwesterly wind event with a

maximum magnitude of 1.0 dyn/cm^2 on June 20. The strength and duration of this wind event results in the strongest upwelling signal so far. Figure 6.11 shows the velocity patterns on June 20. The strongest velocities are observed on June 20 (12 am). Near the coast the surface velocity are off-shore and further away from the coast they are southeastward with speeds as high as 53 cm/s. The high vertical velocities, above 8 m/day, are confined to the top 15 m within 5 km of the coast. Vertical velocities are above 5 m/day all the way to 15 km off-shore.

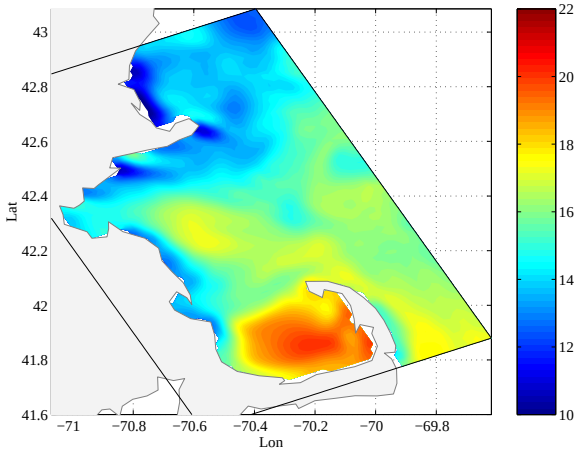

Figure 6.12: Temperature (°C) at 2 m in Massachusetts Bay on June 20 (6 am).

There is a clear upwelling signal in the surface temperature (see Figure 6.12). There is a band of cold temperatures all the way along the coast from Scituate to Nanomet. In this region the temperatures decrease from 16°C to 13°C.

Although this is the strongest upwelling event to date the effect is still fairly weak. Only water is the top 12 to 15 m is upwelled. Below this depth there is no sign of the wind event. The water is upwelling a total distance of about 8 m. The coastal water at the surface is advected about 12 km off-shore.

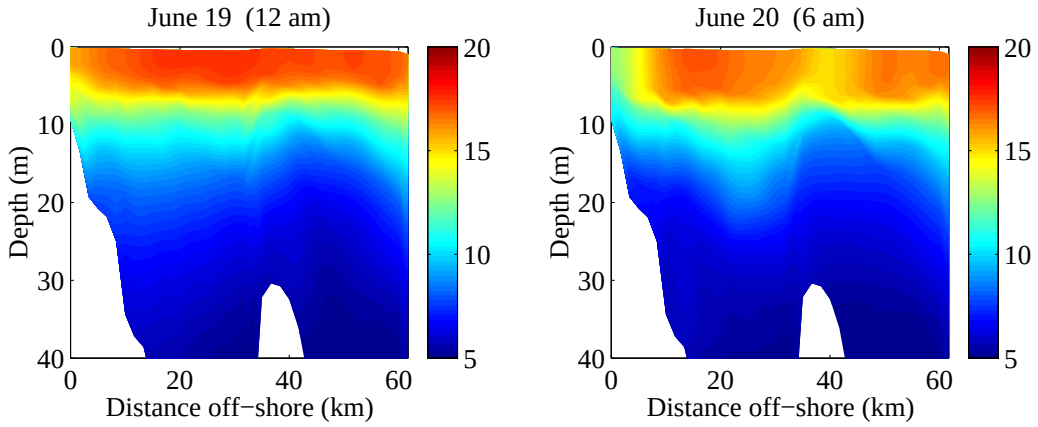

Figure 6.13: Temperature (°C) cross-section in central Massachusetts Bay on June 19, 2001 at 12 am (left), and June 20 at 6 am (right).

June 21 - short downwelling event

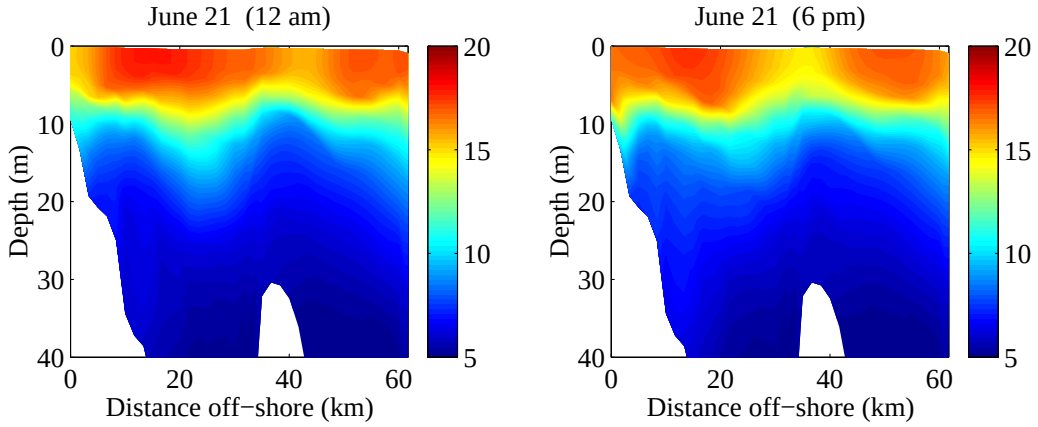

Figure 6.14: Temperature (°C) cross-section in central Massachusetts Bay on June 21 at 12 am (left) and 6 pm (right).

The winds quickly changes direction on June 21 with northeasterly winds with a magnitude of 0.9 dyn/cm^2. During the peak of this event the currents are southward bringing Gulf of Maine water into Massachusetts Bay. This downwelling event erases all traces of the upwelling event from the previous day. It brings warm water closer to shore as seen in Figure 6.14. During this event the coastal surface water is downwelled

about 8 m.

June 23-24 - upwelling event

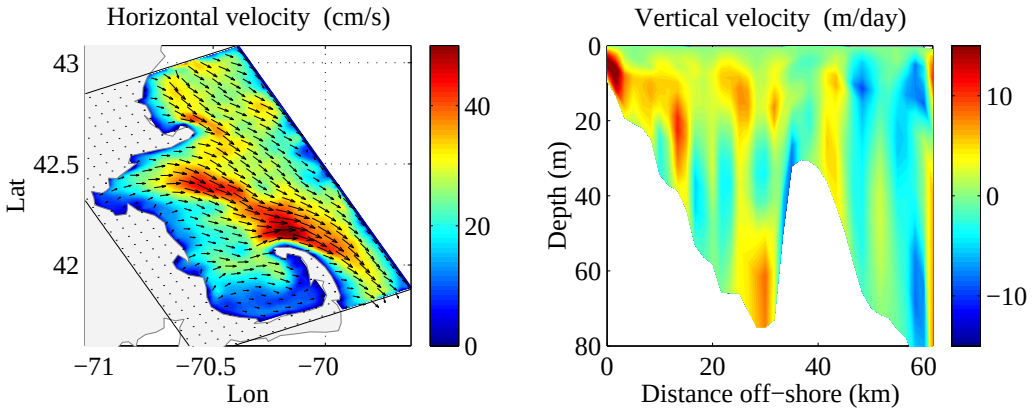

Figure 6.15: The left panel shows the total velocity (cm/s) at 2 m in Massachusetts Bay on June 23. The right panel shows the vertical velocity (m/day) along a cross-section in central Massachusetts Bay on the same date.

The final phase of the simulation is characterized by an upwelling event. On June 23 there is a short southeasterly wind event which exceeds 1 dyn/cm^2. For the following 2 days the wind has a southerly component of 0.5 dyn/cm^2. During this event the velocities along the coast are northward and off-shore (see Figure 6.15). The horizontal velocities are between 20 cm/s to 40 cm/s in Massachusetts Bay. The vertical velocities near the coast are between 5 to 10 m/day. These are not particularly high values but they are maintained (at varying magnitudes) for 2 days, which serves to enhance the upwelling event of June 23.

For three days there is a band of cold temperature along the coast from Boston Harbor to Barnstable (Cape Cod). The cold water extends further off-shore (15 km) than during any of the prior upwelling events (see Figure 6.16). The temperature

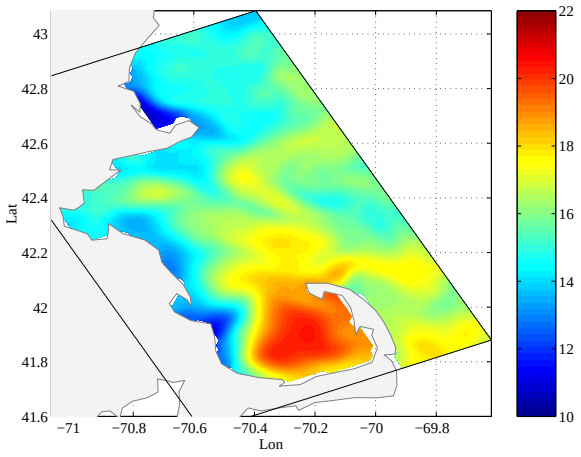

Figure 6.16: Temperature (°C) at 2 m in Massachusetts Bay on June 25 (6 am).

along the coast is drops to 11°C.

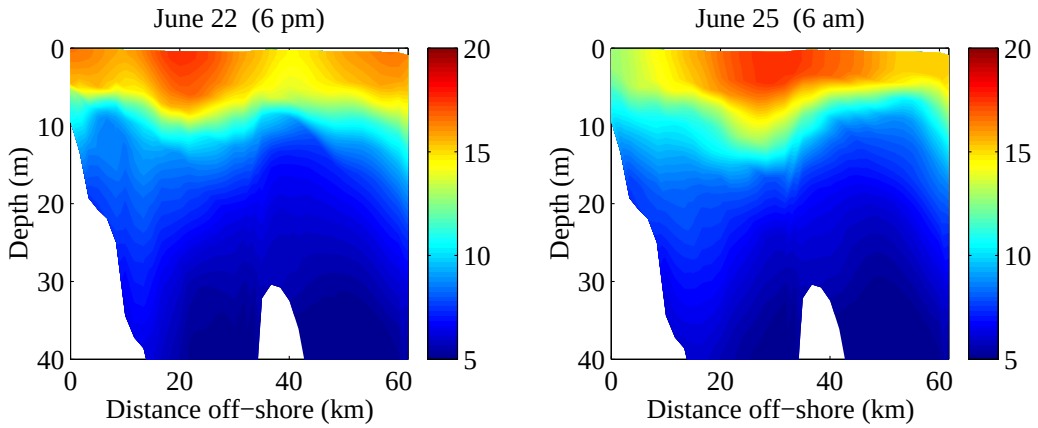

Figure 6.17: Temperature (°C) cross-section in central Massachusetts Bay on June 25 (6 pm), 2001.

During this event water as deep as 15 m is affected by the upwelling. Water that was initially at 5 m reaches the surface. The long duration of the wind event, 2.5 days, allows the surface water to be advected 15-20 km off-shore. This is the furthest distance of all the wind events observed directly in this series.

6.2 Biological response to physics and atmospheric forcing

This section describes the evolution of the biological variables during June 7 to 26, 2001. The emphasis of the analysis is on the biological response to the wind events. We start by calculating the total amount (in mmol N) of nitrate, ammonium, phytoplankton, zooplankton and detritus in the euphotic zone in Massachusetts Bay as a function of time. This analysis gives us a first estimate of the dynamics of the biology.

The vertical distribution of the biological variables along a cross-section in central Massachusetts Bay right before and at the peak of an upwelling event is examined for a more detailed understanding of how the biological variables respond to the wind events. Finally we look at the flow of nitrogen between the biological reservoirs due to biological processes in order to gain an understanding of the relative importance of these.

Volume intergrated biological variables in the euphotic zone

A first overview of the dynamics of the biology is obtained by converting the 3-dimensional biological fields to zero-dimensional box models. This means that we look at the total amount of nutrients and plankton in the euphotic zone as a function of time. The biological variables are expressed in terms of nitrogen concentration (mmol N m^{-3}). By integrating, at each time step, the concentration over the euphotic zone volume we obtain the amount of nitrogen for each biological reservoir as a function

of time. We use a fixed value for the euphotic depth, 23.5 m, which corresponds to the average euphotic depth as measured with a Secchi disk during the ASCOT-01 experiment. The integration of the biological variables is limited to Massachusetts Bay.

Figure 6.18 shows the volume integration of nitrate, ammonium, phytoplankton and Figure 6.19 the volume integration of zooplankton, detritus and total nitrogen as a function of time for June 7 to 26, 2001. Total nitrogen is the sum of nitrogen in all the biological variables.

The nitrate amount in the euphotic zone remains stable throughout the the simulation with an average value of $2.83 \cdot 10^{10}$ mmol N. Towards the end of the simulation there is a small increase of nitrate in the euphotic zone. As the nitrate ADR equation has no biological sources this increase is due to advection (and mixing). The increase of nitrate coincides with the wind events and a small amount of nitrate is brought into the euphotic zone during the June 19-20 and June 23-24 upwelling events.

The ammonium amount also remains stable throughout the simulation. The average amount of ammonium in the euphotic zone is $5.43 \cdot 10^{10}$ mmol N. There are daily variations in the ammonium amount. During the day-time the uptake of ammonium by phytoplankton is the dominant nitrogen uptake term and there is a net loss of ammonium. During the night, when no light is available for photosynthesis, recycling of zooplankton and detritus nitrogen exceeds uptake and thus there is a net gain of ammonium. According to the ammonium data collected during the ASCOT-01 experiment, the ammonium concentration remains low and stable in the euphotic zone during the month of June. We therefore expect the biological processes, ammonium

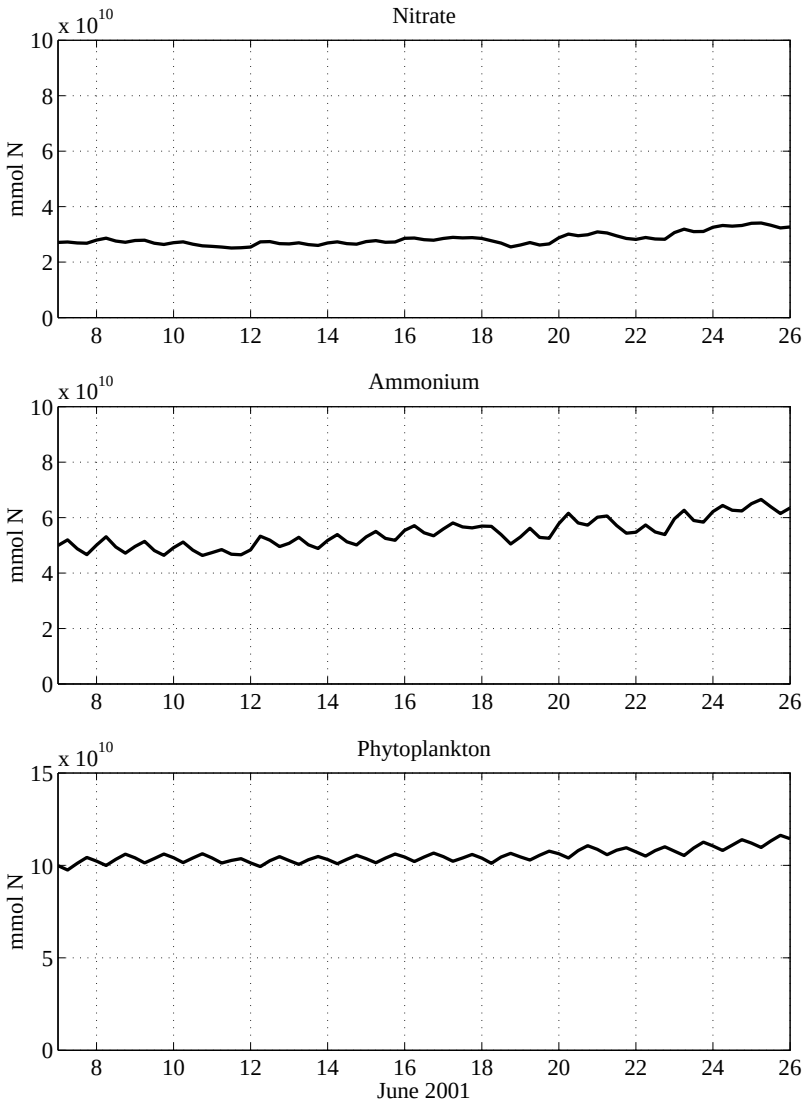

Figure 6.18: Total nitrogen in the euphotic zone in Massachusetts Bay for nitrate (top), ammonium (middle) and phytoplankton (bottom) for June 7-26, 2001. The units are mmol N.

uptake by phytoplankton and recycling, to approximately balance each other over the course of a day. During the 6 last days of the simulation, when wind events occur, there is a small increase of ammonium in the aphotic zone. The largest gradients coincide with the time of the upwelling events.

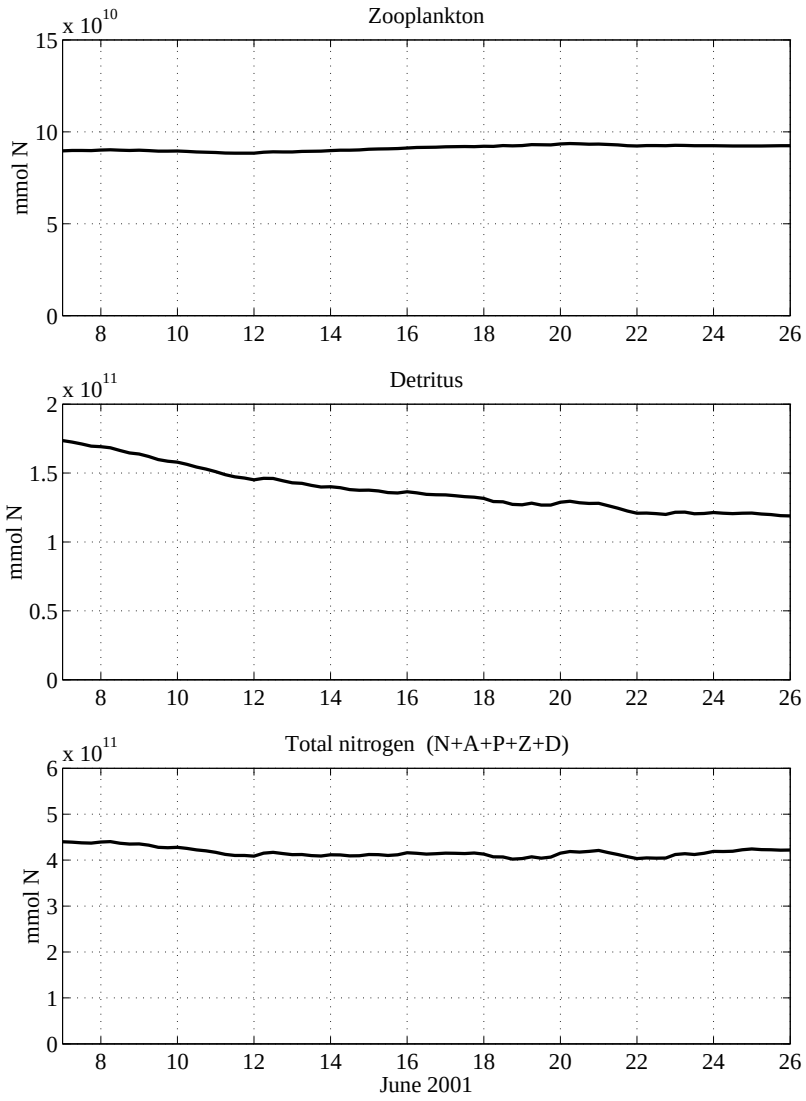

Figure 6.19: Total nitrogen in the euphotic zone in Massachusetts Bay for zooplankton (top), detritus (middle) and total nitrogen (bottom) for June 7-26, 2001. The units are mmol N.

The phytoplankton stock in the euphotic zone remains stable at about $10.5 \cdot 10^{10}$ mmol N throughout the simulation. As with the ammonium there are daily fluctuations. The phytoplankton stock is balanced primarily by primary production and losses due to grazing. During the day photosynthesis is the dominant process,

while during the night losses due to grazing dominate. This gives rise to the daily variations as observed in Figure 6.18. During the last 6 days of the simulation there is a small increase in phytoplankton, which corresponds to an increase in primary production (see below) due to nitrate and ammonium being brought into the euphotic zone during the upwelling events.

The zooplankton stock remains fairly stable at $9.11 \cdot 10^{10}$ mmol N. Zooplankton growth is balanced by mortality. The zooplankton grazing process responds more slowly, so the increase in available phytoplankton is not as readily reflected in zooplankton biomass.

The detritus stock decreases during the simulation due to slow steady sinking out of the euphotic zone. The June 19-20 wind event does not have a significant effect on the detrial concentration in the euphotic zone. There is a small increase due to detritus being brought into the euphotic zone.

The integration of primary production over the entire euphotic zone in Massachusetts Bay gives a total amount of nitrogen being assimilated by the phytoplankton per day. Figure 6.20 shows the volume integrated primary production rate at noon which corresponds to the maximum daily rate. Throughout the simulation the maximum primary production ranges between 1.9 mmol N m^{-3} day^{-1} and 3.0 mmol N m^{-3} day^{-1}. The lowest value is observed on June 11, which corresponds to a cloudy day with low irradiance levels. During the strongest wind events, June 19-20 and June 23-24 there is an increase in primary production. As seen above a small amount of nitrate and ammonium enters the euphotic zone from below during the wind event. The high primary production rates during the upwelling events is not

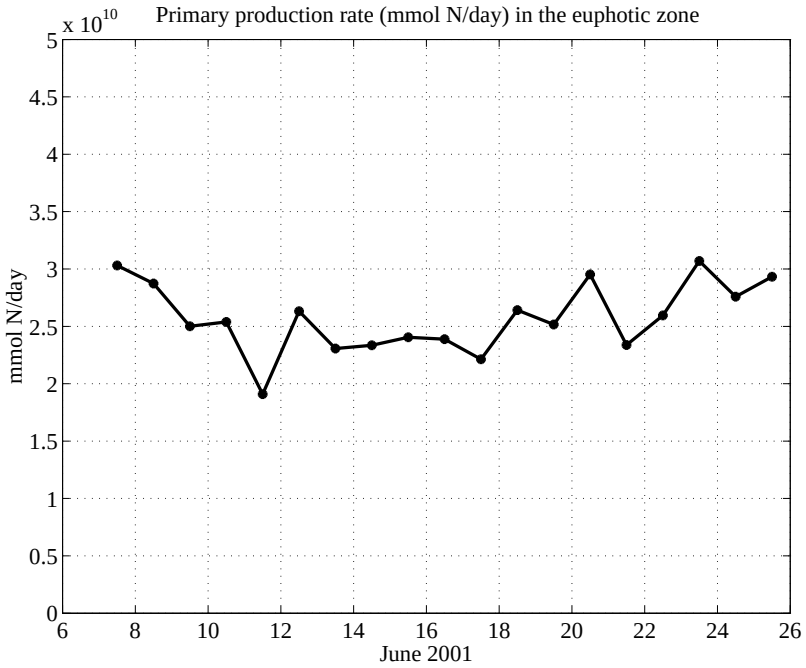

Figure 6.20: Total primary production rate (mmol N/day) in the euphotic zone in Massachusetts Bay for June 7-25, 2001. Only noon values are shown.

necessarily due only to increased nutrient concentration in the euphotic zone. During the upwelling events phytoplankton and nutrient are advected upward towards the surface. With greater light availability the phytoplankton can more efficiently utilize the available nitrate and ammonium.

Biological variables along a central Massachusetts Bay cross-section

To better understand the response of the biological variables to the wind events we analyze the changes in vertical distribution of the biological variables during upwelling events. The strong June 19-20 wind event is selected for this demonstration. As we see in temperature the upwelling occurs mainly within the euphotic zone. The plots below show the biological variables along cross-sections in central Massachusetts Bay

on June 19 at 12 am, just prior to the start of the wind event, and on June 20 (6 am), which is the peak of the event.

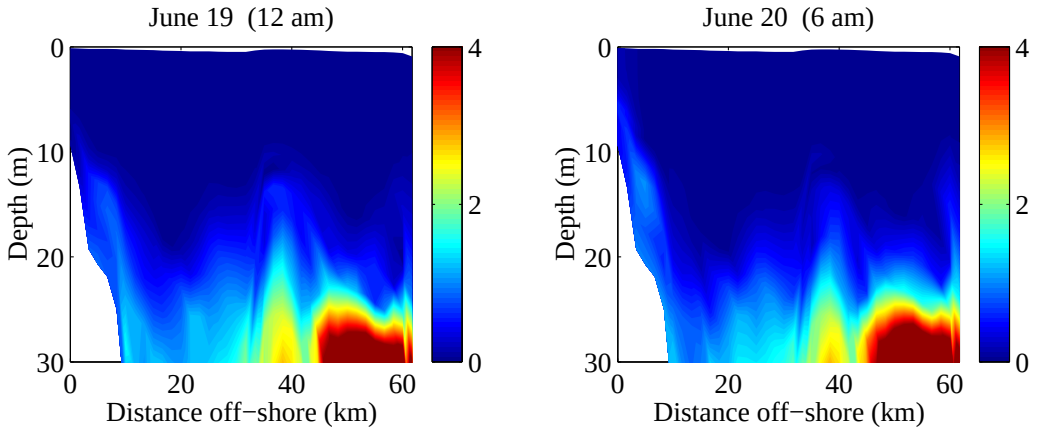

Figure 6.21: Nitrate (mmol N m^{-3}) along central Massachusetts Bay during upwelling event of June 19-20.

Nitrate is depleted (see Figure 6.21) in the near-surface water, which is typical for summer conditions. In the top 10 m the nitrate concentration is below 1 mmol N m^{-3}. As the nitrate concentrations are low in most of the euphotic zone the upwelling effect is barely noticeable. However, a small amount of nitrate is brought in from below the euphotic zone. Due to the preferential uptake of ammonium this upwelled nitrate plays a minor role for primary production during the upwelling event. This new nitrate will be taken up when enough of the upwelled ammonium has been consumed by the phytoplankton to reduce the inhibition effect of ammonium on nitrate uptake.

During the summer the ammonium concentration is also low in the upper euphotic zone. In the top 10 m concentrations are < 0.2 mmol N m^{-3}. As seen earlier, the upwelling event affects mainly the water within the euphotic zone. Near the surface the increase in ammonium concentration is small as the water that reaches the surface originates from a depth with low ammonium concentrations. The depth

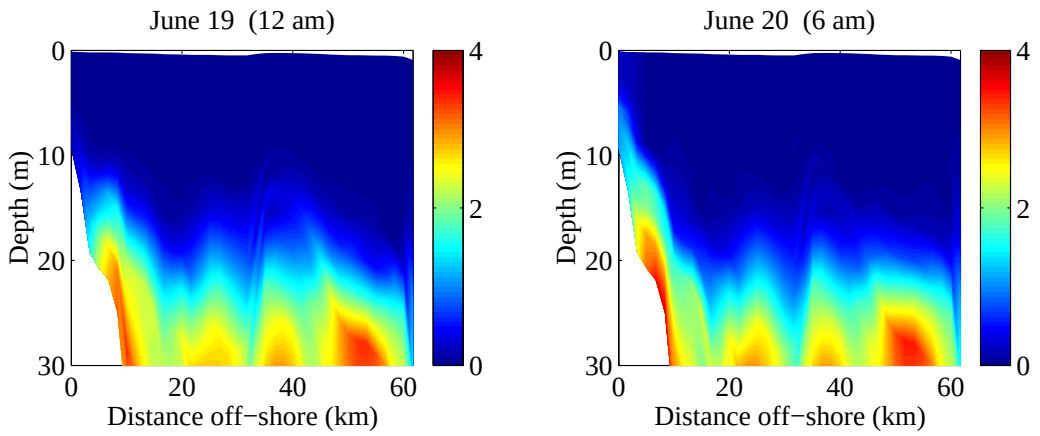

Figure 6.22: Ammonium (mmol N m^{-3}) along central Massachusetts Bay during upwelling event of June 19-20.

of the strongest upwelling signal is the lower portion of the euphotic zone where ammonium concentrations are elevated twofold.

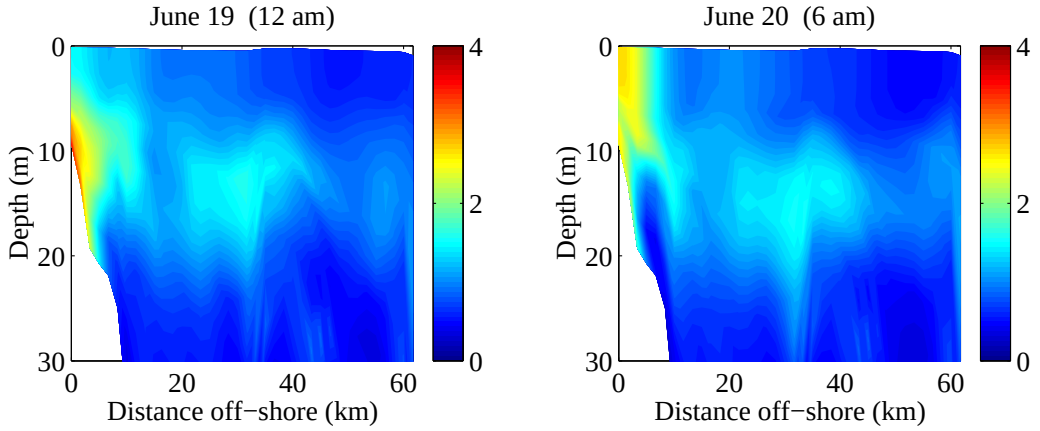

Figure 6.23: Phytoplankton (mmol N m^{-3}) along central Massachusetts Bay during upwelling event of June 19-20.

The phytoplankton distribution is characterized by a subsurface maximum. In Massachusetts Bay this occurs around 10 to 15 m with the maximum value ranging between 2.0 and 3.0 mmol N m^{-3}. During the upwelling event the phytoplankton near the coast are advected upward towards the surface. At the peak of the wind

event the phytoplankton distribution has no subsurface maximum and the highest phytoplankton concentration is at the surface.

Prior to the upwelling event the phytoplankton concentration is low in the lower portion of the euphotic zone where the nutrient concentrations are elevated. Although modest upwelling transports nutrients upwards, phytoplankton are similarly displaced upward, resulting in little initial capability for phytoplankton response to this enrichment of nutrients in the lower portion of the euphotic zone.

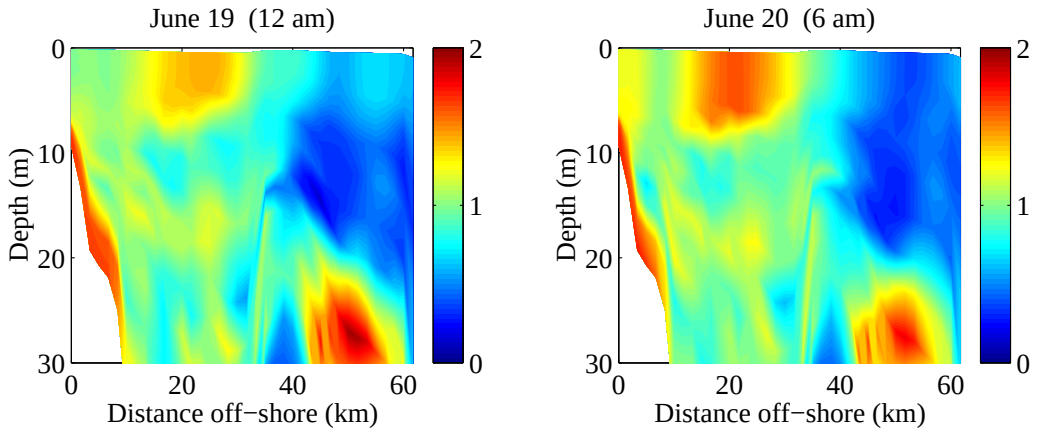

Figure 6.24: Zooplankton (mmol N m^{-3}) along central Massachusetts Bay during upwelling event of June 19-20.

Figure 6.24 shows the zooplankton concentration before and at the peak of the wind event. The zooplankton biomass response to the wind event is similar to the phytoplankton. Along the coast the zooplankton are advected toward the surface which results in an increase of zooplankton concentration from about 1.0 to 1.3 1.0 mmol N m^{-3}. There is also an increase at the surface away from the coast.

The detritus distribution before and at the peak of the wind event is shown in Figure 6.25. The effects of the wind event on the detritus is small. Near the surface by the coast there is an increase and the high values along the bottom extend a few

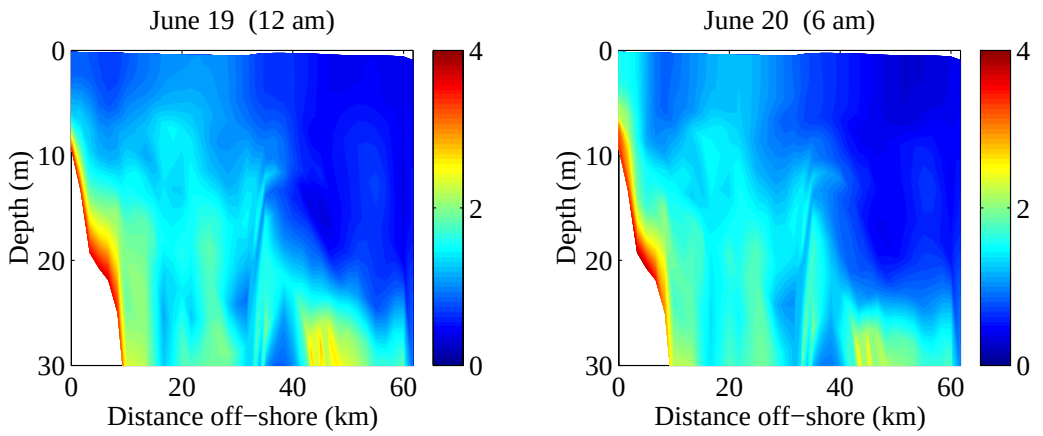

Figure 6.25: Detritus (mmol N m^{-3}) along central Massachusetts Bay during upwelling event of June 19-20.

meters higher up. As detrital processes occur on a longer time scale these changes have no significant near-term impact on the biological processes.

Figure 6.26 shows a timeseries of the primary production rate along central Massachusetts Bay before, during and after the wind event. The peak of the wind event occurs on June 20 at 6 am when the light levels are too low for high primary production rates. The maximum primary production rate is found at the surface by the coast reflecting the distribution of the phytoplankton. On June 20 at noon the phytoplankton have been brought back deeper in the water column where they can utilized the high nutrient concentrations.

6.2.1 Flux of nitrogen due to biological processes

Figure 6.27 shows the flow of nitrogen due to biological processes in the euphotic zone over the course of the simulation, June 7 to 26, 2001. The numbers in the figure indicates the amount of nitrogen ($\cdot 10^{10}$ mmol N) that moves from one biological reser-

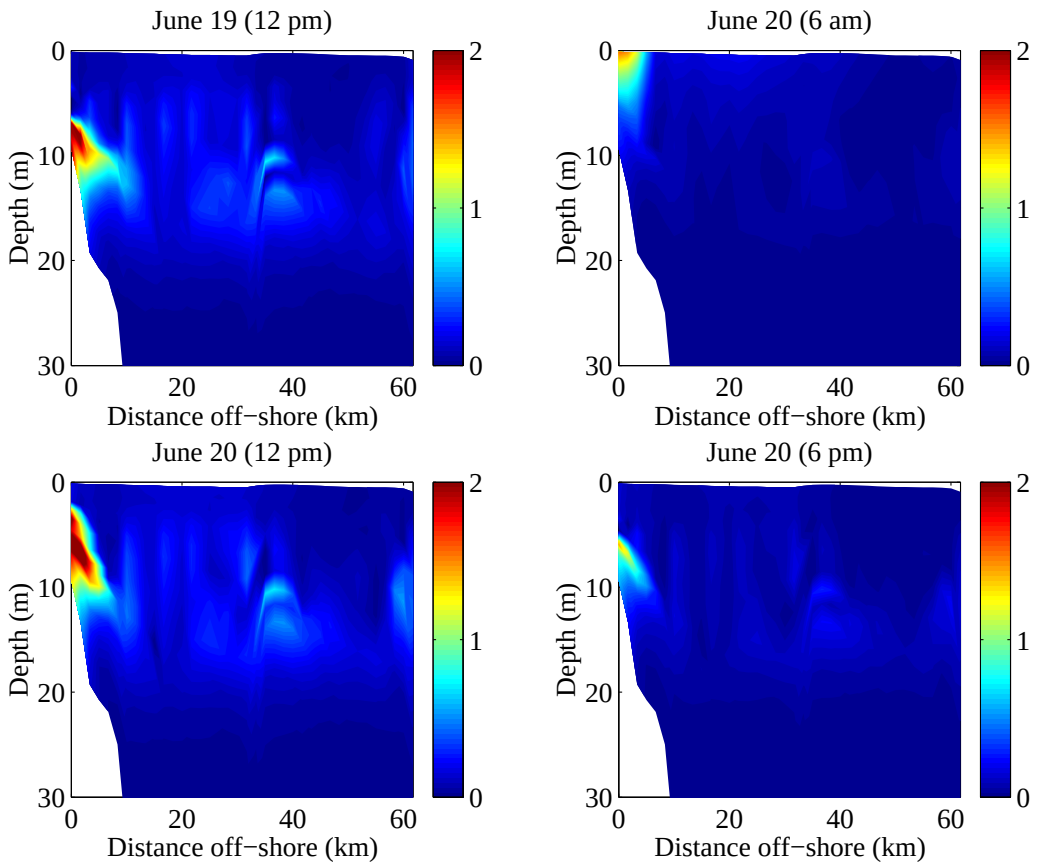

Figure 6.26: Primary production (mmol N m^{-3} day^{-1}) along central Massachusetts Bay Bay during the upwelling event of June 19-20

voir to another in the euphotic zone according to the previously described biological model. $23.4 \cdot 10^{10}$ mmol N is assimilated by phytoplankton. Ammonium assimilation, $18.9 \cdot 10^{10}$ mmol N, is the dominant source of nitrogenous utilization. The computed average f-ratio of 0.19 (= 4.45/23.4) is within the expected range for stratified coastal waters.

Euphotic zone of phytoplankton losses are due to zooplankton grazing and sinking. The dominant term is grazing, which accounts for $18.3 \cdot 10^{10}$ mmol N.

Zooplankton biological sources and sinks are almost balanced. The total zoo-

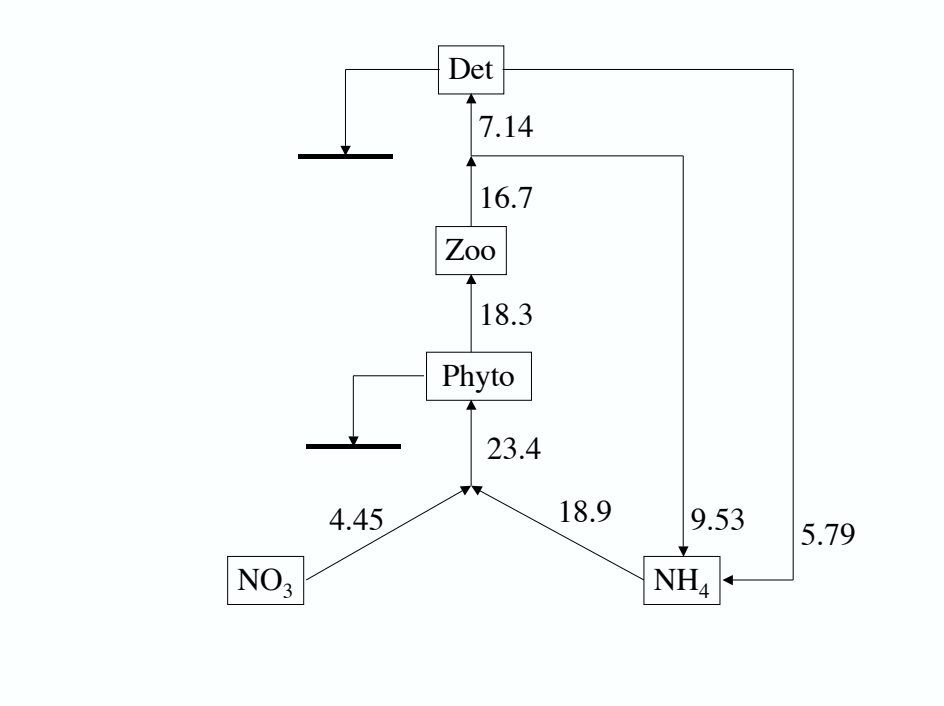

Figure 6.27: Flow of nitrogen between the biological reservoirs due to biological processes between June 7 and 26, 2001.

plankton losses are due to grazing losses and (linear and quadratic) mortality and total $18.3 \cdot 10^{10}$ mmol N. Of this, 57% is recycled to ammonium and the remaining 43% goes to detritus. Detritus remineralization to ammonium amounts to $5.79 \cdot 10^{10}$ mmol N. As seen above, nitrate remains stable throughout the simulation. According to the ADR equation for nitrate there is no biological source term. There is a flux of nitrate into the euphotic zone due to advection and mixing.

6.3 Conclusions

During June 2001 the winds in Massachusetts Bay were weaker than usual. There were 2 wind events that resulted in upwelling along the mainland coast of Massachusetts Bay. However, the wind events were relatively weak and lasted a short time. The induced upwelling was weak and had no significant effect on the biological variables and processes.

The winds were too short and too weak to reach deep enough in the water column to bring substantial amounts of nutrients into the euphotic zone. For a wind event to have an effect on primary production it needs to bring new nitrogen into the euphotic zone where it can be incorporated into the biological foodweb. During the upwelling events in June the surface water is only advected about 15 km away from the coast.

Except for detritus, the biological variables are fairly stable for the first 14 days of the simulation. During the last 6 days of the simulation there are small increases in nitrate, ammonium and phytoplankton due to the upwelling events occuring. For ammonium this increase is about 10%. Although the wind events are weak and the upwelling response is happening mostly within the euphotic zone the nutrient and phytoplankton biomass in the euphotic zone do show a signal of upwelling events.

Chapter 7

Strong episodic wind event simulations

The observed winds during the ASCOT-01 experiment in June 2001 were weaker than usual. The lack of strong wind events made it difficult to study episodic wind-driven upwelling processes. A historical wind data set from 1985 to 2005 for Massachusetts Bay shows that wind events do occur in the summer and last 1-2 days with magnitude as high as 4 dyn/cm^2. To be able to study upwelling processes, strong wind events have been designed based on the historical data set. Two wind events have been designed, both of 2-day duration and maximum strength of 2 and 4 dyn/cm^2. These wind events are then used to substitute for a portion of the real wind forcing. The set-up of the wind event simulations is identical to the data-based one except that neither temperature or salinity is assimilated since the predicted temperature and salinity fields do not represent those of June 2001.

The data-based simulation cannot be used as a reference case as it incorporates

data assimilation. For this purpose a new simulation with the real winds and without assimilation is carried out. This simulation, referred to as "Buoy" in the discussion, shows the distribution of the state variables in the absence of a wind event and is used as reference case.

In this chapter the biological response to these strong episodic wind events is discussed. The focus is on the stronger, 4 dyn/cm^2, wind event as it gives a stronger and clearer response. The physical response to the wind event is analyzed in Section 7.1. The role of horizontal advection during the wind event turns out be an important process and is discussed at length.

The nutrients, biomass and biological processes respond on two time scales to the wind event. During the wind event, advection redistributes the nutrients and biomass (see Section 7.3). For 2-3 weeks after the end of the wind event changes in biological variables are dominated by biological processes (see Section 7.4). This chapter concludes with simulations forced with real historic winds (see Section 7.5).

7.1 Description of the feature wind event

During June 2001 no strong wind events were observed in the NODC buoy wind data. A strong wind event is defined as an event lasting more than 1 day and having a magnitude of at least 2 dyn/cm^2. Wind data for May to August from the same buoy for 1985 to 2005 is available and shows that strong episodic winds event are not unusual. On average the events last 1-2 days and reach magnitudes as high as 4 dyn/cm^2. Based on this information two wind events have been designed which will replace the real wind forcing in the simulations. Both events last 2 days, with a

ramping up and down of 0.25 day. The moderately strong wind event has a maximum magnitude of 2 dyn/cm^2 and the strong one reaches 4 dyn/cm^2. The modeled wind event starts 4 days into the simulation (June 10). Figure 7.1 shows the stickplot for the wind vectors of the 2 dyn/cm^2 event.

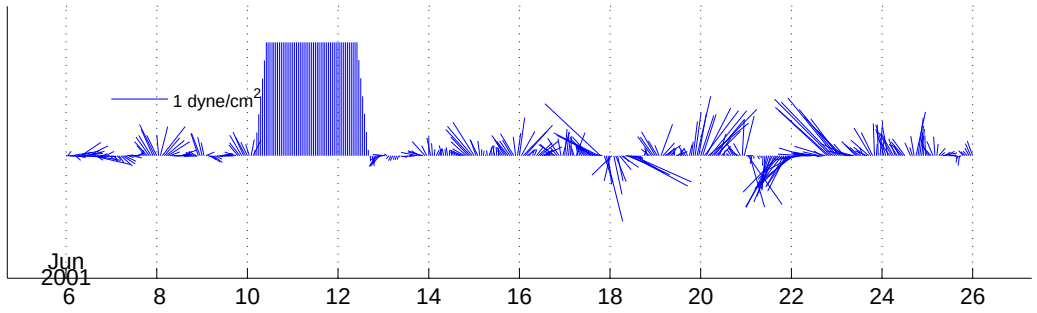

Figure 7.1: Wind vectors for the 2 dyn/cm^2 event.

7.2 Physical response

Circulation pattern during upwelling event

The wind events starts on June 10 (midnight). The surface velocities react immediately to the stronger winds. Figure 7.2 shows the horizontal velocites for the 2 dyn/cm^2 (left) and 4 dyn/cm^2 (right) wind events on June 10 (6 am) when the upwelling is developing. By the time the feature wind event reaches its peak value on June 10 (6 am) the coastal current is no longer evident and the horizontal velocities are approximately 45° to the right of the wind over entire Massachusetts Bay.

The horizontal velocites at 2 m on June 11 (noon) are shown in Figure 7.3. Throughout the wind event the velocities are off-shore. Along the western coast of

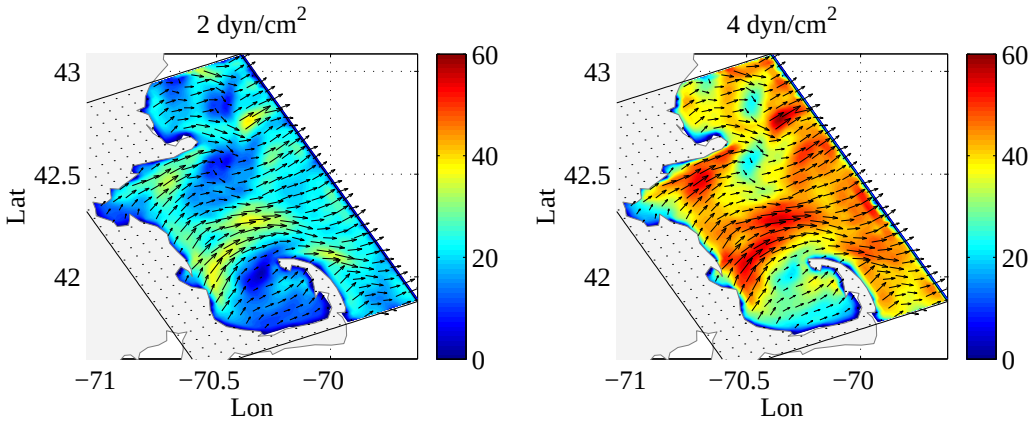

Figure 7.2: Horizontal velocities at 2 m on June 10 (6 am). Build up of the upwelling event.

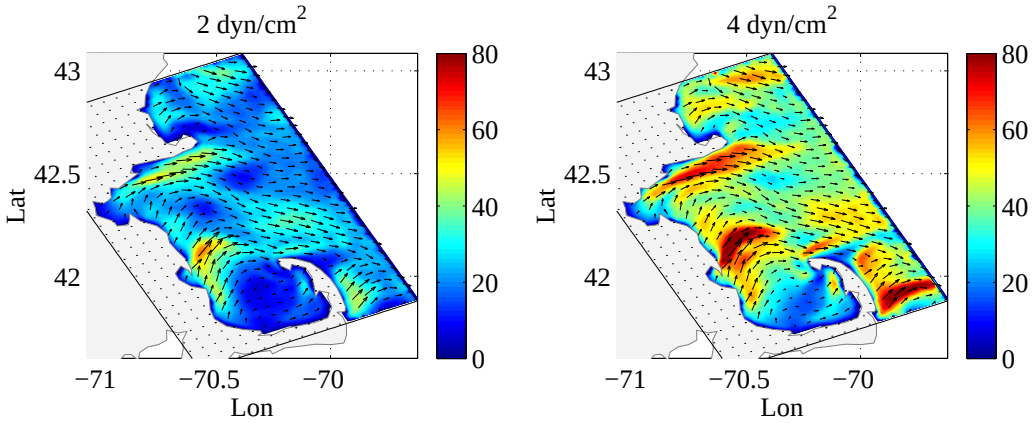

Figure 7.3: Horizontal velocities at 2 m on June 11 (noon). Representative flow for developed/matured upwelling circulation.

Cape Cod Bay there is a strong northward current along the coast. The magnitude is large, comparable to the off-shore currents in Massachusetts Bay. This current gives rise to a distortion of the 2-dimensional upwelling patterns. This along-shore current is important as it will advect the upwelled water northward into Massachusetts Bay. Nutrients will not only be upwelled and advected off-shore but redistributed along the coast.

The wind event starts ramping down on June 12 at 6 am and is completely over by noon. The surface velocities decrease once the wind event is over. For the 4 dyn/cm^2 event the off-shore velocities not only become weaker but they reverse direction (on-shore) and return some of the surface water to Massachusetts Bay.

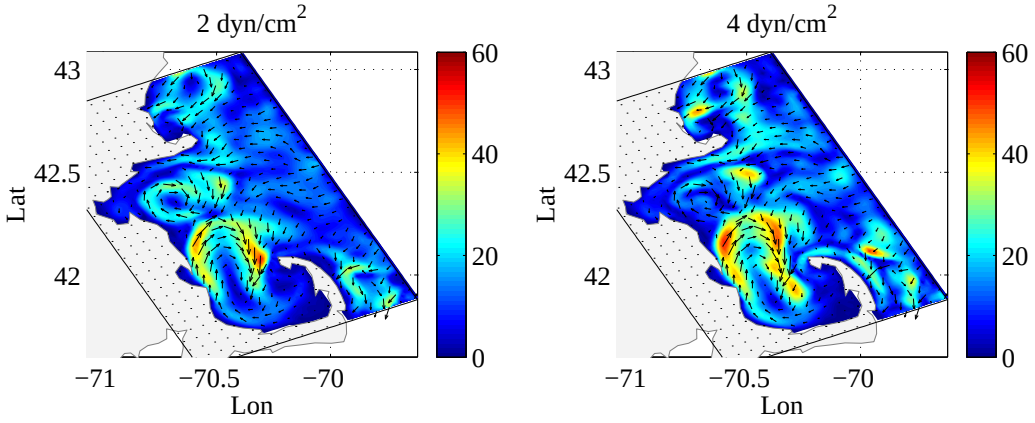

Figure 7.4: Horizontal velocities at 2 m on June 14 (6 am), two days after the end of the wind event.

A few days after the end of the wind event the surface velocities have readjusted. Figure 7.4 shows the horizontal velocites, two days after the end of the wind event, June 14 (6 am), for both wind events. The circulation pattern is dominated by two clockwise gyres in Massachusetts Bay. A strong gyre that covers central Massachusetts Bay and northern Cape Cod Bay. A weaker gyre is located in northern Massachusetts Bay. The simulations with wind events are left with small scale variabilities in the velocity field not observed in the simulation with Buoy winds. The short and strong wind event of June 18 make the wind event simulations and the reference simulation more similar.

Depth dependence of horizontal velocities

The Ekman spiral described in Chapter 1 is apparent in the velocity field at different depths. We are particularly interested in two things when it comes to the horizontal velocites. We want to know the magnitude of the horizontal off-shore currents as this will determine how far off-shore the surface water is advected. This will also determine the fraction of upwelled nutrients that remain in Massachusetts Bay. Secondly, we want to know the depth at which the horizontal current has a large on-shore component. This will determine the degree to which water from the western Gulf of Maine is advected into Massachusetts Bay. Depending on the depth the on-shore currents they can carry a large amount of nitrate.

Figure 7.5 shows profiles for zonal velocity 30 km off-shore along the central Massachusetts Bay cross-section. Below 15 m the zonal velocity reverses direction, and this water, flowing toward the coast, brings new nutrients with it. Such an upwelling event is capable of redistributing nutrients and biomass on scales comparable to the Bay itself.

Surface velocities reach 40 cm/s for the 2 dyn/cm^2 and 55 cm for the 4 dyn/cm^2. The width of Massachusetts Bay is 50 km. This means that coastal surface water in Massachusestts Bay will be advected far out into Gulf of Maine. In fact for the 4 dyn/cm^2 they are advected out of the entire computational domain. As expected the magnitude of the velocity decreases with depth. The reversal of the zonal current occurs for the 2 dyn/cm^2 event at 10-11 m and for the 4 dyn/cm^2 event ar 14-15 m. For the 2 dyn/cm^2 simulation the on-shore velocity peaks around 15 m and are weak (< 5 cm/s). For the 4 dyn/cm^2 event the on-shore are substantially stronger

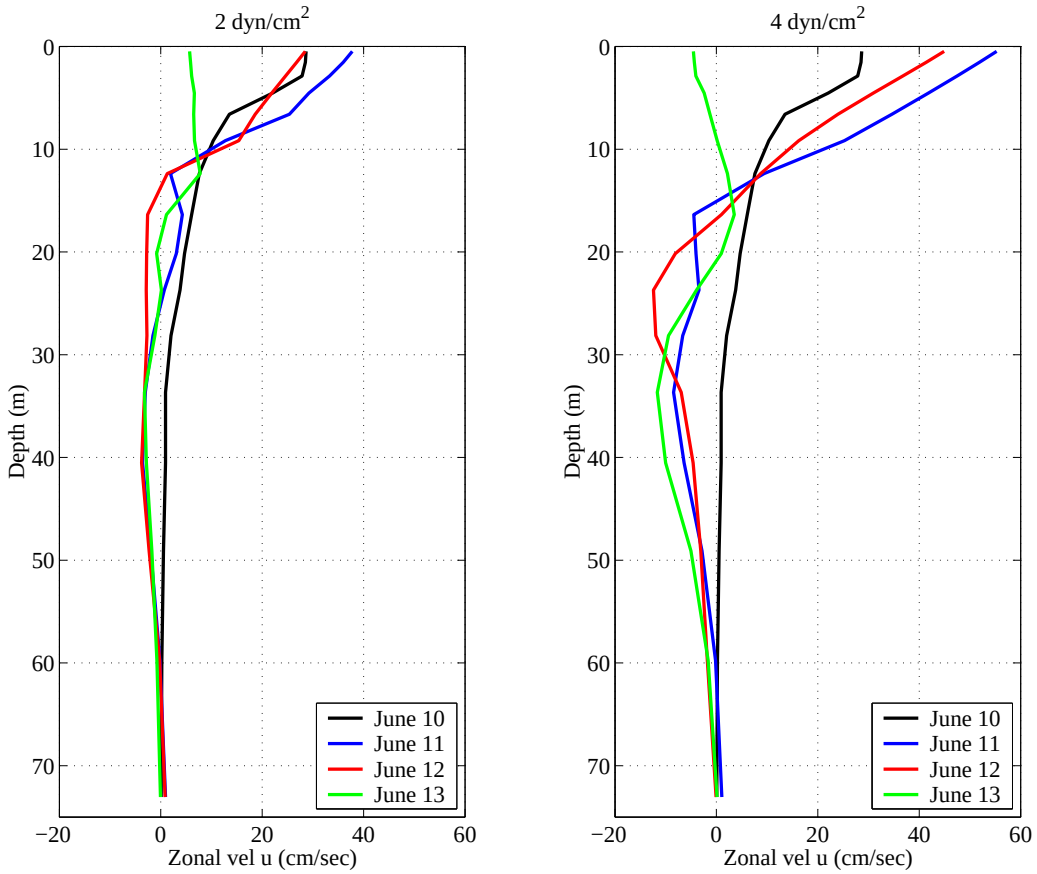

Figure 7.5: Profiles of zonal velocities (cm/s) 30 km off-shore along the central Massachusetts Bay cross-section.

with values as high as 10 cm/s and reach deeper. On June 12 the maximum on-shore velocity is at 25 m.

Once the wind event is over there is a rapid reduction of the zonal velocity in the top 10 m. For the 4 dyn/cm^2 event the zonal velocity reverses direction and is on-shore. Some of the biological material that was advected out of Massachusetts Bay is brought back in. This happens to a lesser degree for the 2 dyn/cm^2.

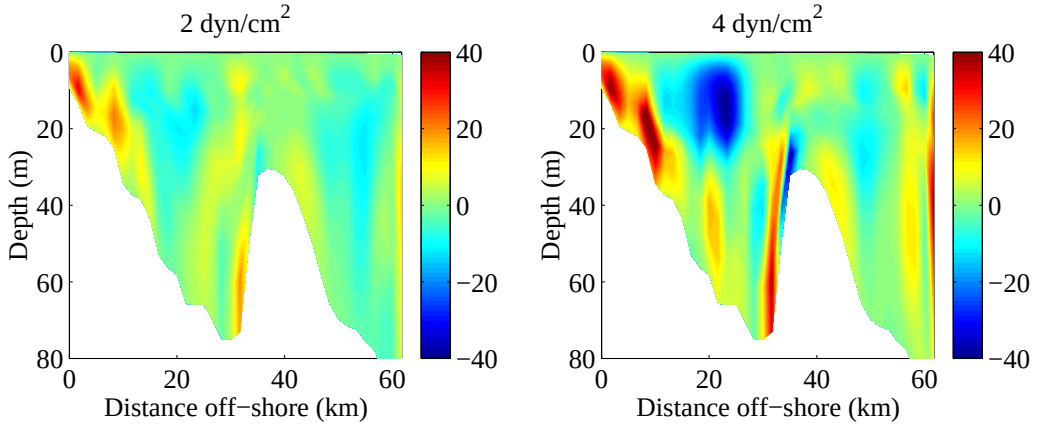

Figure 7.6: Vertical velocities along central Massachusetts Bay on June 11 (noon) for the 2 dyn/cm^2 (left) and 4 dyn/cm^2 (right) wind event.

Vertical velocities

Figure 7.6 shows the vertical velocities for the two wind event simulations. During the ramping up of the wind event there are high vertical velocites all the way from the coast to Stellwagen Bank. For most of the duration of the wind event the positive vertical velocities are confined to a 10-20 m thick band along the bottom. For the 4 dyn/cm^2 the high vertical velocities extend almost 20 km off-shore. The maximum values are about 40 m/day. Compare this with the real buoy wind simulations where the upwelling events have a maximum vertical velocity of 10 m/day. The 4 dyn/cm^2 event has strong downwelling over Stellwagen Basin. The vertical velocities reach -40 m/day here.

The vertical velocities for the 2 dyn/cm^2 have several similar features to that of the stronger wind event but are weaker. The location of the high vertical velocities is the same but they only extend 10-15 km off-shore and maximum values are approximately 25 m/day. The vertical velocities around Stellwagen Bank are positive

for both simulations. The main difference between the two wind event simulations is that the 2 dyn/cm^2 event has no strong downwelling above Stellwagen Basin.

7.3 Advective dominated redistribution of nutrients and biomass during the upwelling event June 10-13

During the wind event both nutrients and plankton are redistributed, not only vertically in the water column, but also horizontally due to the large off-shore currents near the surface and the weak on-shore currents deeper in the water column. This section describes the changes that occur in the distribution of nitrate, ammonium, phytoplankton, zooplankton and detritus during the wind event. This analysis focuses on June 10-13. The wind event ends June 12 at noon but the fluxes of biological variables across the Massachusetts Bay boundaries are still strong for an additional half a day.

The analysis is carried out in two parts. First, the simulations, with the three wind events, are performed with all the biological processes shut-off, including phytoplankton and detritus sinking. The biological variables act as passive tracers and any in changes in their concentrations are due to either advection, mixing or fluxes through the domain boundaries. This makes it possible to isolate the spatial redistribution of nutrient and biomass due to the upwelling event. The simulations are then repeated with all biological processes turned on. The results of simulations with the same wind event but with and without biological processes are compared against each other to determine if any biological processes are important *during* the wind event. The analysis focuses on the 4 dyn/cm^2 event as the signals are stronger and easier to identify.

7.3.1 Simulations with biological variables as passive tracers

A very important parameter for an upwelling event is the source and character of the upwelled water, i.e., the depth and location from which the water originates and the concentration of the biological variables in this water. This is a particularly important parameter for nitrate and ammonium as their concentrations increase with depth. The deeper the upwelled water comes from the more nutrient enters the euphotic zone during the upwelling event. To obtain a first glimpse of the advective redistribution of nutrients and biomass the biological variables are plotted along the west to east cross-section along the central Massachusetts Bay previously used. The (real) buoy winds, which show the distribution of the biological variables in the absence of wind events, is used as reference case. The simulations with wind events (2 and 4 dyn/cm^2) are compared against the buoy one on June 12 at 6 am. This time corresponds to the peak of the wind event and the start of the ramping down of the wind strength.

To predict the response of the biological processes, in particular primary production, it is necessary to determine the flux of nutrient and biomass in and out of the euphotic zone during the wind event. First, each biological variable is integrated in the euphotic zone as a function of time. This gives an insight into the net changes of each biological variable in the euphotic zone. For a complete analysis the volume integrated biological variables are also determined in the aphotic zone.

The flux of nutrients and biomass into the euphotic zone are then calculated. The vertical flux is calculated at the depth of the euphotic zone (23 m) and represents the rate at which nitrogen enters the euphotic zone from below during the wind event.

Due to the geometry of Massachusetts Bay there is only one horizontal flux and it is due to exchange of water with western Gulf of Maine. The net horizontal flux into the aphotic zone is also calculated. The nitrogen flux analysis is summarized in a two-box model of Massachusetts Bay where the top box is the euphotic zone and the lower box the aphotic zone.

The zooplankton and detritus distribution are initialized proportionally to the phytoplankton. For the zooplankton the proportionality constant is 1 and for the detritus 2, i.e., $Z = 1 \times P$ and $D = 2 \times P$. In these simulations, where the biological variables act as passive tracers, the zooplankton distribution is identical to that of the phytoplankton. The detritus distribution is also identical but with values twice as high. Separate analyses for the zooplankton and detritus are therefore not included.

Ammonium

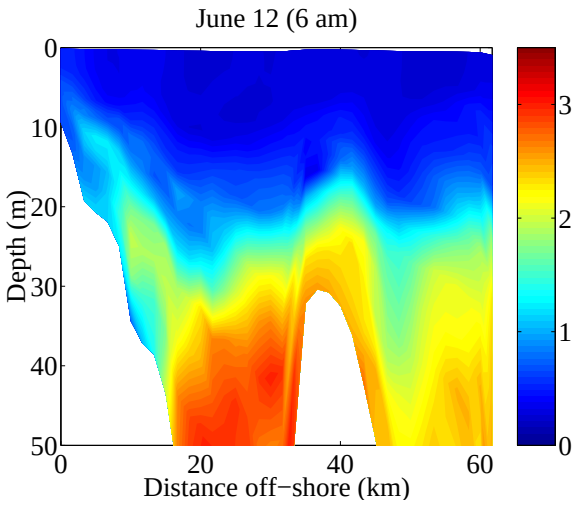

Figure 7.7: Ammonium (mmol N m^{-3}) distribution for June 12 (6 am) for the simulation without a wind event.

Figure 7.7 shows the ammonium concentration on June 12 at 6 am for the sim-

ulation without a wind event. Similarly to the nitrate distribution, we have low concentrations near the surface. The ammonium concentration increases with depth and at the bottom of the euphotic zone we have concentrations of 2.0 mmol N m^{-3} and above. Below the euphotic zone in Massachusetts Bay the ammonium concentrations reach above 3.0 mmol N m^{-3}. The ammonium concentrations are low in the deep water of the western Gulf Maine.

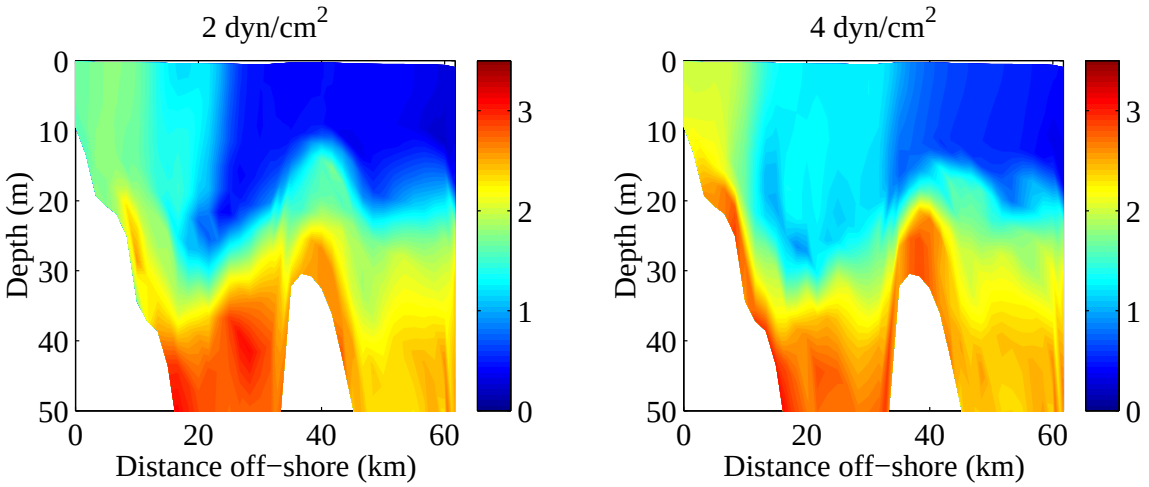

Figure 7.8: Ammonium (mmol N m^{-3}) distribution for June 12 (6 am) for 2 dyn/cm^2 (left) and 2 dyn/cm^2 (right) wind event simulation.

The response of the ammonium to the two wind events is shown in Figure 7.8. For both wind events there is a large increase of ammonium in the euphotic zone, especially at the coast. The 4 dyn/cm^2 wind event results in an increase of ammonium from below 0.5 mmol N m^{-3} to above 2.0 mmol N m^{-3} near the coast. The entire euphotic zone in Massachusetts Bay ends up with concentrations above 1.0 mmol N m^{-3}. The half-saturation constant for ammonium, k_2, is 0.1 mmol N m^{-3}, which implies that in the entire euphotic zone the phytoplankton are nutrient saturated. Near the surface the large off-shore currents advect ammonium rich water far off-shore

and the high ammonium concentrations extend 45 km off-shore. Deeper in the water column the currents are on-shore and bring ammonium into Massachusetts Bay. This amount of ammonium is smaller than for nitrate as the ammonium concentrations are lower in the Gulf of Maine. After the event a portion of the ammonium that was advected off-shore at the surface is brought back into Massachusetts Bay.

The 2 dyn/cm^2 upwelling event leads to ammonium concentrations of about 2.0 mmol N m^{-3}, which is not very different from the 4 dyn/cm^2 event. The most notable difference between the two events is the distance off-shore that the ammonium rich water reaches. For the 2 dyn/cm^2 this distance is only 30 km, i.e., only a small fraction of the ammonium is advected out of Massachusetts Bay.

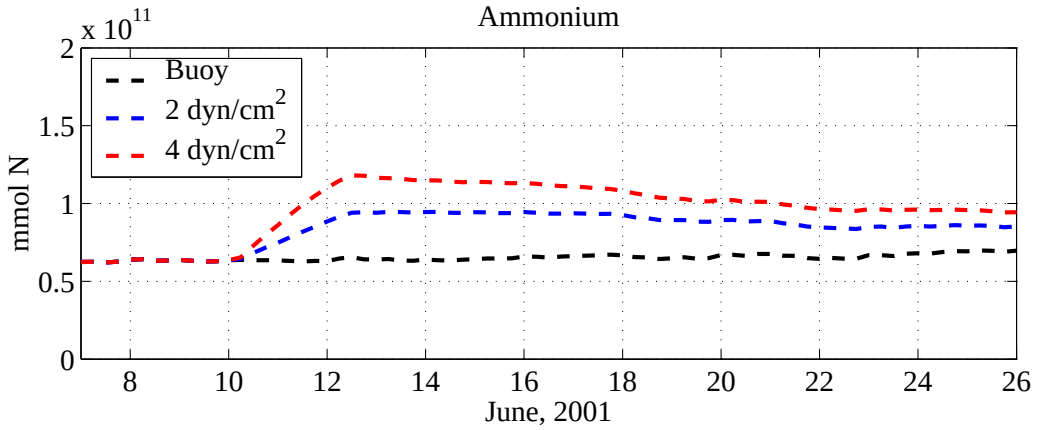

Figure 7.9: Ammonium (mmol N) in the euphotic zone in Massachusetts Bay for simulations with varying winds and no biological processes.

Figure 7.9 shows the total ammonium in the euphotic zone as a function of time. For both wind events there is a substantial increase of ammonium in the euphotic zone. This ammonium is upwelled from the aphotic zone during the wind event. Prior to the wind events the total ammonium in the euphotic zone is $6.35 \cdot 10^{10}$ mmol N. At the end of the wind event the ammonium has increased to $11.7 \cdot 10^{10}$ mmol N.

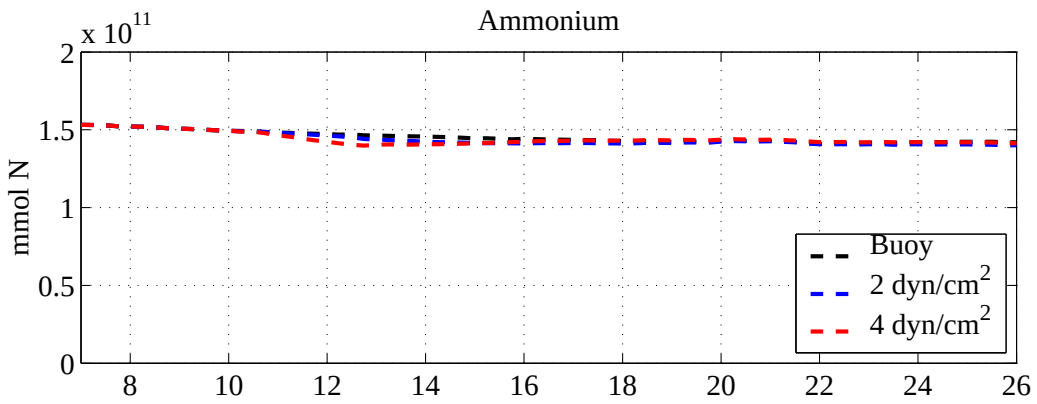

Figure 7.10: Ammonium (mmol N) in the aphotic zone in Massachusetts Bay for simulations with varying winds and no biological processes.

The total ammonium in the aphotic zone as a function of time is shown in Figure 7.10. Neither of the wind events result in large changes in ammonium in the aphotic zone. The 4 dyn/cm^2 simulation shows a small decrease in ammonium during the upwelling event. The flux of ammonium from the western Gulf of Maine is smaller and not sufficient to balance the vertical flux of ammonium into the euphotic zone. The simulation with the 2 dyn/cm^2 wind event shows a very small change during the wind event June 10-12.

Figure 7.11 shows the fluxes of ammonium in and out of Massachusetts Bay. The top box represents the euphotic zone and the lower box aphotic zone. For the 4 dyn/cm^2 event $7.1 \cdot 10^{10}$ mmol N of ammonium is transferred from the aphotic zone to the euphotic zone during the upwelling event while $1.6 \cdot 10^{10}$ mmol N are lost out of the euphotic zone due to horizontal advection. The net gain of ammonium in the euphotic zone is therefore $5.5 \cdot 10^{10}$ mmol N. The ammonium flux into the aphotic zone is $6.0 \cdot 10^{10}$ mmol N which results in a net loss of ammonium from the aphotic zone. The 4 dyn/cm^2 leads to a small, $1.09 \cdot 10^{10}$ mmol N, loss of ammonium

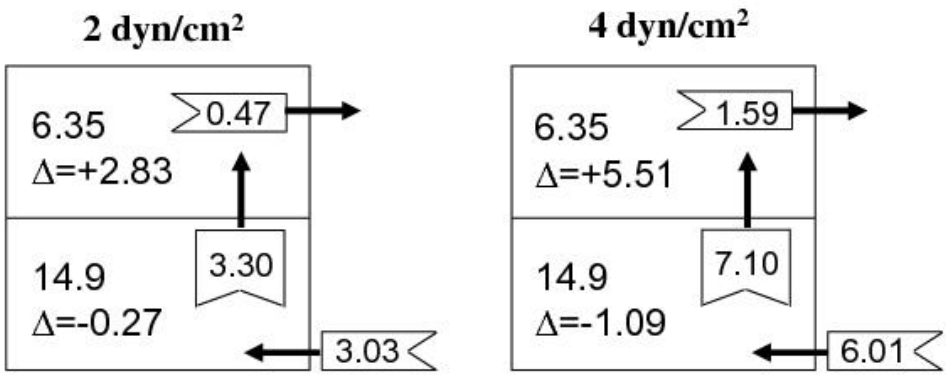

Figure 7.11: Amount ($\times 10^{10}$ mmol N) of ammonium advected in and out of the euphotic (top) and aphotic (bottom) zone during the upwelling event June 10-13. The amount of ammonium prior to the wind event as well as the resulting changed due to advection are given for each box.

from the aphotic zone. However, the decrease is small in comparison with the total amount of ammonium in the aphotic zone. In the aphotic zone for the 2 dyn/cm^2 simulation ammonium losses to the euphotic zone are nearly balanced by the flux in from the western Gulf of Maine. In the euphotic zone the ammonium losses due to off-shore advection are relatively smaller (compared to the stronger event) leading to a proportionally larger accumulation of ammonium in the euphotic zone.

Nitrate

Figure 7.12 shows the nitrate distribution from the simulation without a wind event. This is a typical distribution for summer conditions in Massachusetts Bay where nitrate is nearly depleted in the top of the water column. At the bottom of the euphotic zone (23 m) the nitrate concentration is around 1.0 mmol N m^{-3}. Below the euphotic zone the concentration ranges between 1.5 to 4.0 mmol N m^{-3}. Outside

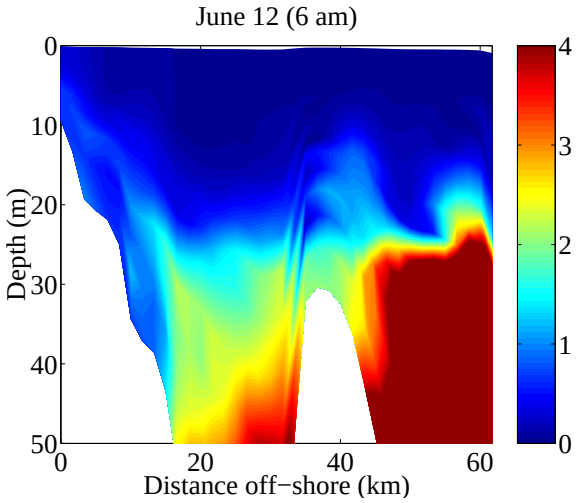

Figure 7.12: Nitrate (mmol N m^{-3}) distribution for June 12 (6 am) for simulation without wind event.

Massachusetts Bay there are high nitrate concentrations, > 10 mmol N, deep in the water column.

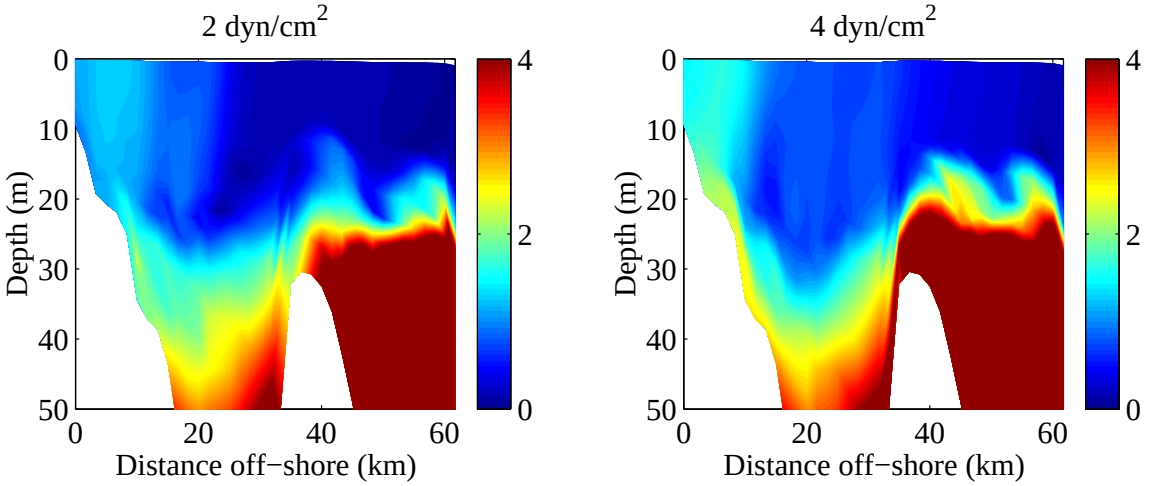

Figure 7.13: Nitrate (mmol N m^{-3}) distribution for June 12 (6 am) for 2 dyn/cm^2 (left) and 4 dyn/cm^2 (right) wind event simulation.

Figure 7.13 shows the nitrate concentration along the central Massachusetts Bay cross section for the 2 dyn/cm^2 (left) and the 4 dyn/cm^2 (right) on June 12 at 6 am.

Both wind events have a significant impact on the nitrate distribution. During the wind event nitrate is upwelled into the euphotic zone near the coast, resulting in a large nitrate increase. During the 4 dyn/cm^2 wind event water as deep as 60 m is upwelled. Contrast this with the upwelling induced by the real buoy winds, which affected only the water within the euphotic zone. In the euphotic zone the wind event has resulted in an increase of nitrate concentration from nearly depleted conditions to values in the vicinity of 2.0 mmol N m^{-3}. This nitrate concentration is well above the half-saturation constant for nitrate uptake, $k_1 = 0.1$ mmol N m^{-3}. However, to determine the nitrate uptake rate the ammonium concentration must be determined to estimate the effects of ammonium inhibition.

During the wind event the surface water is advected off-shore. The 4 dyn/cm^2 wind event advects water almost 60 km off-shore. Thus water upwelled along the coast is advected out of Massachusetts Bay. The upwelling event is no longer a local event as it redistributes the water on scales of the size of Massachusetts Bay itself. Recall that for for the real buoy wind events the water was advected no more than 15 km off-shore. The large distances that the nitrate is advected implies that the nitrate utilization after the end of event will happen away from the upwelling site. In other words, the upwelling happens in one place and the subsequent bloom elsewhere.

Deeper in the water column, below 15 m, there are on-shore currents during the upwelling event. These currents bring nitrate in from the western Gulf of Maine. The strongest on-shore zonal velocities are at the bottom of and below the euphotic zone. This flux of nitrate is evident above Stellwagen Bank. Here the nitrate concentration has increased from approximately 2.0 mmol N m^{-3} to above 4 mmol N m^{-3}. Once

the wind event is over the horizontal (zonal) velocities decay very quickly. For the 4 dyn/cm^2 event they even reverse direction near the surface (see Figure 7.5). This means that some of the nitrate that was brought out to western Gulf of Maine is brought back into Massachusetts Bay.

Above Stellwagen Basin there is downwelling and nitrate is brought deeper into the water column. Below the euphotic zone water is replaced by surface water with very low nitrate concentration. For the 4 dyn/cm^2 wind event the nitrate decreases from approximately 2.0 to 1.0 mmol N m^{-3}.

The 2 dyn/cm^2 wind event has a similar response. Water is upwelled from about 40 m depth and near the coast the nitrate concentration increases to approximately 1.5 mmol N m^{-3}. This concentration is also well above the half-saturation constant for nitrate uptake. The surface water is advected less than 30 km off-shore. This means that water that is upwelled near the coast remains inside Massachusetts Bay. Only water originally at the surface is advected out of Massachusetts Bay. The 2 dyn/cm^2 event has a slight reversal of zonal currents at the end of the wind event, thus the nitrate advected out of Massachusetts Bay is not brought back. Deeper in the water column some nitrate returns with the on-shore currents.

Figure 7.14 shows the volume integrated nitrate as a function of time in the euphotic zone in Massachusetts Bay for the three simulations. The stronger the wind event the larger the increase of nitrate in the euphotic zone. During the 4 dyn/cm^2 event the total nitrate in the euphotic zone increases from $3.1 \cdot 10^{10}$ mmol N to $8.6 \cdot 10^{10}$ mmol N, which is almost a three-fold increase. As the nitrate concentrations are, prior to the wind event, low in the near surface waters we expect only a small horizontal

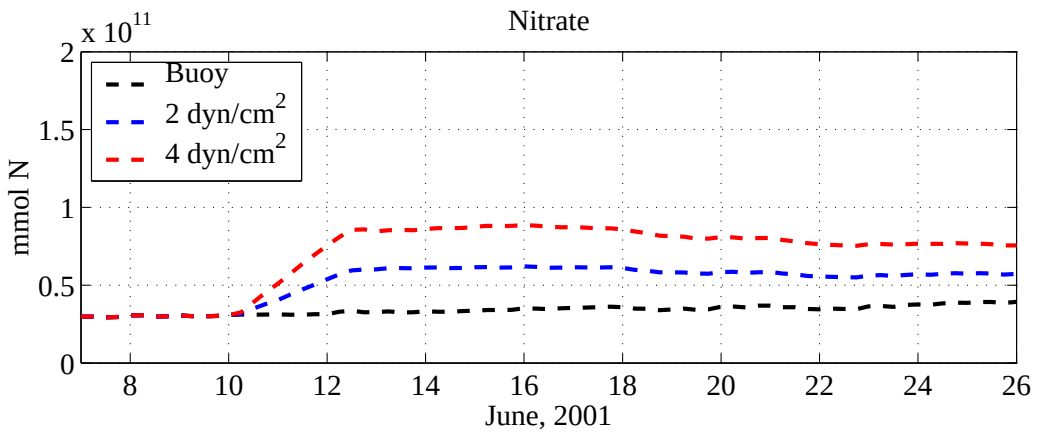

Figure 7.14: Nitrate (mmol N) in the euphotic zone in Massachusetts Bay for simulation with varying winds and no biological processes.

flux of nitrate out of the euphotic zone due to the off-shore currents. The change of nitrate in the euphotic zone is therefore dominanted by the vertical flux of nitrate from the aphotic zone (the fluxes in and out of the euphotic zone are quantified and summarized below).

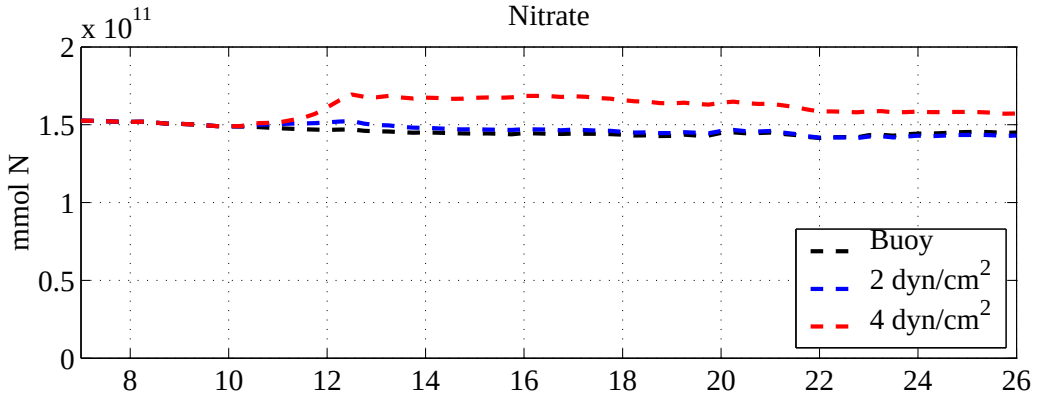

Figure 7.15: Nitrate (mmol N) in the aphotic zone in Massachusetts Bay for simulation with varying winds and no biological processes.

The volume integrated nitrate in the aphotic zone for the three wind simulations is shown in Figure 7.15. The total nitrate in the aphotic zone for the 4 dyn/cm^4

simulation shows a strong response to the wind event. During the wind event, nitrate is lost to the euphotic zone due to upwelling while at the same time, nitrate enters the aphotic zone due to horizontal on-shore advection from western Gulf of Maine.

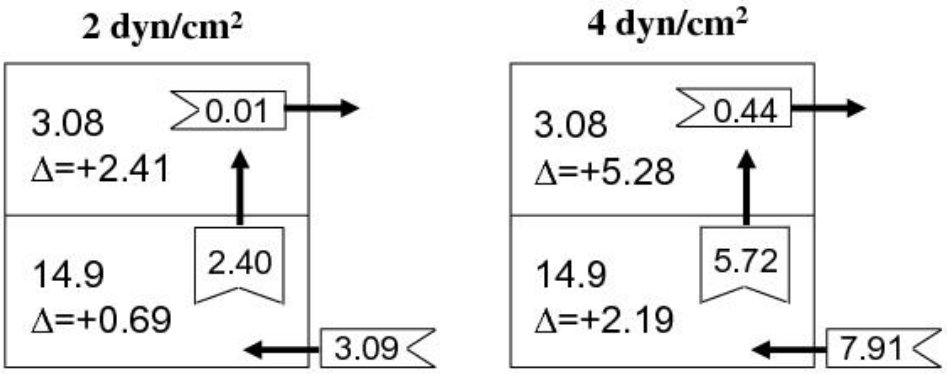

Figure 7.16: Amount ($\times 10^{10}$ mmol N) of nitrate advected in and out of the euphotic (top) and aphotic (bottom) zone during the upwelling event June 10-13. The amount of nitrate prior to the wind event as well as the net accumulation due to advection are given for each box.

Figure 7.16 summarizes the nitrate flux in Massachusetts Bay. For the 4 dyn/cm^2, $5.7 \cdot 10^{10}$ mmol N flow from the aphotic to the euphotic zone due to upwelling. In the euphotic zone, $0.4 \cdot 10^{10}$ mmol N are advected off-shore into the Gulf of Maine. This results in a net increase of $5.3 \cdot 10^{10}$ mmol N in the euphotic zone. In the aphotic zone nitrate influx from western Gulf of Maine is $7.9 \cdot 10^{11}$ mmol N. This results in a net gain of nitrate in the aphotic zone of $2.2 \cdot 10^{10}$ mmol N. A 4 dyn/cm^2 event not only replenishes the nitrate in the aphotic zone, but leads to an increase of nitrate. The fate of this new nitrate depends on the subsequent winds and resulting circulation.

For the 2 dyn/cm^2 event $2.4 \cdot 10^{10}$ mmol N enters the euphotic zone from below while the net horizontal flux is negligible. The total amount of nitrate in the aphotic

zone is barely affected by the 2 dyn/cm^2 wind event. From the western Gulf of Maine $3.1 \cdot 10^{10}$ mmol N enters the aphotic zone. The net gain of nitrate in the euphotic zone is $0.7 \cdot 10^{10}$ mmol N. The 2 dyn/cm^2 event has less of an recharging power but nevertheless replenishes the nitrate in the aphotic zone.

Phytoplankton

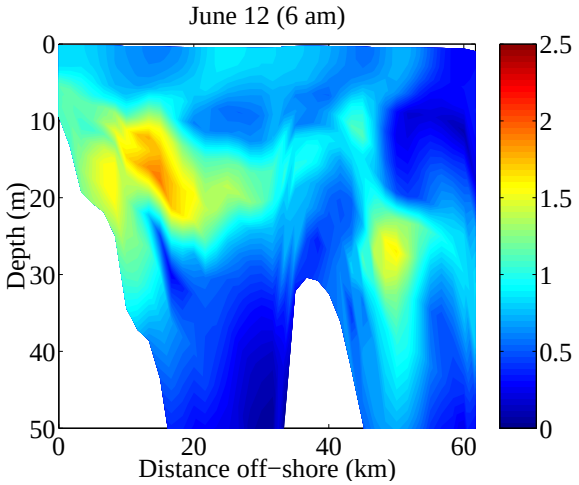

Figure 7.17: Phytoplankton (mmol N m^{-3}) distribution for June 12 (6 am) for simulation without wind event.

Figure 7.17 shows the phytoplankton concentration along the central Massachusetts Bay cross-section on June 12 at 6 am. Without a wind event the phytoplankton distribution is characterized by a subsurface maximum between 10 to 20 m with concentrations ranging from 1.2 to 1.5 mmol N m^{-3}.

The phytoplankton distribution along the central Massachusetts Bay cross-section for the two wind events are show in Figure 7.18. Both wind events are strong enough to change the characteristics of the phytoplankton distribution. During the first day of the wind event the phytoplankton subsurface maximum moves closer to the surface.

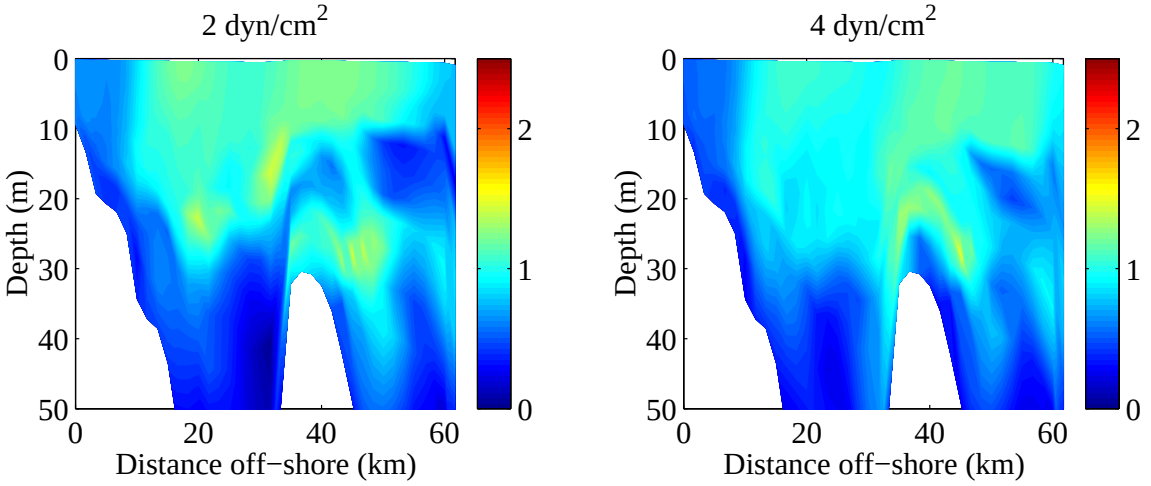

Figure 7.18: Phytoplankton (mmol N m^{-3}) distribution for June 12 (6 am) for 2 dyn/cm^2 (left) and 2 dyn/cm^2 (right) wind event simulation.

By the end of the first day of the event the maximum phytoplankton concentrations are found at the surface.

For the phytoplankton, the depth of the deepest upwelled water is not as important a parameter as it is for nitrate and ammonium. Below the euphotic zone there are only small quantities of phytoplankton to upwell. On the second day, deep phytoplankton poor water makes it into the euphotic zone and reaches the surface at the coast. Within 10 km off the coast the phytoplankton concentration is below 1.0 mmol N m^{-3}. As the upwelling event progresses phytoplankton are advected further and further off-shore. A fraction of the phytoplankton are advected out of Massachusetts Bay for both wind events. For the stronger, 4 dyn/cm^2 wind event, the highest phytoplankton concentrations are found outside of Massachusetts Bay. A small amount of phytoplankton enters the Bay with the deep on-shore currents from the western Gulf of Maine. This flux is not as prominent as it is for the nutrienta as the phytoplankton concentrations decrease with depth below the subsurface maxima.

The phytoplankton distribution over Stellwagen Bank shows that "coastal" upwelling occurs on the Gulf of Maine side of the Bank, facilitating the inflow of biomass in the Massachusetts Bay.

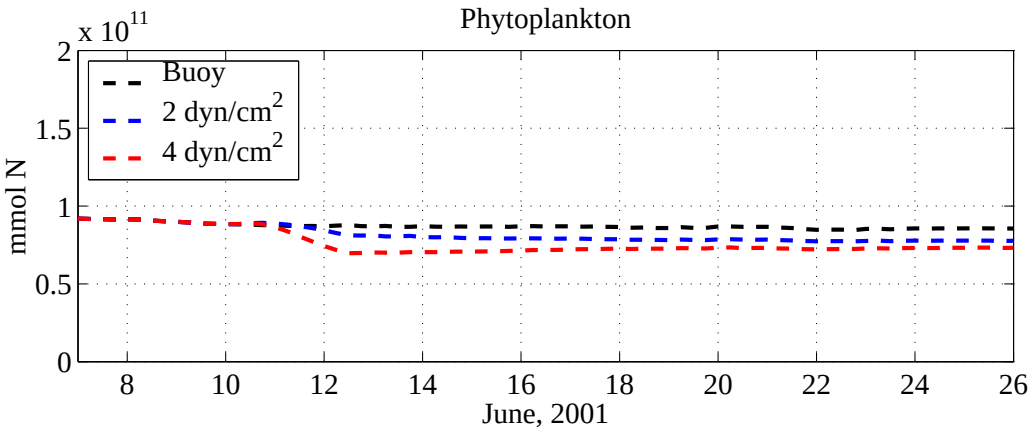

Figure 7.19: Phytoplankton (mmol N) in the euphotic zone in Massachusetts Bay for simulations with varying winds and no biological processes.

Figure 7.19 shows the phytoplankton stock in the euphotic zone as a function of time. During the first day of the wind event, June 10, the phytoplankton are upwelled into the euphotic zone. This results in an increase in the phytoplankton as the off-shore currents have not yet advected large quantities of phytoplankton out of Massachusetts Bay. During the second day of the upwelling event, June 11, the flux of phytoplankton from the aphotic zone is diminished as the successively upwelled water has lower and lower phytoplankton concentration. The dominant flux on June 11 is the loss of phytoplankton out of Massachusetts Bay due the off-shore surface currents. The phytoplankton decreases from $8.8 \cdot 10^{10}$ mmol N to $7.0 \cdot 10^{10}$ mmol N.

The phytoplankton stock in the aphotic zone is shown in Figure 7.20. The phytoplankton biomass increases in the aphotic zone for all simulations. The wind events have barely any effect on the phytoplankton stock in the aphotic zone. For both wind

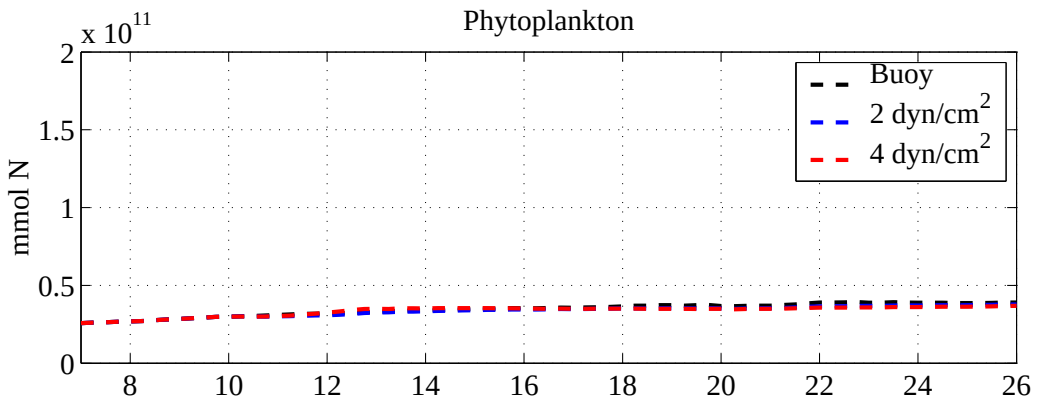

Figure 7.20: Phytoplankton (mmol N) in the aphotic zone in Massachusetts Bay for simulations with varying winds and no biological processes.

events the loss of phytoplankton to the euphotic zone is nearly balanced by the influx from the western Gulf of Maine.

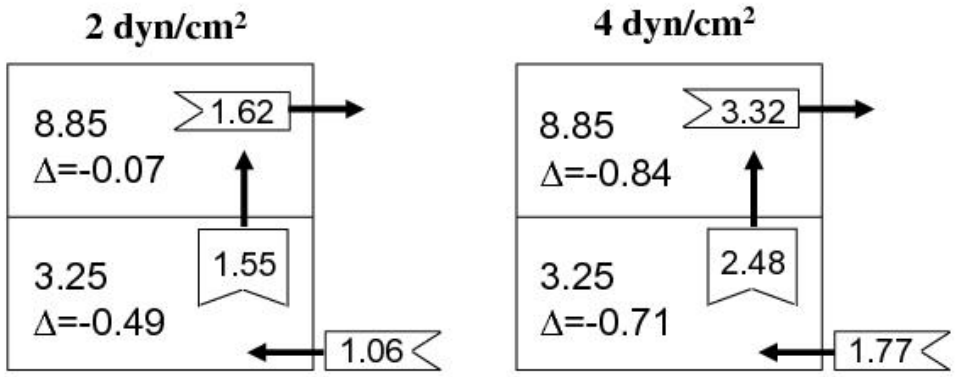

Figure 7.21: Amount ($\times 10^{10}$ mmol N) of phytoplankton advected in and out of the euphotic (top) and aphotic (bottom) zone during the upwelling event June 10-13. The amount of phytoplankton prior to the wind event as well as the net accumulation due to advection are given for each box.

7.3.2 Simulations with biological processes included

In this section the importance of biological processes during the upwelling event June 10-13, is determined. The volume integrated rates for primary production (due to nitrate, ammonium and the sum of the two) and zooplankton grazing are calculated for the euphotic zone for the buoy, 2 dyn/cm^2, and 4 dyn/cm^2 wind event simulations. The biological variables are also volume integrated in the euphotic zone. The values for a simulation with biological processes is compared against one without. The comparison is first made for the 4 dyn/cm^2 simulation as it is the one that has the strongest response and is therefore easier to analyze.

Ammonium

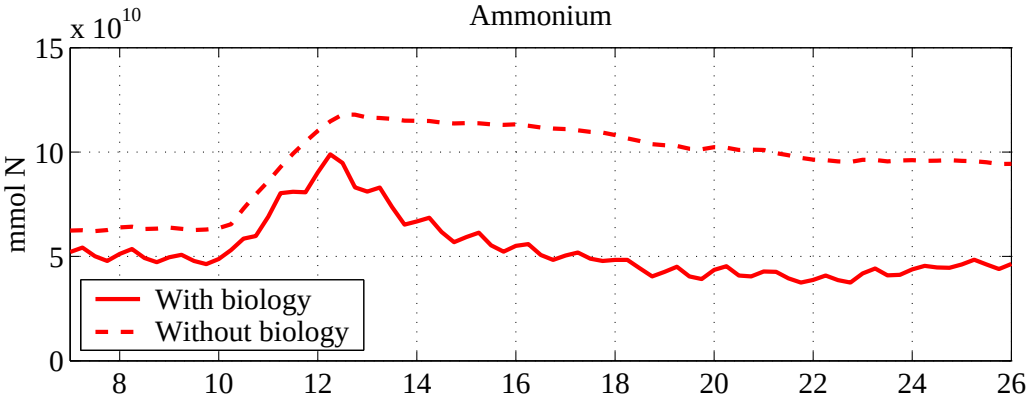

Figure 7.22: Total ammonium (mmol N) in the euphotic zone for 4 dyn/cm^2 simulation with and without biological processes present.

The total ammonium in the euphotic zone for the 4 dyn/cm^2 wind event simulation with and without biological processes is shown in Figure 7.22. The determination of the amount of ammonium is made difficult by the fact that in the simulation with biological processes the phytoplankton take up ammonium during the first four days

before the start of the wind event. The uptake is particularly high on the first day of the simulation. However, it is still possible to determine from Figure 7.22 if ammonium is influenced by biological processes during the wind event. If ammonium is taken up during the upwelling event it will increase at a slower rate than the ammonium without biological processes. The curve for the two simulations should therefore diverge during the upwelling event. On June 10, at the start of the wind event, the difference between the two simluations is smaller than at the the end of the event (June 12). The difference is small, but nevertheless shows that ammonium is taken up during the upwelling event. A more precise picture of the ammonium can be obtained by shutting off the biological processes at the start of the wind event rather than at the start of the simulation.

Nitrate

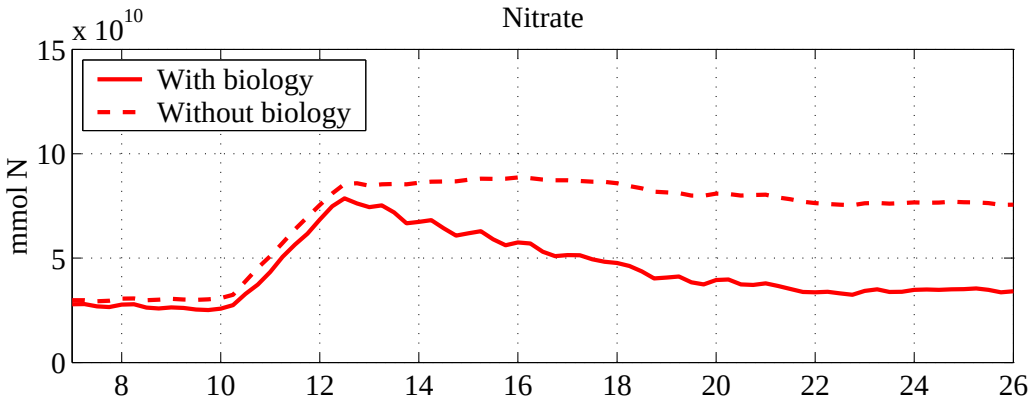

Figure 7.23: Total nitrate (mmol N) in the euphotic zone for 4 dyn/cm^2 simulation with and without biological processes present.

Figure 7.23 shows the total amount of nitrate in the euphotic zone for the 4 dyn/cm^2 simulation with and without biological processes present. The nitrate

amount is almost the same for the two simulations during the wind event. The nitrate in the simulation without biological sources shows a somewhat larger increase during the upwelling event that the simulation with biological processes. The difference between the two simulations represent the amount of nitrate taken up by the phytoplankton during the wind event, which as we have already seen is small.

Phytoplankton

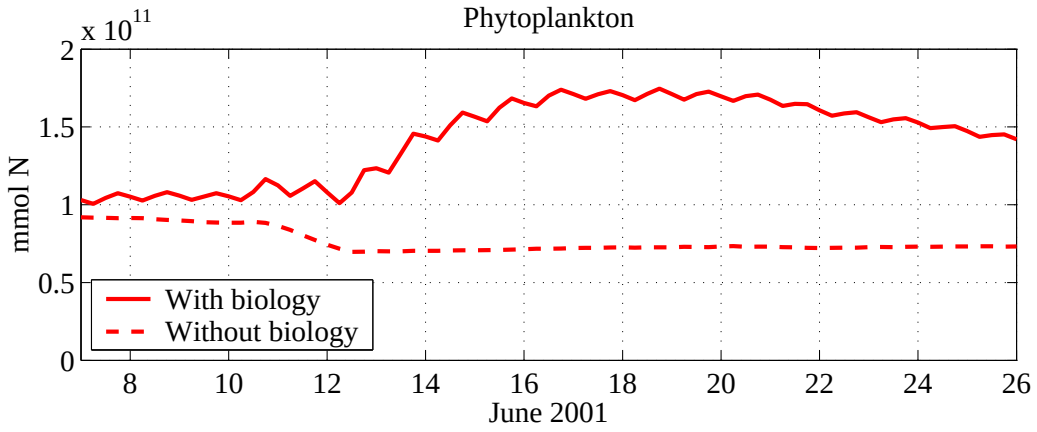

Figure 7.24: Total phytoplankton (mmol N) in the euphotic zone for 4 dyn/cm^2 simulation with and without biological processes present.

The phytoplankton stock in the euphotic zone for the 4 dyn/cm^2 simulation with and without biological processes is shown in Figure 7.24. Phytoplankton is the biological variable that shows the largest difference between the two simulations. Without biological processes the phytoplankton decrease due to advective losses to the Gulf of Maine. With biological processes, the phytoplankton assimilate sufficient nitrogen to more than balance these losses. Nutrient uptake is therefore an important biological process during the upwelling event.

Zooplankton

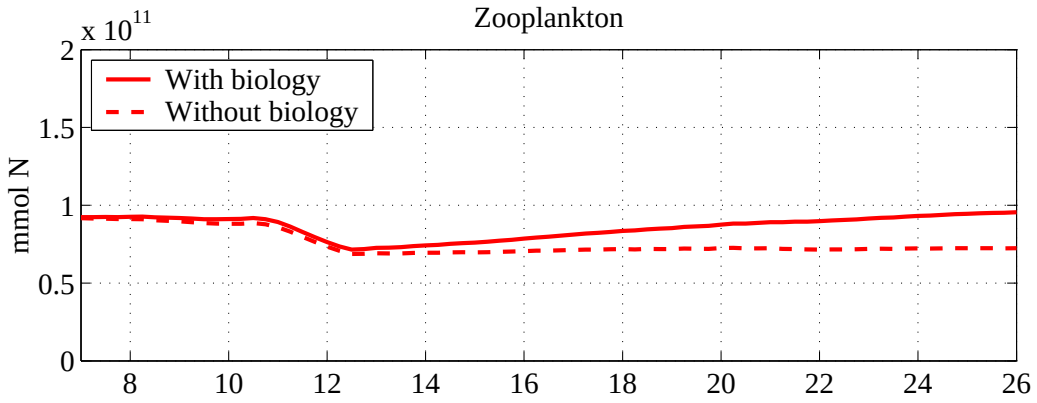

Figure 7.25: Total zooplankton (mmol N) in the euphotic zone for 4 dyn/cm^2 simulation with and without biological processes present.

Figure 7.25 shows the zooplankton stock for the 4 dyn/cm^2 simulation with and without biological processes. The zooplankton stock is almost the same for the two simulations during the upwelling event. Compared to the rate of advective losses, the zooplankton grazing rate is very small. Unlike the phytoplankton, that are able to compensate the advective losses with high nutrient uptake rates, the zooplankton are lost at a higher rate than they can graze the phytoplankton. The zooplankton grazing does not play a major role in regulating phytoplankton concentration during the upwelling event.

Detritus

The total detrital material in the euphotic zone for the simulations with and without biological processes is shown in Figure 7.26. The difference between the two simulations is small and largely due to differential sinking losses. During the first 4 days, before the start of the wind event, in the simulation with biological

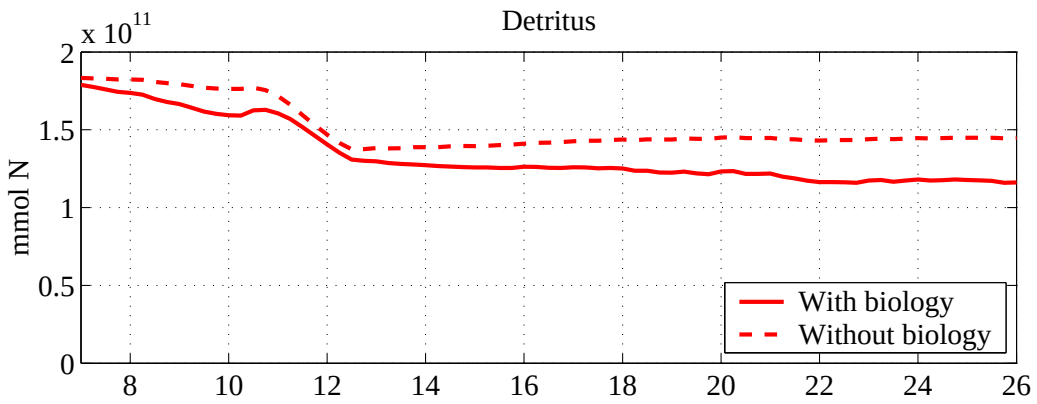

Figure 7.26: Total detritus (mmol N) in the euphotic zone for 4 dyn/cm^2 simulation with and without biological processes present.

processes the detritus sinks out of the euphotic zone. During the first day of the wind event detritus is brought into the euphotic zone from below. For the simulation with biological processes there is less detritus at the start of the wind event (as it has sunk out of the euphotic zone) but more is brought in. During the second day of the wind event the detritus concentration is most influenced by the advective losses out of the euphotic zone. For the detritus, biological processes play no significant role during the wind event.

Total primary production

Figure 7.27 shows the total volume integrated primary production rate for nitrate and ammonium. For the simulation without wind events the primary production rate is stable at approximately $2.5 \cdot 10^{10}$ mmol N/day. With an average phytoplankton biomass of $11.0 \cdot 10^{10}$ mmol N in the euphotic zone, this primary production rate corresponds to an average doubling time of 4.4 days.

Both wind event simulations show elevated primary production rates on the first

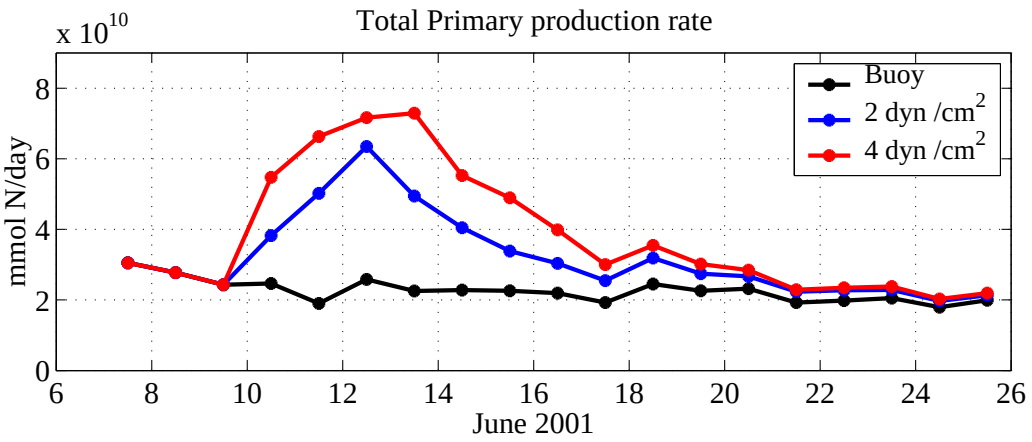

Figure 7.27: Total primary production rate (mmol N/day) in the euphotic zone for simulations with varying winds.

day of the upwelling event. Throughout the wind event the primary production rate increases. Notice that the difference between the 4 and 2 dyn/cm^2 events is relatively small. During the wind the concentrations of nitrate (see Figure 7.13) and ammonium (see Figure 7.8) in the euphotic zone are much higher than the half-saturation constants for nitrogen uptake. During the wind event the phytoplankton in the euphotic zone are therefore nutrient saturated which results in the primary production rates for the two wind events to only differ a little (14%).

Primary production due to ammonium uptake

Figure 7.28 shows the primary production rate due to ammonium uptake only. During the wind event the majority of the nutrient uptake is due to ammonium, which is not surprising due to the preferential uptake of ammonium.

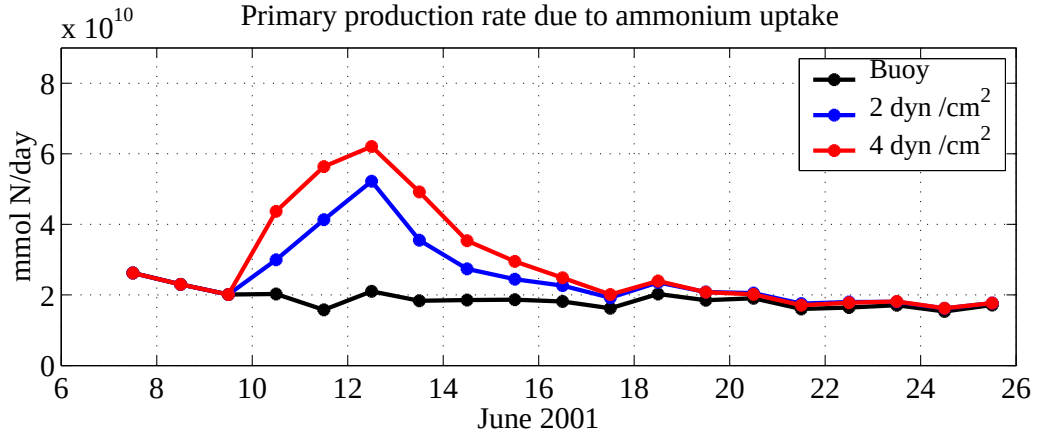

Figure 7.28: Total ammonium uptake rate (mmol N/day) in the euphotic zone for simulations with varying wind.

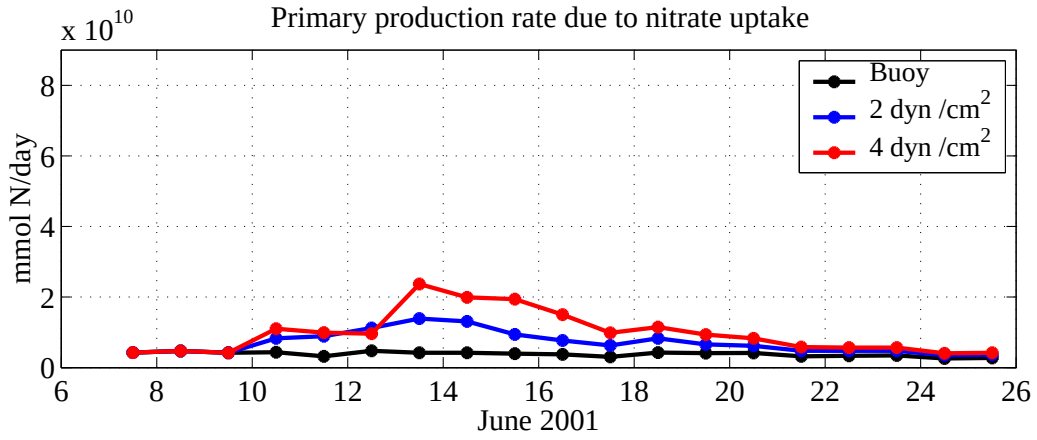

Figure 7.29: Total nitrate uptake rate (mmol N/day) in the euphotic zone for simulations with varying wind.

Primary production due to nitrate uptake

The primary production rate due to nitrate uptake as a function of time is shown in Figure 7.29. The nitrate uptake rate shows only slightly elevated values during the wind event. During the wind event there are high ammonium concentrations in the euphotic zone, inhibiting nitrate uptake. The maximum nitrate uptake rates are found after the end of the upwelling event, once the upwelled ammonium has been

assimilated by the phytoplankton and the ammonium concentration is low enough to allow nitrate to be taken up.

Zooplankton grazing

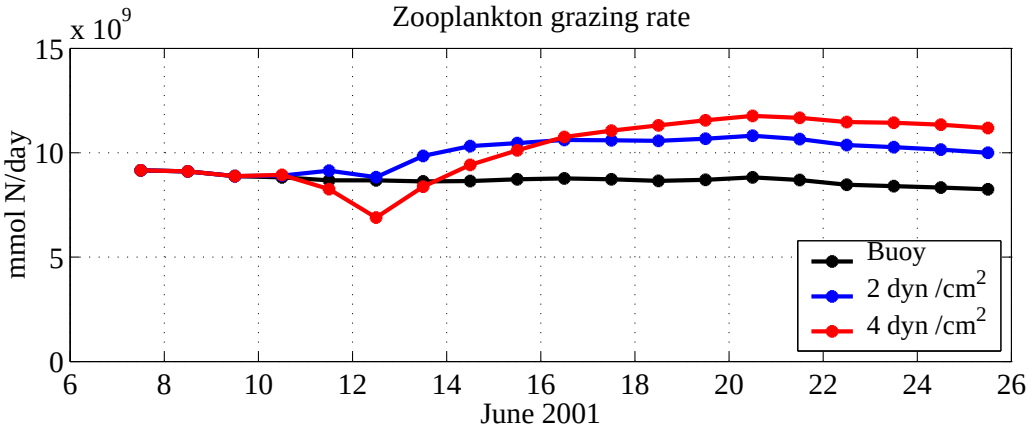

Figure 7.30: Zooplankton grazing rate in the euphotic zone.

Figure 7.30 shows the total grazing rate in the euphotic zone. For the 4 dyn/cm^2 the zooplankton grazing rate decreases throughout the upwelling event. On June 10 the grazing rate is approximately $9.0 \cdot 10^9$ mmol N/day, which corresponds to a decrease of 22%. The reason for the low grazing rate is the decrease in zooplankton stock during the wind event, when a fraction of the zooplankton are advected out of Massachusetts Bay. This decrease in grazing rate give the phytoplankton a growth advantage at the start of the bloom that follows the wind event. For the 2 dyn/cm^2 wind event there is only a small decrease in zooplankton grazing rate. On June 11 the grazing rate shows a small increase, followed by a small dip on June 12. However, the grazing rate does not fall below the (reference) value of the buoy simulation.

Summary

Figure 7.31, 7.32, and 7.33 show the balance of terms integrated over June 10-13 in the euphotic zone and its boundaries. They quantify the advective and biological dynamical results in this section.

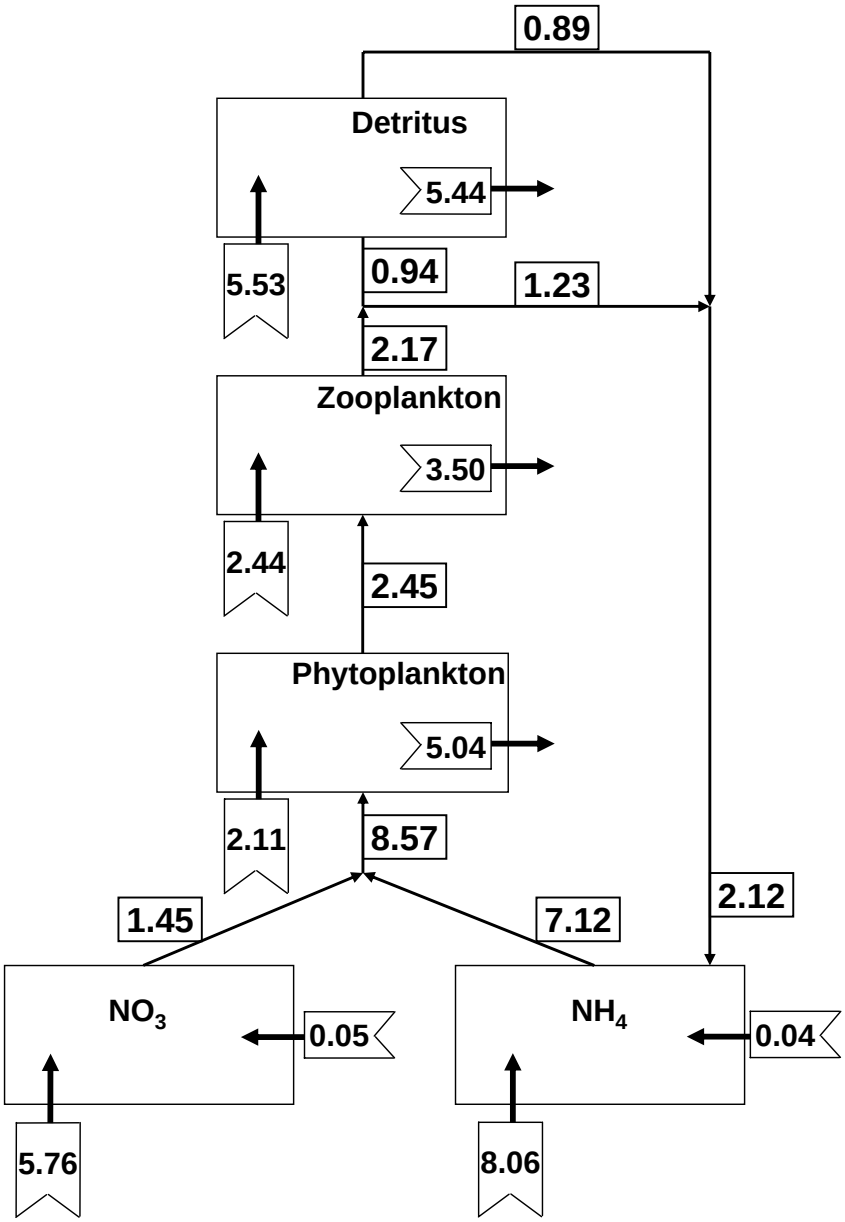

Figure 7.31: Advective dominant balance of terms in the euphotic zone, June 10-13, for 4 dyn/cm^2 wind event.

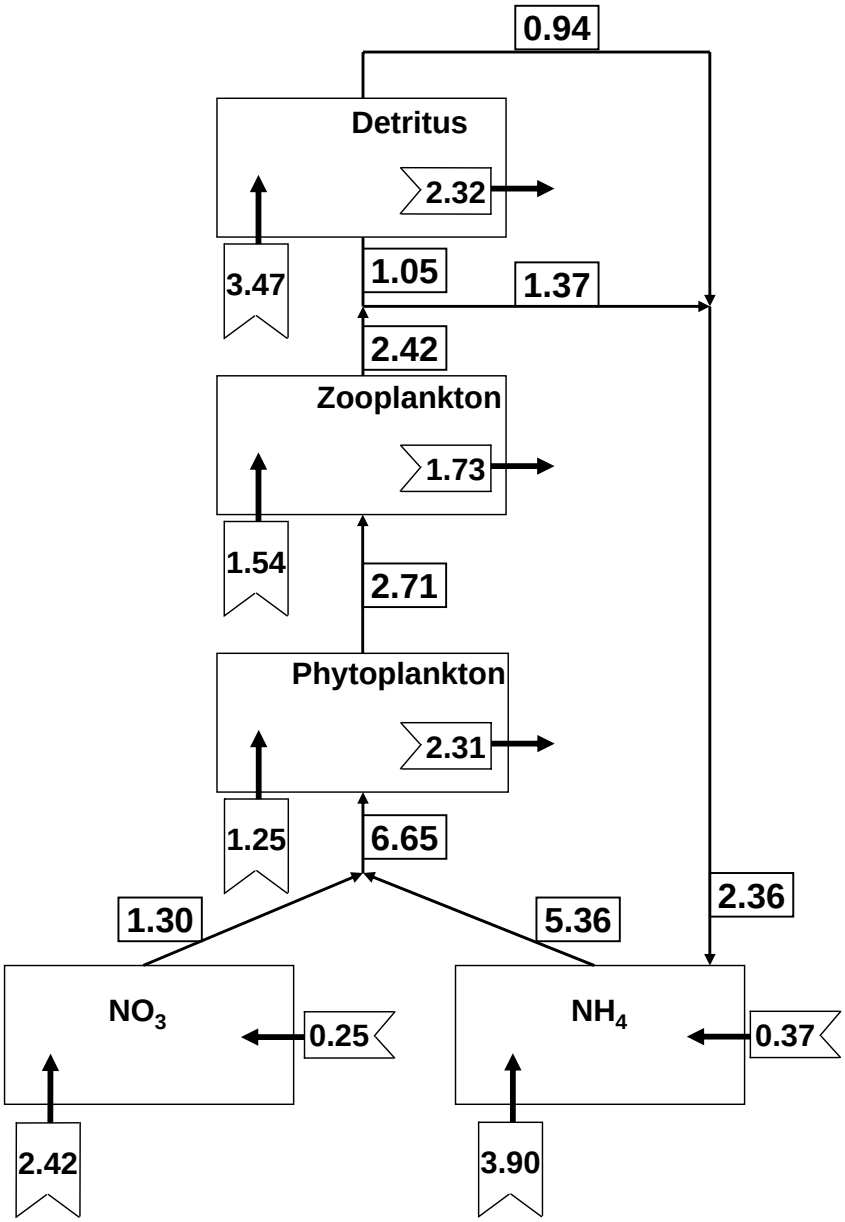

Figure 7.32: Advective dominant balance of terms in the euphotic zone, June 10-13, for 2 dyn/cm^2 wind event.

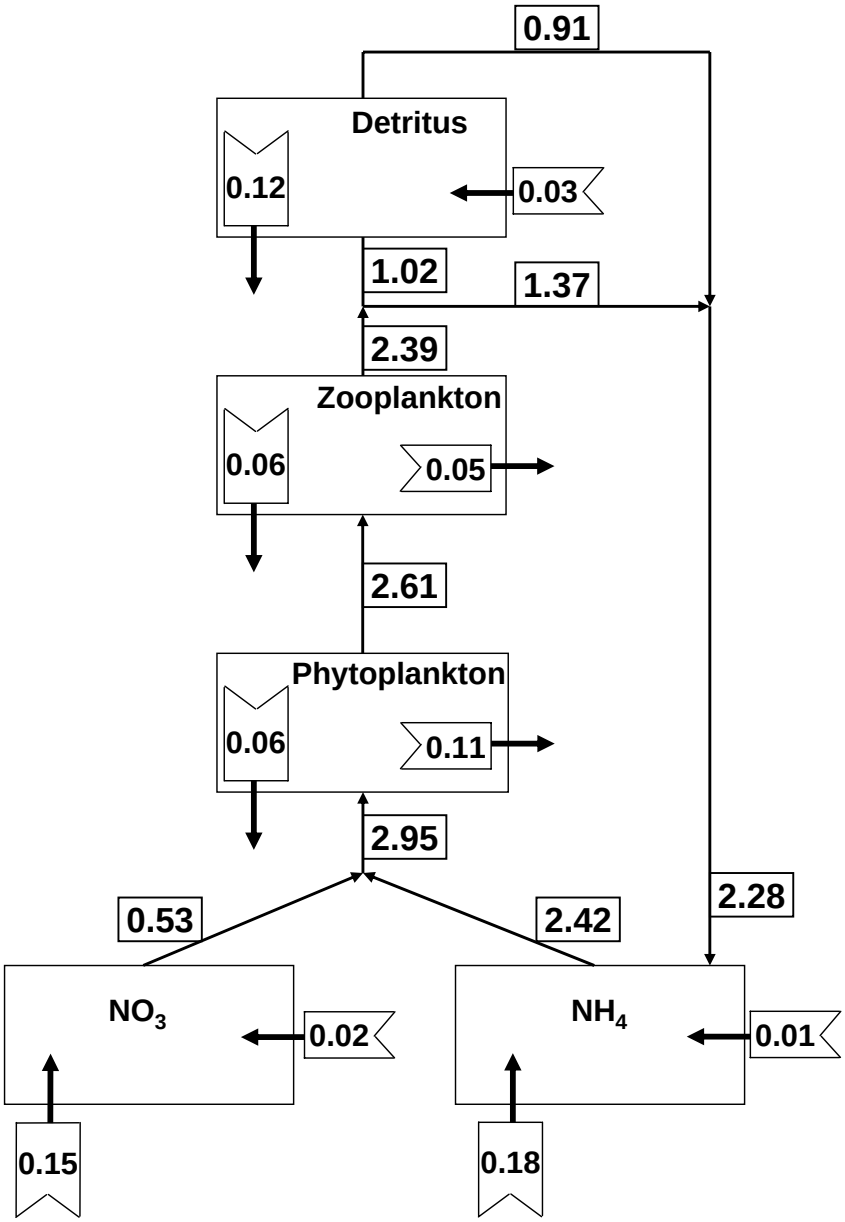

Figure 7.33: Advective dominant balance of terms in the euphotic zone, June 10-13, for Buoy winds.

7.4 Biologically dominant changes June 13-26

After the end of the upwelling event the advective fluxes of nitrogen in and out of the euphotic zone are very small. From the end of the wind event to the end of the simulation changes in biological variables are mainly due to biological processes. This sections deals with the biological variables and processes after the wind event.

Total Primary Production

The total primary production rate (see Figure 7.27) already has high values during the upwelling event. Throughout the upwelling event the nutrient uptake rate increases and reaches its maximum value at the end of the event. The maximum nutrient uptake rate for the 4 dyn/cm^2 event is about $7.0 \cdot 10^{10}$ mmol N/day and occurs on June 13. This is a large increase in uptake rates compared to the buoy wind simulation that has, on average, a nutrient uptake of $2.5 \cdot 10^{10}$ mmol N/day. After June 13 the total primary production decreases quickly for 4-5 days and on June 17 the rates are back close to non-event values. The primary production rate keeps decreasing for about 5 more days and by the end of the simulation on June 26 the primary production rates for the three simulations are almost the same.

The primary production rate for the 2 dyn/cm^2 simulation is similar to the stronger event, not only during the upwelling event, but all through the decay. Both wind events lead to nutrient concentrations well above the half-saturation constants so that although the weaker event brings less nutrient into the euphotic zone, the phytoplankton are nutrient saturated. The maximum primary production rate for the 2 dyn/cm^2 event is about $6.0 \cdot 10^{10}$ mmol N/day. The decline of the primary

production rate for the 2 dyn/cm^2 happens on the same time scale as for the stronger event. The main difference between the two wind simulations is that the 2 dyn/cm^2 reaches it maximum rate on June 12 while the stronger event reaches its maximum a day later. The difference between the two wind event simulations is the biggest on June 13 when the primary production rate for the 2 dyn/cm^2 is $5.0 \cdot 10^{10}$ mmol N/day and for the 4 dyn/cm^2 $7.0 \cdot 10^{10}$ mmol N/day. The difference is due to that on June 13 the 4 dyn/cm^2 has much higher nitrate uptake than the weaker event.

Nitrate

As seen earlier, only a small amount of nitrate is assimilated during the upwelling event (see Figure 7.23). The nitrate uptake rate is high after the end of the wind event until enough of the upwelled ammonium has been taken up to weaken the ammonium inhibition. For the 4 dyn/cm^2 event the nitrate uptake rate reaches $2.4 \cdot 10^{10}$ mmol N/day, which is a three-fold increase compared to the buoy wind simulation. The uptake rates remain high, but declining, for about 5 days. It takes another 5 days for the upwelling signal to disappear from the nitrate uptake rate. After the wind event the nitrate in the 2 dyn/cm^2 simulation has lower uptake rates but takes the same time, about 10 days, to reach non-wind event (buoy) values.

After the wind event the nitrate concentrations decrease slowly due to uptake by the phytoplankton (see above). There is a quick decrease of nitrate for 10 days following the end of the wind event, which corresponds to the time when the nitrate uptake rates are high. By the end of the simulation on June 26 the nitrate concentration for the wind event simulations is still higher than for the buoy wind simulation.

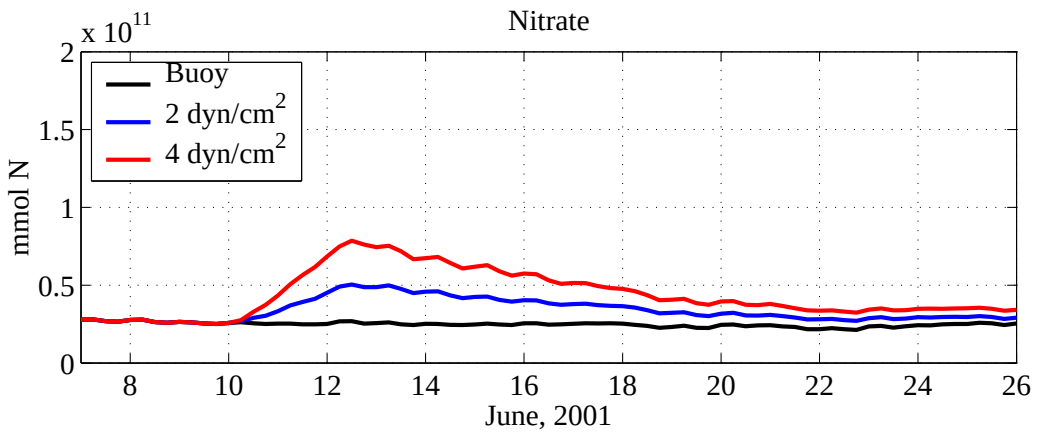

Figure 7.34: Total nitrate (mmol N) in the euphotic zone for simulations with real winds, 2 dyn/cm^2 wind event and 4 dyn/cm^2 wind event.

Ammonium

The ammonium uptake rate peaks on June 12, the last day of the wind event (see Figure 7.28). The maximum ammonium uptake rate for the 4 dyn/cm^2 event is about $6.0 \cdot 10^{10}$ mmol N/day. After the wind event the ammonium uptakes remains high for 5 days. Four days later there is barely any difference between the wind event simulations and the buoy simulation. The ammonium uptake rate for the 2 dyn/cm^2 event is similar to the stronger wind event due to saturated ammonium concentrations.

The ammonium that is brought into the euphotic zone during the upwelling event is quickly assimilated by the phytoplankton (see Figure 7.35). About half of the ammonium brought in is consumed during the wind event. The reminder is taken up within 4 days after the end of the wind event. On June 17, the total amount of ammonium in the euphotic zone is the same for the wind event and buoy simulations. Compare this with the nitrate distribution where 8-10 days after the end of the

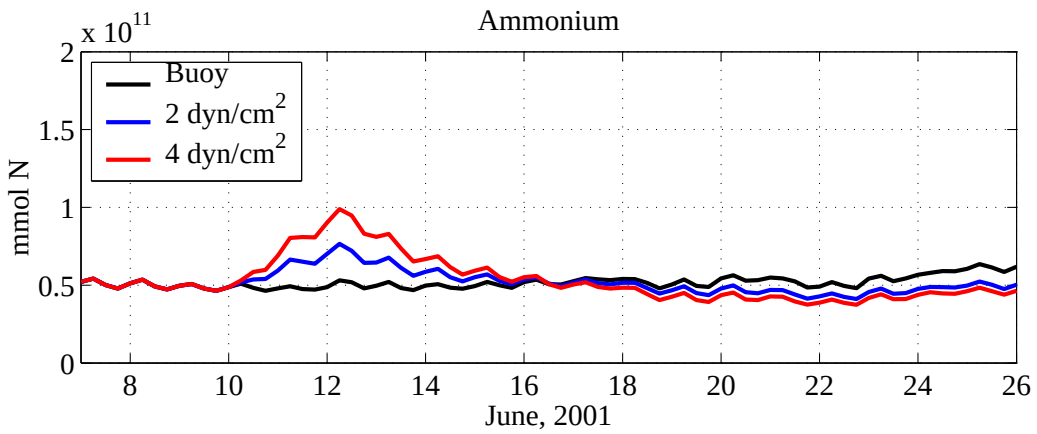

Figure 7.35: Total ammonium (mmol N) in the euphotic zone for simulations with real winds, 2 dyn/cm^2 wind event and 4 dyn/cm^2 wind event.

wind event there are elevated nitrate concentrations in the euphotic zone due to the upwelling event. It is interesting to notice that beyond June 17 the ammonium for the wind event simulations continues to decrease. During and after the wind event the phytoplankton stock in the euphotic zone is substantially higher than for the buoy wind simulation. As the nutrient uptake rates are proportional to the phytoplankton concentrations there is a higher ammonium uptake rate and the ammonium keeps decreasing for the wind event simulations.

Phytoplankton

In spite of high primary production rates during the wind event there is only a small increase of phytoplankton as a fraction is lost out of Massachusetts Bay due to advection. After the wind event the phytoplankton keep increasing. For the 4 dyn/cm^2 event the maximum phytoplankton stock is $1.7 \cdot 10^{11}$ mmol N and occurs on June 17. From then on there is a very slow decay of the phytoplankton stock in the euphotic zone. Two weeks after the end of the wind event there are still elevated

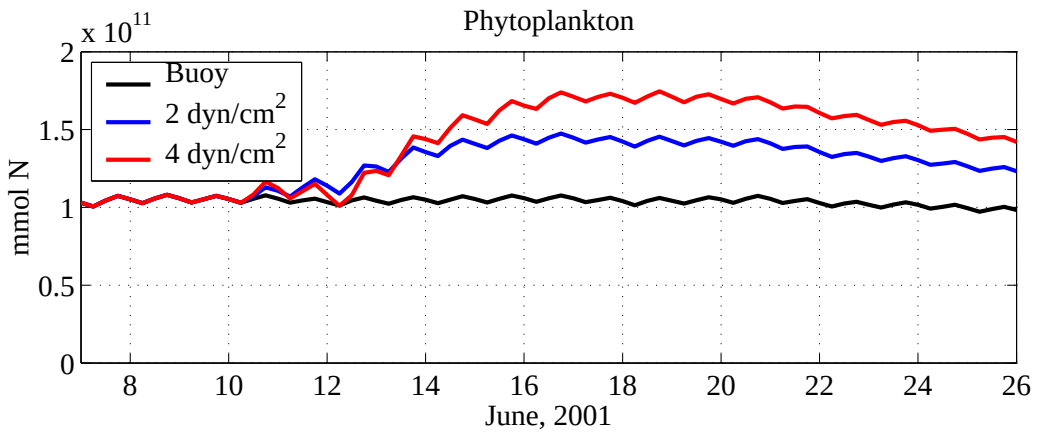

Figure 7.36: Total phytoplankton (mmol N) in the euphotic zone for simulations with real winds, 2 dyn/cm^2 wind event and 4 dyn/cm^2 wind event.

phytoplankton biomass values.

Throughout the upwelling event the phytoplankton biomass for the 2 dyn/cm^2 simulation differs little from the simulation with the stronger wind event. For the weaker wind event the maximum phytoplankton value is $1.4 \cdot 10^{11}$ mmol N and occurs on June 15, which is a day earlier. More ammonium and nitrate enters the euphotic zone during the stronger wind event. As the phytoplankton are nutrient saturated it will take longer for them to consume the new nutrients, thus reaching the maximum value later.

Zooplankton

The zooplankton grazing rate has its minimum value during the upwelling event (see Figure 7.30). From the end of the wind event to the end of the simulation the grazing rate remains elevated. Right after the wind event the grazing rate has a large increase. For the 4 dyn/cm^2 event the grazing rate increases from about $0.7 \cdot 10^{10}$ mmol N/day to $1.2 \cdot 10^{10}$ mmol N/day in only four days, from June 12 to 16. The

grazing rate keeps increasing for four more days but at a much smaller rate. During the last three days of the simulation there is a small decrease in the grazing rate.

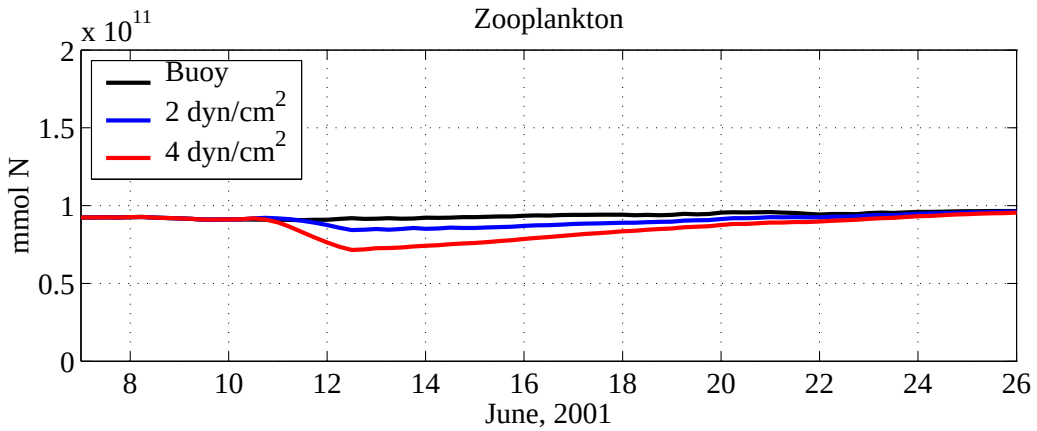

Figure 7.37: Total zooplankton (mmol N) in the euphotic zone for simulations with real winds, 2 dyn/cm^2 wind event and 4 dyn/cm^2 wind event.

During the wind event the zooplankton are lost, advected out of the euphotic zone (see Figure 7.37). For the 4 dyn/cm^2 this loss is 22% of the biomass. After the wind event, as the phytoplankton biomass increases, the grazing rate increases. The zooplankton biomass increases steadily till the end of the simulation. Within two weeks after the end of the wind event the zooplankton biomass has recovered.

For the 4 dyn/cm^2 event simulation the increase of zooplankton is on average $0.016 \cdot 10^{10}$ mmol N/day for June 13-26 which is twice as high as for the 2 dyn/cm^2 event which has a rate of $0.008 \cdot 10^{10}$ mmol N/day. The grazing rate is proportional to the zooplankton biomass and depends on the phytoplankton stock. Despite the 4 dyn/cm^2 having lower zooplankton biomass the grazing rate is higher. For the 4 dyn/cm^2 event the phytoplankton biomass is much larger. The grazing term is given by $R_m(1 - e^{-\lambda P})Z$, which for low (relative to the Ivlev constant) values of phytoplankton depends linearly on the phytoplankton. After the wind event the

zooplankton are phytoplankton limited. This makes the Ivlev constant a sensitive parameter.

Detritus

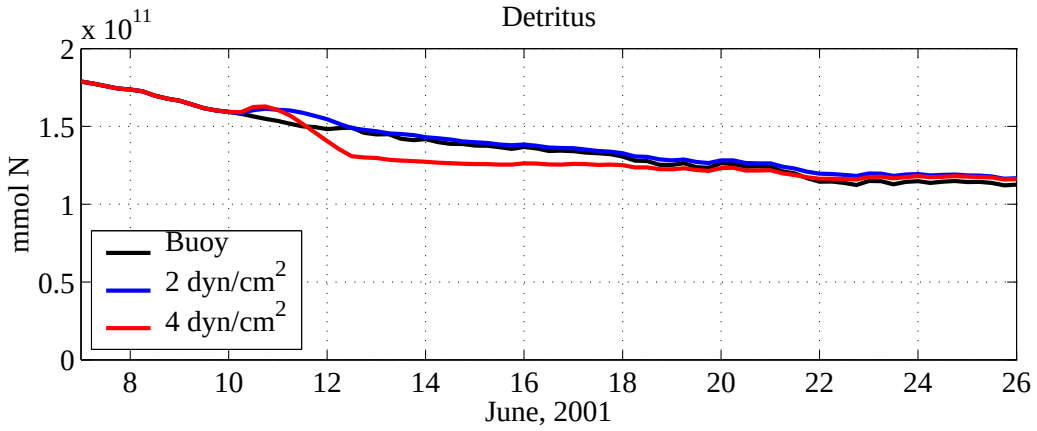

Figure 7.38: Total detritus (mmol N) in the euphotic zone for simulations with real winds, 2 dyn/cm^2 wind event and 4 dyn/cm^2 wind event.

The effect of the upwelling event on the detritus distribution is very local in time. The upward vertical velocities during the wind event slow reverses the sinking of detritus and brings detritus into the euphotic zone. On June 20 the upwelling signal in the detritus has vanished. The biological processes involving detritus occur on a much slower timescale compared to primary production so the changes in detritus during the wind event have a small influence on the biological dynamics.

Summary

Figure 7.39, 7.40, and 7.41 show the balance of terms integrated over June 13-26 in the euphotic zone and its boundaries. They quantify the advective and biological dynamical results in this section.

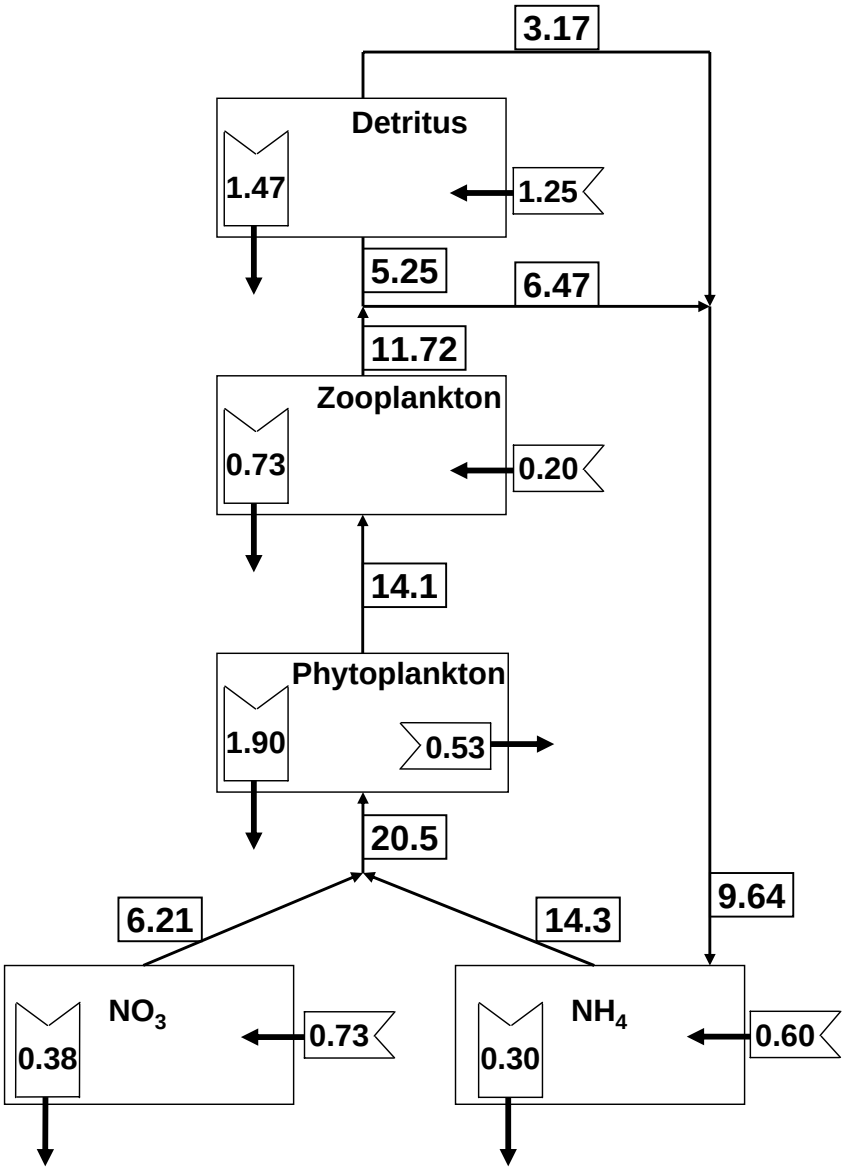

Figure 7.39: Biological dominant balance of terms in the euphotic zone, June 13-26, for 4 dyn/cm^2 wind event.

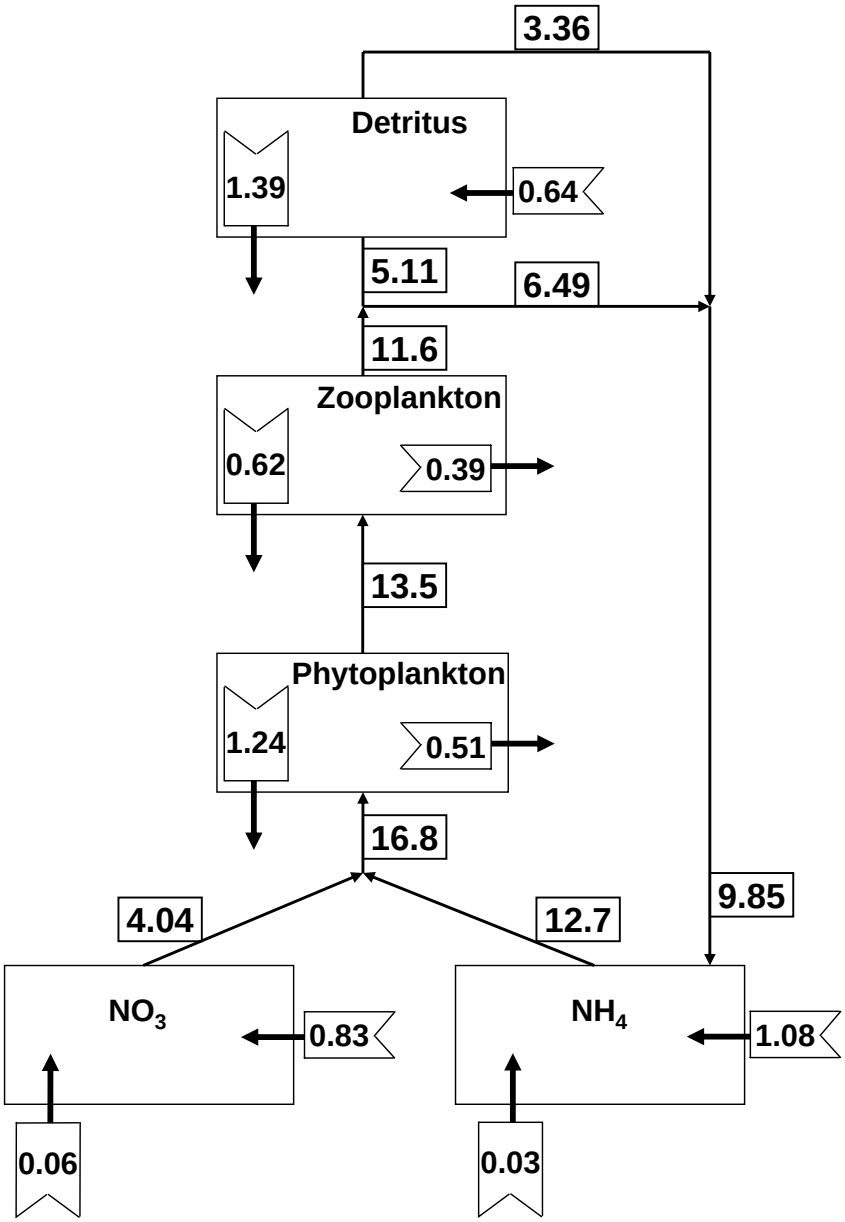

Figure 7.40: Biological dominant balance of terms in the euphotic zone, June 13-26, for 2 dyn/cm^2 wind event.

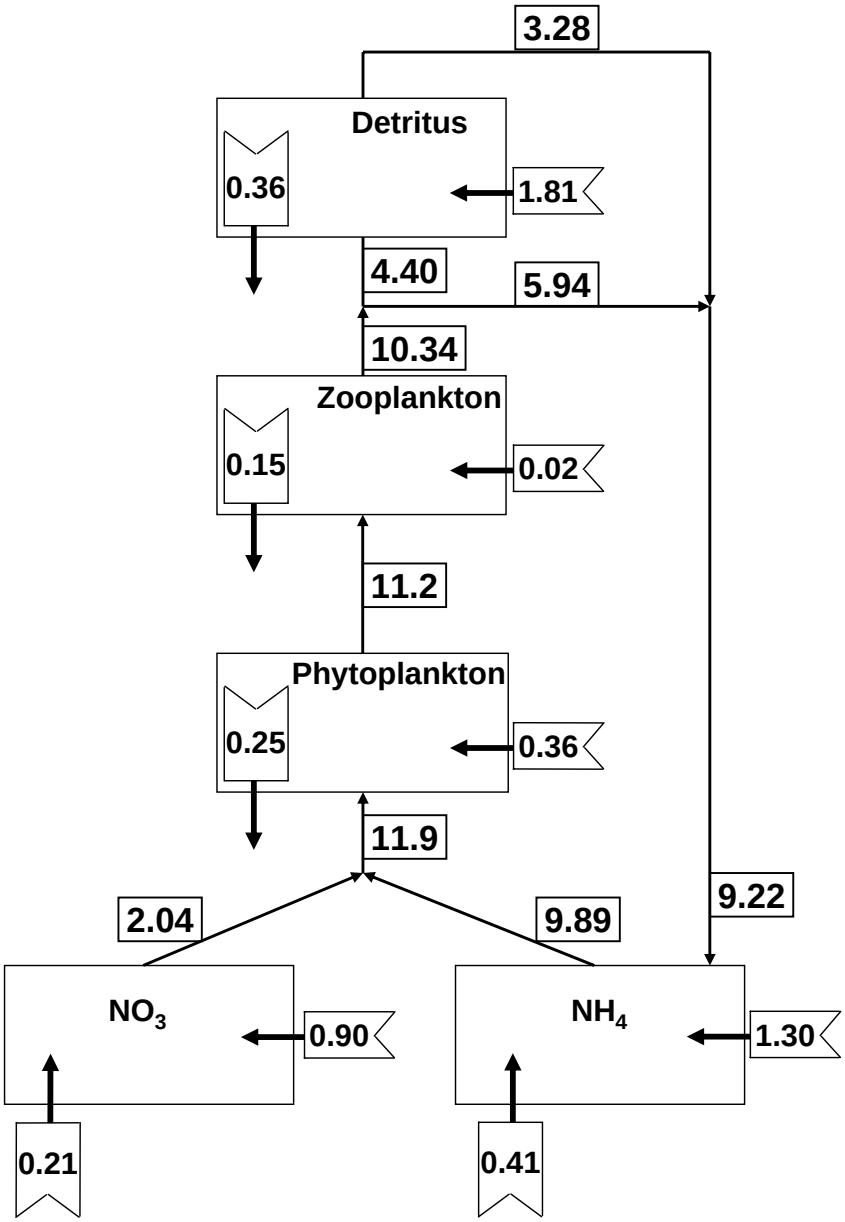

Figure 7.41: Biological dominant balance of terms in the euphotic zone, June 13-26, for Buoy winds.

7.5 Historical wind simulations

In Sections 7.1 through 7.4 simulations with data-based modeled wind events are described. These simulations provide a basic understanding of the biological response to upwelling events.

In this section an initial exploration of simulations with real historical winds is presented. From the 1985-2005 wind record the dynamically most interesting years are subjectively selected. Summers with either very strong (close to 4 dyn/cm^2) or long-lasting (more than 2 days) events are selected. Also years with multiple smaller events are selected. The dynamically interesting years are found to be 1985, 1989, 1990, 1991, 1997, and 2000.

Simulations are carried out combining the wind forcing from these years with other actual atmospheric forcing (heat flux, fresh water flux, and shortwave radiation) from 2001. The simulations start on May 15 and last three months. The same initialization is used as for the data-based and model wind event simulations.

For an initial study of these simulations the total volume integrated primary production rate in the euphotic zone is used as a measure of the strength of the biological response to the wind events. For each year a description of the wind is provided as well as a discussion on the resulting primary production rate. These simulations with real historical winds are to be considered as a first step in a more detailed study of upwelling events with real winds on a longer timescale.

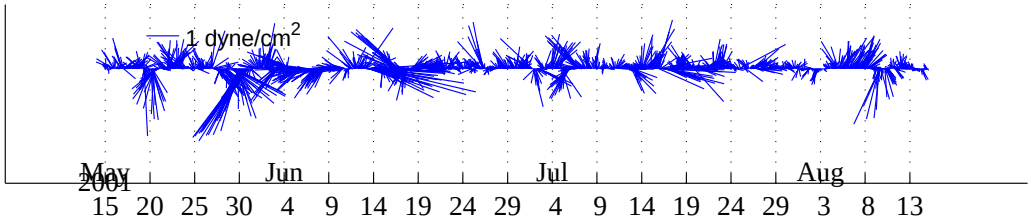

Figure 7.42: Wind vectors for summer 2001 in Massachusetts Bay.

Reference 2001

Figure 7.42 shows the wind vectors as measured by the NODC buoy in Massachusetts Bay for May 15 through August 15, 2001. A comparison with the 1985-2005 wind record shows that in 2001 the winds were weaker than usual. We use 2001 as reference case and compare the 2001 primary production rate with that from the dynamically interesting years.

1985

Figure 7.43 shows the wind vectors for the summer of 1985. The wind series from summer 1985 has three consecutive wind event on 5/25, 5/30 and 6/4. These three event all last about 2 days, have an average strength of 1 dyn/cm^2, and peak magnitudes of about 2 dyn/cm^2. The 5/30 wind event is somewhat weaker with a peak magnitude of 1.5 dyn/cm^2. All of these wind events are weaker than the designed 2 dyn/cm^2 event.

Figure 7.44 shows the the total volume integrated primary production rate in the euphotic zone in Massachusetts Bay. The primary production rate for 2001 is also plotted. The two strongest wind events in the timeseries, 5/25 and 6/4 are evident

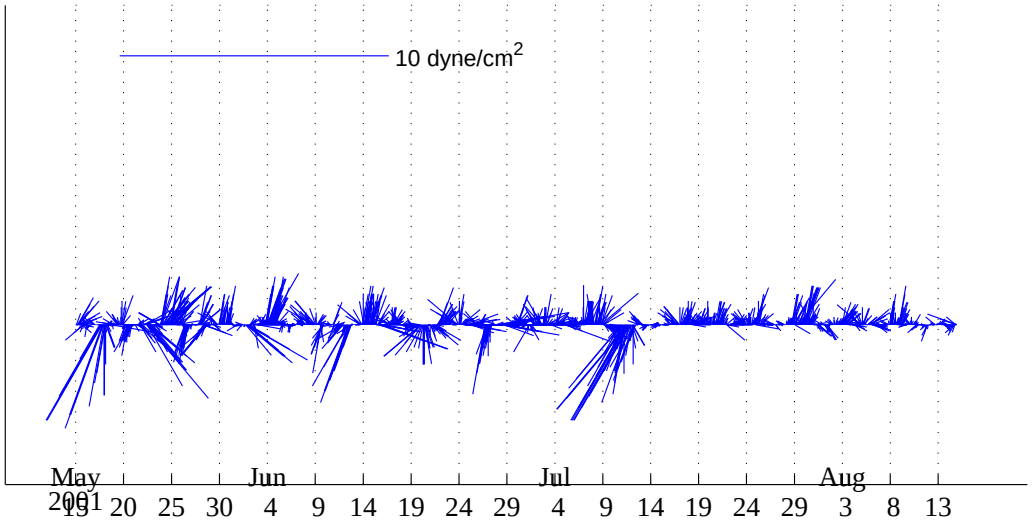

Figure 7.43: Wind vectors for summer 1985.

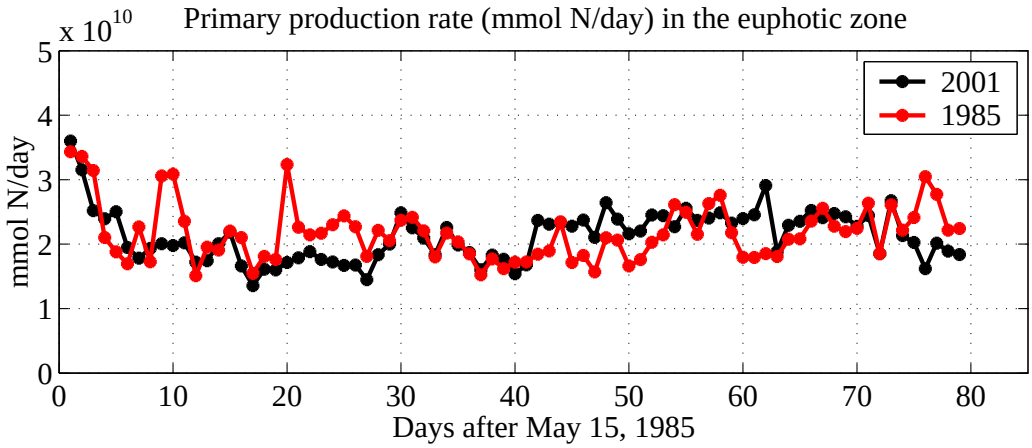

Figure 7.44: Primary production rate (mmol N/day) in the euphotic zone for summer 1985 in Massachusetts Bay.

in the primary production rate. During these days primary production rates reach just above $3.0 \cdot 10^{10}$ mmol N/day in the Bay. Compare this value with the 2 dyn/cm^2 2-day feature wind event which resulted in a maximum total primary production rate of $6.0 \cdot 10^{10}$ mmol N/day.

1989

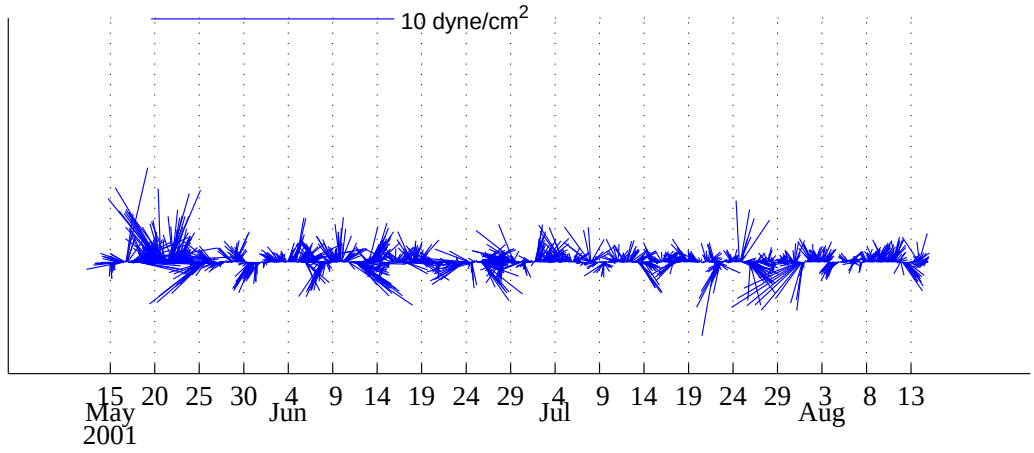

Figure 7.45: Wind vectors for summer 1989 in Massachusetts Bay.

The wind vectors for the summer of 1989 are shown in Figure 7.45. The 1989 wind timeseries includes the strongest wind event from 1985 to 2005. A strong wind event starts on 5/19 and lasts 4 days, during which the strength of the wind is at least 1.5 dyn/cm^2 and has peaks of about 3 dyn/cm^2. This event is followed 2.5 weeks later by 3 small wind events, each lasting a day with an average strength of 1 dyn/cm^2.

Figure 7.46 shows the primary production rate for summer 1989. The largest difference with the 2001 primary production rate occurs at the beginning of simulation during the very strong event. This wind event results in a maximum primary production rate of $6.0 \cdot 10^{10}$ mmol N/day. Compared to the 2001 primary production rate this is an 3-fold increase. This wind event results in elevated primary production rates for 10 days! The smaller wind events are also visible in the primary production as elevated rates during June. Due to their weakness the primary production rate remains below $3.0 \cdot 10^{10}$ mmol N/day during this time.

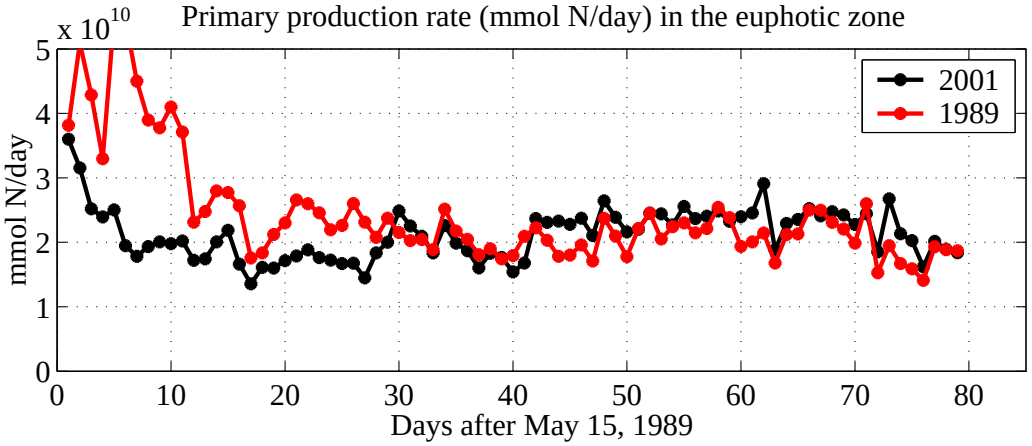

Figure 7.46: Primary production rate (mmol N/day) in the euphotic zone for summer 1989.

1990

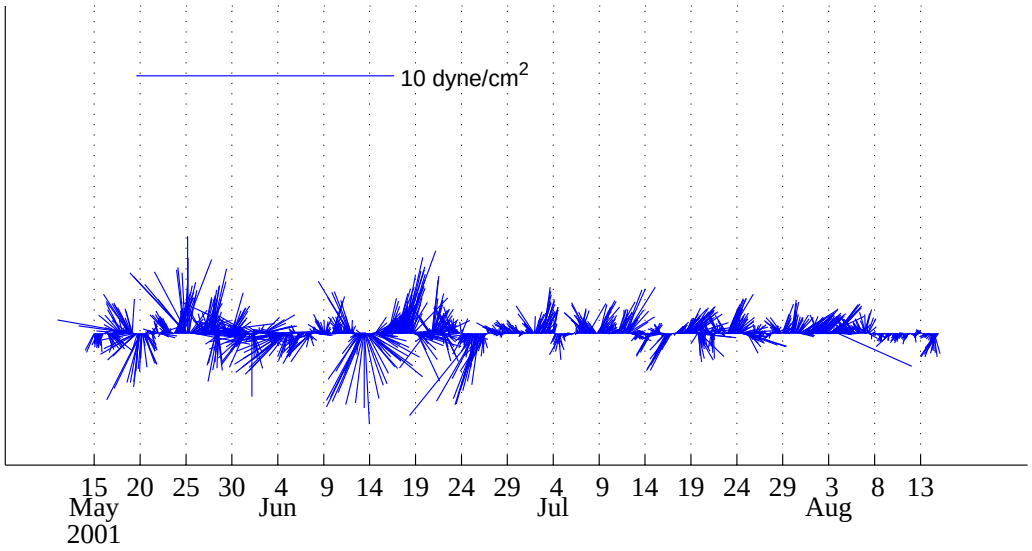

Figure 7.47: Wind vectors for summer 1990 in Massachusetts Bay.

The wind vectors for summer 1990 are shown in Figure 7.47. During the summer of 1990 there are two wind events of interest. On 5/22 there is a strong wind event which last two days. For one day the strength of the wind is above 2 dyn/cm^2 and

reaches briefly 4 dyn/cm^2. On 6/14 there is a four-day long event with sustained winds of at least 1 dyn/cm^2 and a maximum value of 4 dyn/cm^2.

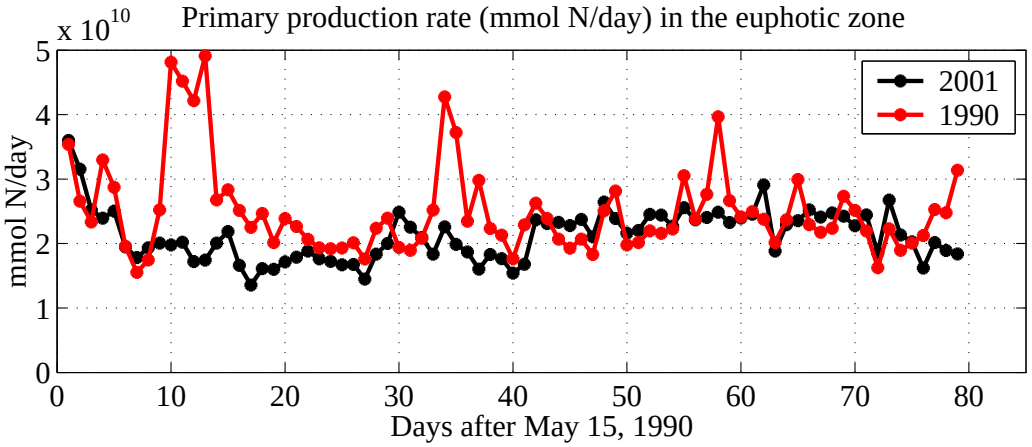

Figure 7.48: Primary production rate (mmol N/day) in the euphotic zone for summer 1990.

Figure 7.48 shows the primary production rate for 1990. The two wind events described above are clearly observed in the primary production rate of 1990. The first wind events leads to higher primary production rates for 4 days with values as high as $5.0 \cdot 10^{10}$ mmol N/day. The second wind event results in higher primary production rates for two days only and values are approximately $4.0 \cdot 10^{10}$ mmol N/day.

1991

The wind vectors for 1991 are shown in Figure 7.49. Starting 5/22 there are 3 weeks of small wind events. Each event lasts a day or less and reaches a peak magnitude of 2 dyn/cm^2. The gap between the wind events is on average 1 day. On 6/23 there is a 1-day wind event with a magnitude of 1.5 dyn/cm^2

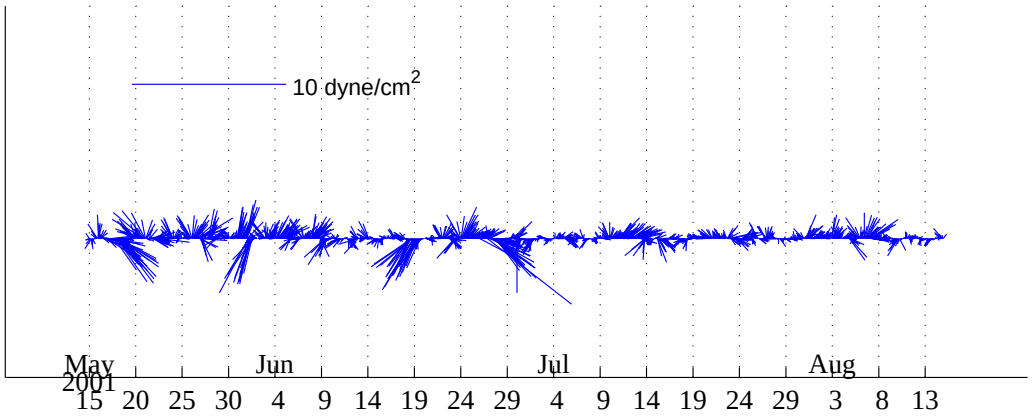

Figure 7.49: Wind vectors for summer 1991 in Massachusetts Bay.

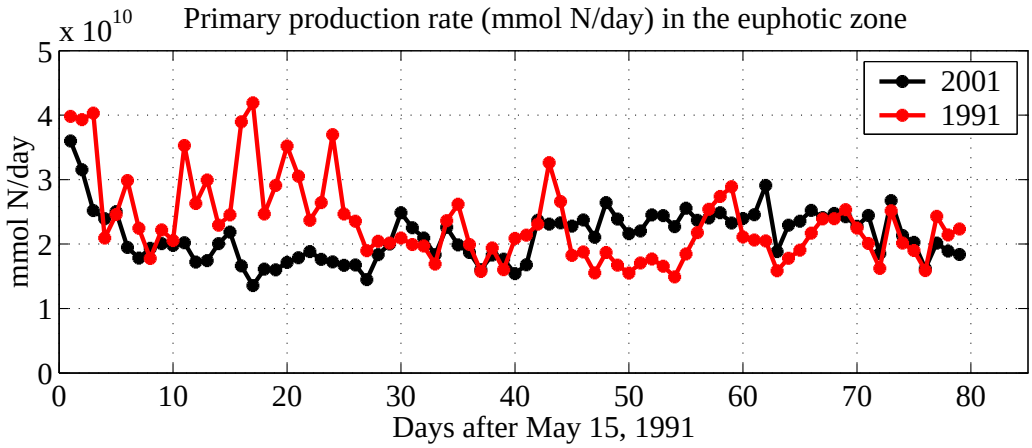

Figure 7.50: Primary production rate (mmol N/day) in the euphotic zone for summer 1991

Figure 7.50 shows the primary production rate for the summer of 1991. The three weeks with small wind events is evident in the primary production rate. During this time period the primary production rate is elevated and reaches values as high as $4.2 \cdot 10^{10}$ mmol N/day.

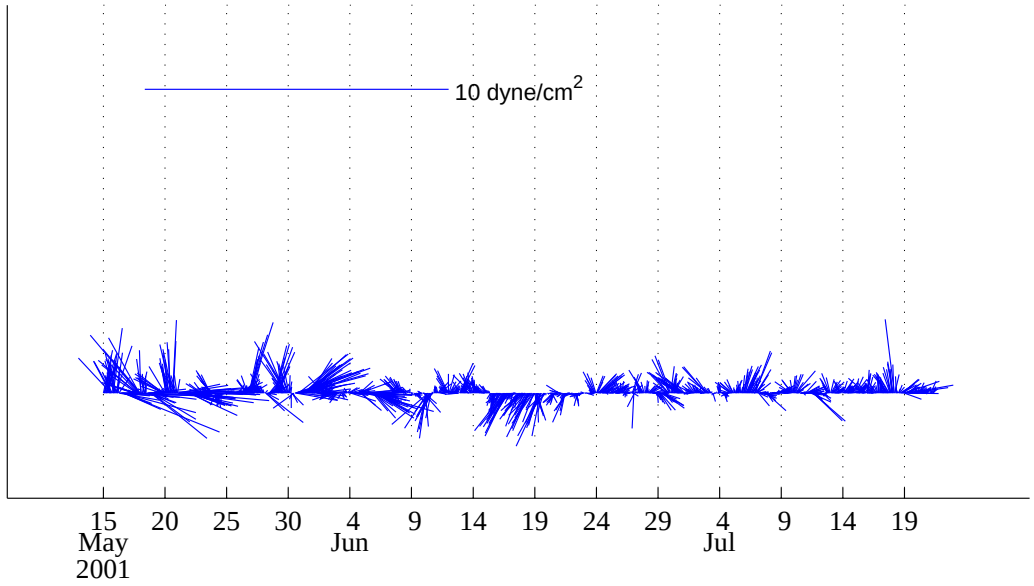

Figure 7.51: Wind vectors for summer 1997 in Massachusetts Bay.

1997

Figure 7.51 shows the winds during summer 1997. Most of the summer was dull except for May when there are two sets of wind events 5 days apart. Both of these sets consist of three 1-1.5-day long events with average magnitude of 1 dyn/cm^2 and peak values of 2 dyn/cm^2. The gap between the small events is less than a day.

The primary production rate for summer 1997 is shown in Figure 7.52. The first wind event (5/15) gives rise to elevated primary production rates for 7 days. The primary production rate peaks corresponds to the peaks in the wind event. The second set of wind events results in a weaker response. There is a graduate increase in the primary production rate with only one peak which corresponds to the last wind event. A strong downwelling event leads to a decrease in primary production over the summer months.

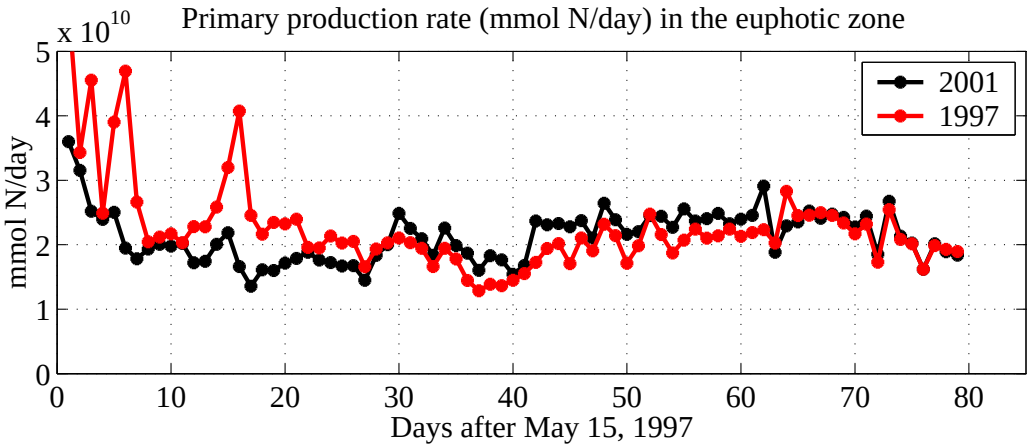

Figure 7.52: Primary production rate (mmol N/day) in the euphotic zone for summer 1997.

2000

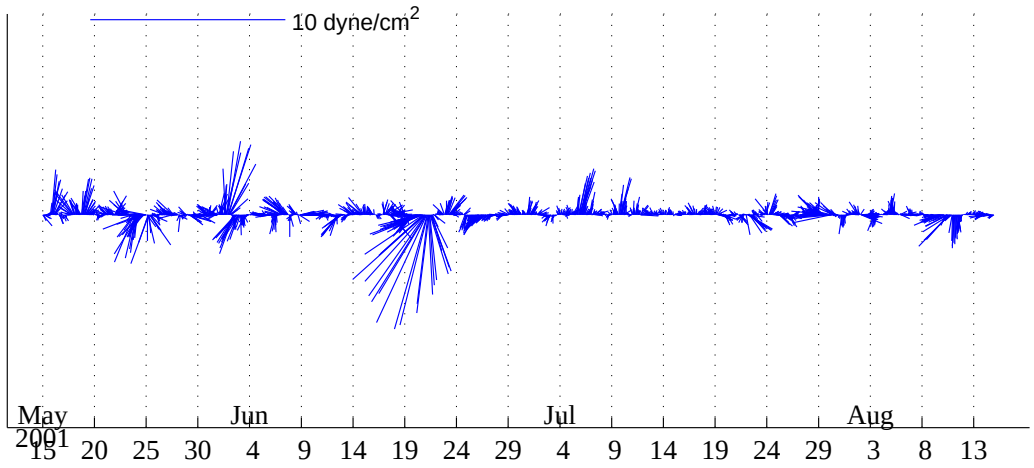

Figure 7.53: Wind vectors for summer 2000 in Massachusetts Bay.

The winds for summer 2000 are shown in Figure 7.53. The summer of 2000 starts with two 1 to 1.5-day events of peak magnitude of 2 dyn/cm^2. The second of these two events maintains a strength of 1 dyn/cm^2 for two days. On 6/1 there is a strong, 4 dyn/cm^2, event that lasts less than a day. On 7/5 there is a one-day wind event with a sustained magnitude of 2 dyn/cm^2.

The primary production rate for the summer of 2000 is shown in Figure 7.54. The two wind events at the start of the wind simulation results in elevated primary production rates with values above $4.0 \cdot 10^{10}$ mmol N/day. The two other wind events during the summer results in one-day peaks of primary production with values approximately $3.5 \cdot 10^{10}$ mmol N/day.

The conclusions of this chapter are found in Chapter 8.

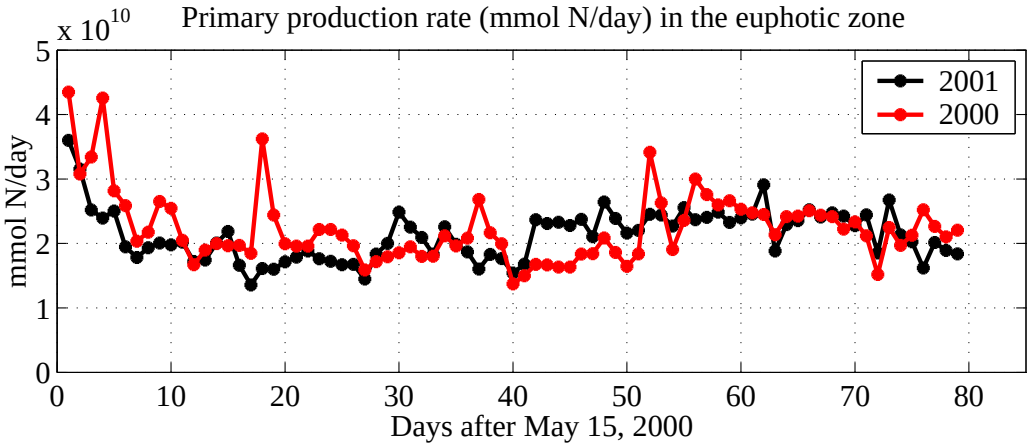

Figure 7.54: Primary production rate (mmol N/day) in the euphotic zone for summer 2000.

Chapter 8

Summary and conclusions

Introduction

- In this work the role of episodic wind events (storms) on the circulation and biological processes in Massachusetts Bay in early summer are studied. The winds in Massachusetts Bay are characterized by frequent changes in direction and magnitude. The box-like geometry of Massachusetts Bay and the varying direction of the winds mean that upwelling can happen anywhere along the coast on Massachusetts Bay. Here the focus is on southerly winds as they give rise to upwelling along the mainland coast, which is the longest one, and therefore have the largest impact on primary production. The importance of horizontal advection during upwelling events is a major focus of the analysis. Three-dimensional physical-biological simulations are carried out in Massachusetts Bay for June 6-26, 2001. During this time the ASCOT-01 experiment took place and data were collected for initialization, assimilation and biological parameter determination. The simulations are forced with three different kinds of winds

1) real winds from June 2001, 2) data-based strong feature model wind events and 3) real historical winds. The results of these simulations are summarized below.

- Massachusetts Bay is a semi-enclosed embayment adjacent to a large shallow shelf-sea and the processes studied here are anticipated to have more general applicability. The modeling approach and methods are designed to represent realistic physical-biological processes with (sub)mesoscale and mesoscale space and time scale resolution. Careful attention must be paid to the complex physical and biological interactions.

Issues in coupled physical-biological modeling

- To initialize the physical-biological simulation 3-dimensional fields of all the state variables are required. The observable physical and biological data is objectively analyzed to create initial fields. For the non-observable physical variables (e.g. vertical velocity) there are well-developed methods and fundamental equations to determine them based on the observable ones (commonly temperature and salinity). The initialization of non-observable biological variables is more difficult as no fundamental expressions exist between the observable and non-observable variables. A common approach is to assume that the non-observable variables are an empirical functional of observable physical and/or biological variables.

- In this work nitrate, ammonium and chlorophyll are the observable variables while phytoplankton, zooplankton and detritus are the non-observable ones.

Zooplankton and detritus data are available but are not of high enough resolution to use directly for initialization. Instead it is used as a guide for determining relationships between the observable and non-observable biological variables. With a fixed carbon to chlorophyll ratio of 80 mg C to 1 mg Chl the relationship between phytoplankton (P) and Chlorophyll (Chl) becomes $P = 1 \times Chl$. The zooplankton (Z) are assumed to be proportional to the phytoplankton. The ratio between these two variables is determined by comparing zooplankton tow data with average phytoplankton concentrations in the euphotic zone. This results in $Z = 1 \times P$. The detritus is also assumed to be proportional to the phytoplankton. The proportionality factor is determined using particulate organic nitrogen and phytoplankton data. The detritus (D) is set to $D = 2 \times P$.

- A challenging task in biological modeling is the determination of the model parameters. They have to be tuned for the particular geographical location, time of year and ecosystem characteristics. It is difficult to determine the biological parameters as measurements of biological processes in the ocean are not abundant and biological processes depend on the history of their environment.

- The nutrient, phytoplankton and zooplankton data collected during the ASCOT-01 experiment, to a first approximation do not show any temporal gradient, they remain stable. This implies that for each variable the biological sources are approximately balanced by the biological sinks. The phytoplankton biomass is maintained stable by a balance between nutrient uptake and zooplankton grazing. A balance between zooplankton growth and mortality keeps the zooplank-

ton biomass stable. The final set of biological model parameters are determined through model tuning guided by ASCOT-01 data and literature surveys taking into account the balance of terms described above.

Real 2001 wind simulation

- The real winds from June 2001 showed no strong or long-lasting wind event. The wind events that occurred resulted in weak upwelling events which affected mainly the euphotic zone and the region closest to the coast. Only small quantities of nutrients are upwelled from the aphotic zone during the upwelling events. The primary production does increase during the upwelling events but only by a small amount. Thus June 2001 was unfortunately not an adequate time to study upwelling processes.

Data-based strong modeled wind events

- The weak winds of June 2001 in Massachusetts Bay made it difficult to study the effects of wind events on the nutrients, biomass and biological processes. For this reason a feature model wind event was designed. The definition of a strong wind event is an event with a maximum wind stress of at least of 2 dyn/cm^2 and a duration of at least one day. Strong wind events are identified from a 20-year historical data set shown in an appendix. Two feature wind events are designed, one of 2 dyn/cm^2 and another one of 4 dyn/cm^2, both lasting 2 days. The maximum peak wind stress observed was 4 dyn/cm^2 and wind events lasted on average 2 days. The 2 dyn/cm^2 event was common in the data set. There

was no event that maintained 4 dyn/cm^2 for two days but it is, based on the strong events that do occur, reasonable. These winds are southerly and give rise to upwelling on the mainland coast of Massachusetts Bay.

Advective effects: See Figure 7.31-7.33

- The physical response to the southerly wind events in Massachusetts Bay is characterized by three processes: 1) Upwelling along the mainland coast, 2) large off-shore currents near the surface, and 3) on-shore currents deeper in the water column. The last point, the deep on-shore current, plays an important biological role in the upwelling process in Massachusetts Bay.

- During the upwelling event there is a deep on-shore current that advects Gulf of Maine water into Massachusetts Bay. In the open Gulf of Maine the nitrate concentration increases with depth. Gulf of Maine has higher nitrate concentrations than Massachusetts Bay and acts as a reservoir of nitrate. During the wind event, deep in the water column nitrate and, to a lesser extent, ammonium are advected into Massachusetts Bay.

- A strong upwelling event will not only upwell nitrate into the euphotic zone but it will also recharge the aphotic zone with nitrate. The strong, 4 dyn/cm^2, wind event leads to a a substantial increase of nitrate in the aphotic zone. While the moderately strong, 2 dyn/cm^2, results in only a small nitrate increase in the aphotic zone. Thus there is no net loss of nitrate in the aphotic zone during an upwelling event.

- The fact that it is nitrate that is mainly brought in is important as when nitrate is assimilated by the phytoplankton it becomes part of the foodweb. Compare with ammonium: a foodweb can be maintained by ammonium only as it is recycled.

Biological dynamics: See Figure 7.39-7.41

- The biological response to the wind event happens on two time scales. First, the nutrients and biomass are redistributed during the wind event mainly by advection which dominates biological dynamics. Then, after the end of the wind event, a phytoplankton bloom occurs and changes in nutrient and biomass are dominated by biological processes with only small advective effects.

- During the wind event nitrate and ammonium are upwelled near the coast into the euphotic zone. The resulting nutrient concentrations is well above the half-saturation constant for nutrient uptake which implies that the phytoplankton uptake is nutrient saturated.

- Phytoplankton and zooplankton are advected out of Massachusetts Bay at the surface by the strong off-shore currents during the wind event. However, during the upwelling event primary production rates are already elevated. This allows the phytoplankton losses due to advection to be more than balanced by nutrient uptake. Zooplankton grazing rate during the upwelling event, on the other hand, is too low to balance the advective losses. The zooplankton decrease by advective losses during the wind event gives the phytoplankton an advantage at the start of the bloom that follows the upwelling event.

- After the wind event there is a phytoplankton bloom. The upwelled ammonium is taken up on a time scale of 4-5 days. The new nitrate is taken up once the ammonium concentration decreases. Phytoplankton peak a few days after the end of the wind event. Two weeks after the end of the wind event, phytoplankton concentrations are still higher than for the reference simulation. At this point the phytoplankton biomass is decreasing due to zooplankton grazing. The zooplankton recover quickly from the advective losses during the wind event. Increasing grazing rates leads to a recovery of zooplankton biomass on a time scale of 10 days and thereafter increase.

Real historical winds

- Simulations are also carried out using real historical winds. The dynamically most interesting summers from the 1985-2005 wind data set are selected. The simulations use the initialization from 2001 and the atmospheric forcing, except for the wind, from 2001.

- The total primary production rate is used as a measure of the strength of the biological response to the wind events. Table 8.1 summarizes this results. It shows the total amount of nitrogen taken up by the phytoplankton for the duration of the simulation (May 15-August 15) as well as the difference relative to the primary production of 2001. The last column shows the percentage increase of primary production relative to 2001.

  For three simulations, 1989, 1990, and 1991, the total primary production is at least 10% higher than in 2001. The wind events that lead to these high values

Year	Total PP	$PP_{year} - PP_{2001}$	% increase
1985	0.91	0.03	3
1989	1.00	0.12	14
1990	1.04	0.16	18
1991	0.97	0.09	10
1997	0.94	0.06	7
2000	0.93	0.05	6
2001	0.88	-	-

Table 8.1: Total primary production (PP) for May 15-Aug15 and difference relative to primary production relative to 2001. The units are: 10^{12} mmol N

are

1990 Two strong wind events with peaks of 4 dyn/cm.

1989 One strong event that lasts four days.

1991 3 weeks of weak wind events.

- The winds from 1985, 1997, and 200 resulted in primary production values close to the reference value (2001). 1985 and 1997 were summers when there are 2-3 wind events close in time. Each event lasts 1-2 days and reach peak magnitudes of 2 dyn/cm^2. Despite their closeness in time they do not play a major role in the summer primary production. In 2001 only one strong event occurred.

Research issues

- Resulting primary production during the wind event must be put in context. At this time we are able to compare areal primary production rate (mmol N/m^2/day). The maximum primary production rate during the wind event is approximately equal to the maximum rate during the spring bloom. A more

complete comparison needs to take into account the duration and spatial coverage of spring bloom and the annual sequence of wind events.

- Further analysis of the primary production includes looking at the annual budget and determining what fraction of it is due to the spring bloom, what fraction is due to all the wind events within a year and what fraction is due to the background primary production.

- A relevant question that needs to be answered in the future is whether a primary production burst due to a wind event has a significant effect on higher trophic levels, specially commercial fish. This question can be addressed by initially analyzing the fate of the quadratic mortality losses of zooplankton (recall that quadratic mortality represent losses to higher trophic levels).

- Massachusetts Bay is an embayment connected to a shelf-sea (Gulf of Maine) which allows for the particular upwelling and horizontal transport patterns described above. An interesting future research topic would be to determine what geometries and topography in bays allow for this type of nitrate influx to occur and to explore embayments in the global coastal ocean analogous to Massachusetts Bay.

Bibliography

[1] L. A. Anderson and A. R. Robinson. Physical and biological modeling in the Gulf Stream region: II. physical and biological processes. *Deep-Sea Res. Part I - Oceanographic Research Papers*, 48(5):1139–1168, 2001.

[2] L. A. Anderson, A. R. Robinson, and C. J. Lozano. Physical and biological modeling in the Gulf Stream region: I. data assimilation methodology. *Deep-Sea Res. Part I - Oceanographic Research Papers*, 47(10):1787–1827, 2000.

[3] K. Bendschneider and R.J. Robinson. New spectrophotometric determination of nitrite in seawater. *J. Mar. Res.*, 11:87–96, 1952.

[4] S.T. Besiktepe, P.F.J. Lermusiaux, and A.R. Robinson. Coupled physical and biochemical data driven simulations of Massachusetts Bay in late summer: real-time and post-cruise data assimilation. *J. of Mar. Sys.*, 40:171–212., 2003. In "The use of data assimilation in coupled hydrodynamic, ecological and bio-geochemical models of the oceans", M. Gregoire, P. Brasseur and P.F.J. Lermusiaux (Eds.)
http://people.deas.harvard.edu/ pierrel/Papers/besiktepe_pfjl_arr_jms03.pdf.

[5] R.R. Bidigare and M.E. Ondrusek. Spatial and temporal variability of phytoplankton pigment distributions in the central equatorial Pacific Ocean. *Deep-Sea Res. II*, 43:809–833, 1996.

[6] Edwards. C.A., H.P. Batchelder, and T.P. Powell. Modeling microzooplankton and macrozooplankton dynamics within a coastal upwelling system. *J. Plank. Res.*, 22(9):1619–1648, 2000.

[7] M.-E. Carr. A numerical study of the effect of periodic nutrient supply on pathways of carbon in a coastal upwelling regime. *J. Plank. Res.*, 20(3):491–516, 1998.

[8] E. F. Carter and A. R. Robinson. Analysis models for the estimation of oceanic fields. *Journal of Atmospheric and Oceanic Technology*, 4:49–74, 1987.

[9] F. Chai, R.C. Dugdale, T.-H. Peng, F.P. Wilkerson, and R.T. Barber. One-dimensional ecosystem model of the equatorial Pacific upwelling system. Part I: model development and silicon and nitrogen cycle. *Deep-Sea Res. II*, 49:2713–2745, 2002.

[10] B. Cushman-Roisin. *Introduction to Geophysical Fluid Dynamics*. Prentice Hall, 1994.

[11] R. Daley. *Atmospheric data analysis*, volume 2 of *Cambridge atmospheric and space science series*. Cambridge University Press, Cambridge, 1991.

[12] V.W. Ekman. On the influence of the earth's rotation on ocean-currents. *Arkiv For Matematik, Astronomi och Fysik*, 2(11):1–53, 1905.

[13] R.W. Eppley and B.J. Peterson. Particulate organic matter flux and planktonic new production in the deep ocean. *Nature*, 282:677–680, 1979.

[14] M. J. R. Fasham and G. T. Evans. The use of optimization techniques to model marine ecosystem dynamics at the JGOFS station. *Phil. Trans. R. Soc. Lond., Ser. B*, 348:203–209, 1995.

[15] M.J.R. Fasham, H.W. Ducklow, and S.M. McKelvie. A nitrogen-based model of plankton dynamics in the oceanic mixed layer. *J. Mar. Res.*, 48:591–639, 1990.

[16] M.G. Foy and J.T. Anderson. Marine plankton computer codes for the Northwest Atlantic Fisheries Centre. Technical Report 595, Can. Data Rep. Fish. Aquat. Sci., 1986.

[17] P.J.S. Franks, J.S. Wroblewski, and G.R. Flierl. Behavior of a simple plankton model with food-level acclimation by herbivores. *Marine Biology*, 91:121–129, 1986.

[18] E. E. Hofmann and A. M. Friedrichs. Predictive modeling for marine ecosystems. In M. N. Hill, Allan R. Robinson, James J. McCarthy, and Brian J. Rothschild, editors, *Biological-Physical Interactions in the Ocean*, volume 12 of *The Sea: The Global Coastal Ocean*. John Wiley and Sons, New York, 2002.

[19] E.E. Hofmann and J.W. Ambler. Plankton dynamics on the outer southeastern US continental shelf. Part II: a time-dependent model. *J. Mar. Res.*, 9:235–248, 1988.

[20] E.E. Hofmann and C.M. Lascara. Overview of interdisciplinary modeling for marine ecosystems. In K.H. Brink and A.R. Robinson, editors, *Processes and Methods*, volume 10 of *The Sea: The Global Coastal Ocean*, pages 507–540. John Wiley and Sons, New York, 1998.

[21] V.S. Ivlev. *Experimental ecology of the feeding of fishes.* Yale University Press, New Haven, 1955.

[22] A.A. Keller, C. Taylor, C. Oviatt, T. Dorrington, G. Holcombe, and L. Reed. Phytoplankton production patterns in Massachusetts Bay 1992–1994. *Marine Biology*, 138:1051–1062, 2001.

[23] J.T.O. Kirk. *Light and photosynthesis in aquatic ecosystems, 2nd ed.* Cambridge University Press, 1994.

[24] R.M. Kudela. *Characterization and prediction of planktonic nitrogenous nutrition and new production in Monterey Bay, California: nutrient and physiological interactions.* Ph.d. thesis, University of Southern California, 1995.

[25] P. F. J. Lermusiaux. Evolving the subspace of the three-dimensional multiscale ocean variability: Massachusetts bay. *J. Marine Systems, Special issue on 'Three-dimensional ocean circulation: Lagrangian measurements and diagnostic analyses'*, 29(1-4):385–422, 2001.

[26] P.S. Libby, C. Gagnon, C.S. Albro, M.J. Mickelson, A.A. Keller, D.G. Borkman, J.T. Turner, and C.A. Oviatt. Combined work/quality assurance plan (CWQAPP) for water column monitoring 2004 - 2005 - tasks 9, 10, 12, 13, 14, 15. Technical Report 2005-09, Massachusetts Water Resources Authority, 2005.

[27] P.S. Libby, L.A. McLeod, C.J. Mongin, A.A. Keller, C.A. Oviatt, and J.T. Turner. Semiannual water column monitoring report: February - June 2001. Technical Report 2002-10, Massachusetts Water Resources Authority, 2002.

[28] J.J. McCarthy, C. Garside, and J.L. Nevins. Nitrogen dynamics during the Arabian Sea Northeast monsoon. *Deep-Sea Res. II*, 46(8-9):1623–1664, 1999.

[29] J.J. McCarthy, C. Garside, J.L. Nevins, and R.T. Barber. New production along 140W in the equatorial Pacific during and following the 1992 El Nino event. *Deep-Sea Res. II*, 43(4-6):1065–1093, 1996.

[30] D. J. McGillicuddy, J. J. McCarthy, and A. R. Robinson. Coupled physical and biological modelling of the spring bloom in the North Atlantic (I): model formulation and one dimensional bloom processes. *Deep-Sea Res. I*, 42(8):1313–1357, 1995.

[31] D. J. McGillicuddy, A. R. Robinson, and J. J. McCarthy. Coupled physical and biological modelling of the spring bloom in the North Atlantic (II): Three-dimensional bloom and post-bloom effects. *Deep-Sea Res. I*, 42(8):1359–1398, 1995.

[32] C. Miller. *Biological Oceanography.* Blackwell Publishing, 2004.

[33] A.W. Morris and J.P. Riley. The determination of nitrate in seawater. *Anal. Chim. Acta.*, 29:272–279, 1963.

[34] J.C.J. Nihoul and S. Djenidi. Coupled physical, chemical and biological models. In K.H. Brink and A.R. Robinson, editors, *Processes and Methods*, volume 10 of *The Sea: The Global Coastal Ocean*, pages 483–506. John Wiley and Sons, New York, 1998.

[35] J.J. O'Brien. Models of coastal upwelling. In *Numerical Models of Ocean Circulation*, pages 204–215. National Academy of Sciences, Washington, 1975.

[36] R.O. Olivieri and F.P. Chavez. A model of plankton dynamics for the coastal upwelling system of Monterey Bay, California. *Deep-Sea Res. II*, 47:1077–1105, 2000.

[37] T.R. Parsons, Y. Maita, and C.M. Lalli. *A manual of chemical and biological methods for seawater analysis.* Pergamon Press, 1984.

[38] T.R. Parsons, M. Takahashi, and B. Hargrave. *Biological Oceanographic Processes.* Pergamon Press, Oxford, 1984.

[39] F. A. Richards, editor. *Coastal Upwelling.* Coastal and Estuarine Sciences 1. American Geophysical Union, Washington, D.C., 1981.

[40] A. R. Robinson. Physical processes, field estimation and an approach to interdisciplinary ocean modeling. *Earth-Science Reviews*, 40(1–2):3–54, 1996.

[41] A. R. Robinson and P. F. J. Lermusiaux. Data assimilation for modeling and predicting coupled physical-biological interactions in the sea. In A.R. Robinson, J.R. McCarthy, and B.J. Rothschild, editors, *Biological-Physical Interactions in the Ocean*, volume 12 of *The Sea: The Global Coastal Ocean.* John Wiley and Sons, New York, 2002. http://people.deas.harvard.edu/ pierrel/sea/arr$_{pjfl_chap}$12.*pdf*.

[42] A. R. Robinson and W. G. Leslie. Estimation and prediction of oceanic eddy field. *Prog. Oceanog.*, 14:485–510, 1985.

[43] A. R. Robinson and the LOOPS Group. Realtime forecasting of the multidisciplinary coastal ocean with the Littoral Ocean Observing and Predicting System (LOOPS). In *Third Conference on Coastal Atmospheric and Oceanic Prediction and Processes*, pages 30–35, New Orleans, LA, 3-5 November 1999. American Meteorological Society. http://www.deas.harvard.edu/ robinson/PAPERS/AMS_NO.html.

[44] A. R. Robinson and L. J. Walstad. The Harvard Open Ocean Model: Calibration and application to dynamical process, forecasting, and data assimilation studiess. *Applied Numerical Mathematics*, 3:89–131, 1987.

[45] A.R. Robinson. On the theory of advective effects on biological dynamics in the sea. *Proceedings of the Royal Society, A*, 453:2295–2324, 1997.

[46] P.E. Smith and S.L. Richardson. Standard techniques for pelagic fish egg and larva surveys. Technical Report 175, FAO Fisheries, 1977.

[47] L. Solorzano. Determination of ammonia in natural waters by the phenol-hypochlorite method. *Limnol. and Oceanog.*, 14:799–801, 1969.

[48] Y.H. Spitz, J.R. Moisan, and M.R. Abbott. Configuring an ecosystem model using data from the Bermuda-Atlantic Time Series (BATS). *Deep-Sea Res. II*, 48:1733–1768, 2001.

[49] I. Valiela. *Marine ecological processes, 2nd ed.* Springer-Verlag, 1995.

[50] L. Van Guelpen, D.F. Markle, and D.J. Duggan. An evaluation of accuracy, precision, and speed of several zooplankton subsampling techniques. *J. Cons. int. Explor. Mer.*, 40:226–236, 1982.

[51] J. J. Walsh and R. C. Dugdale. Nutrient submodels and simulation models of phytoplankton production in the sea. In J. Kramer and H. Allen, editors, *Nutrients in Natural Waters*, pages 171–191. John Wiley, New York, 1972.

[52] K.K. White and R.C. Dugdale. Silicate and nitrate uptake in the Monterey Bay upwelling system. *Cont. Shelf Res.*, 17(5):455–472, 1997.

[53] J. Wroblewski. A simulation of the distribution of *acartia clausii* during Oregon upwelling August 1973. *J. Plankton Res.*, 2:43–68, 1977.

[54] J.S. Wroblewski, J.L. Sarmiento, and G.R. Flierl. An ocean-basin scale model of plankton dynamics in the North Atlantic. Part I. solutions for the climatological oceanographic conditions in May. *Global Biogeochemical Cycles*, 2:199–218, 1988.

Appendix A

Wind data 1985-2005

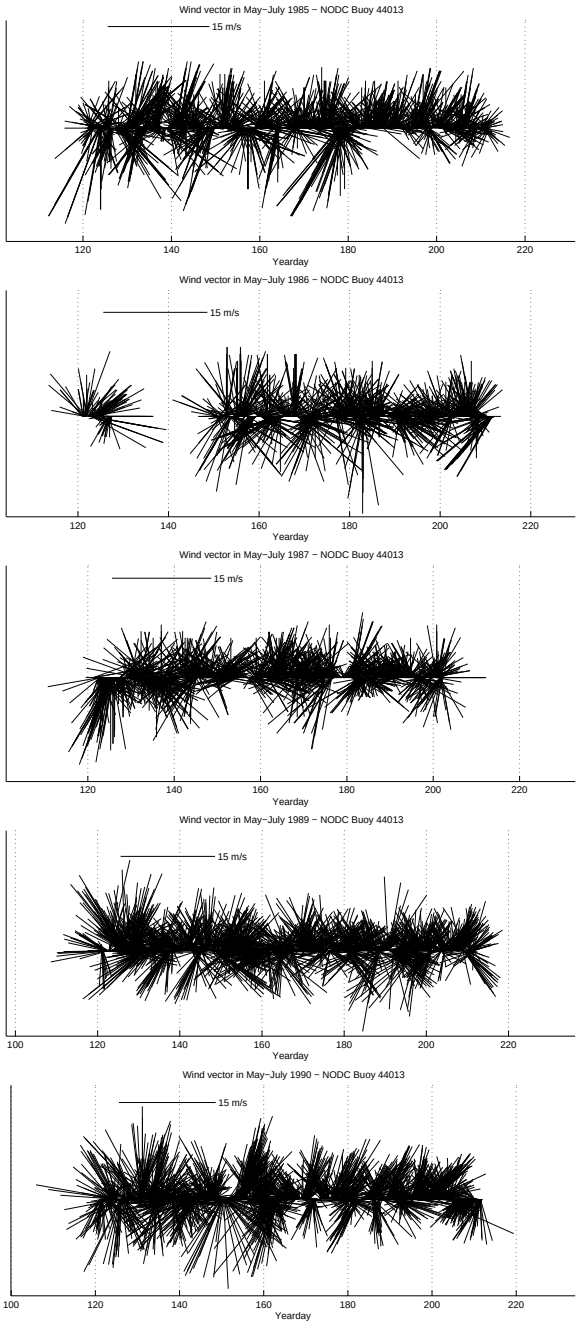

Figure A.1: Wind Vectors at MassBay Buoy: May-July, 1985-1990 (no 1988)

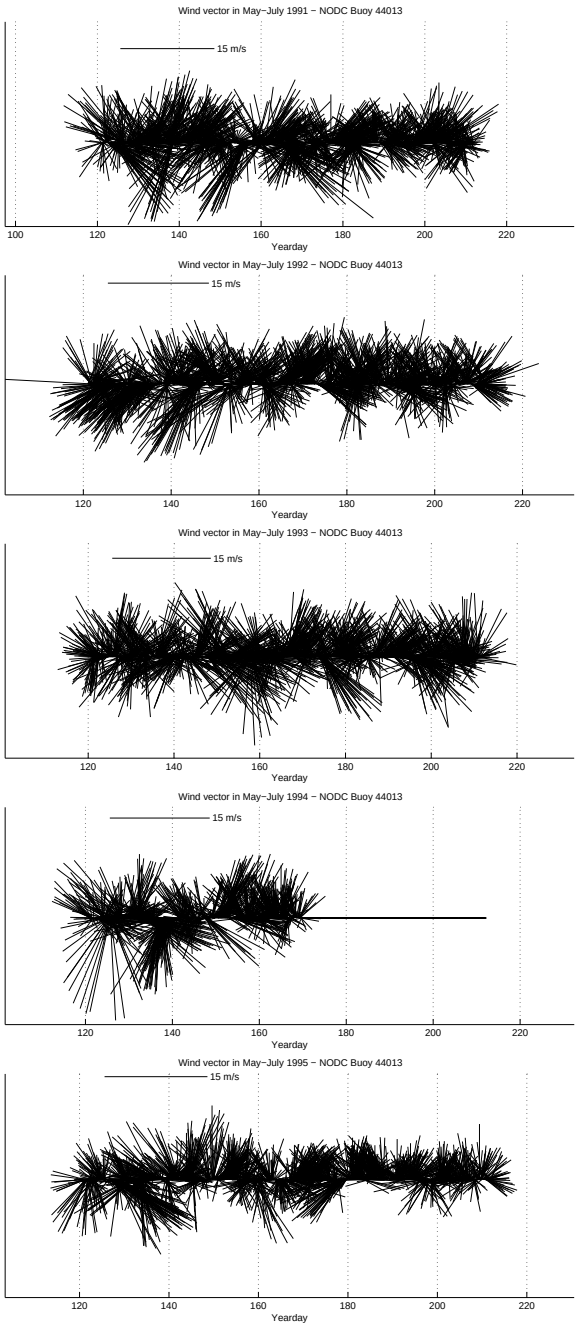

Figure A.2: Wind Vectors at MassBay Buoy: May-July, 1991-1995

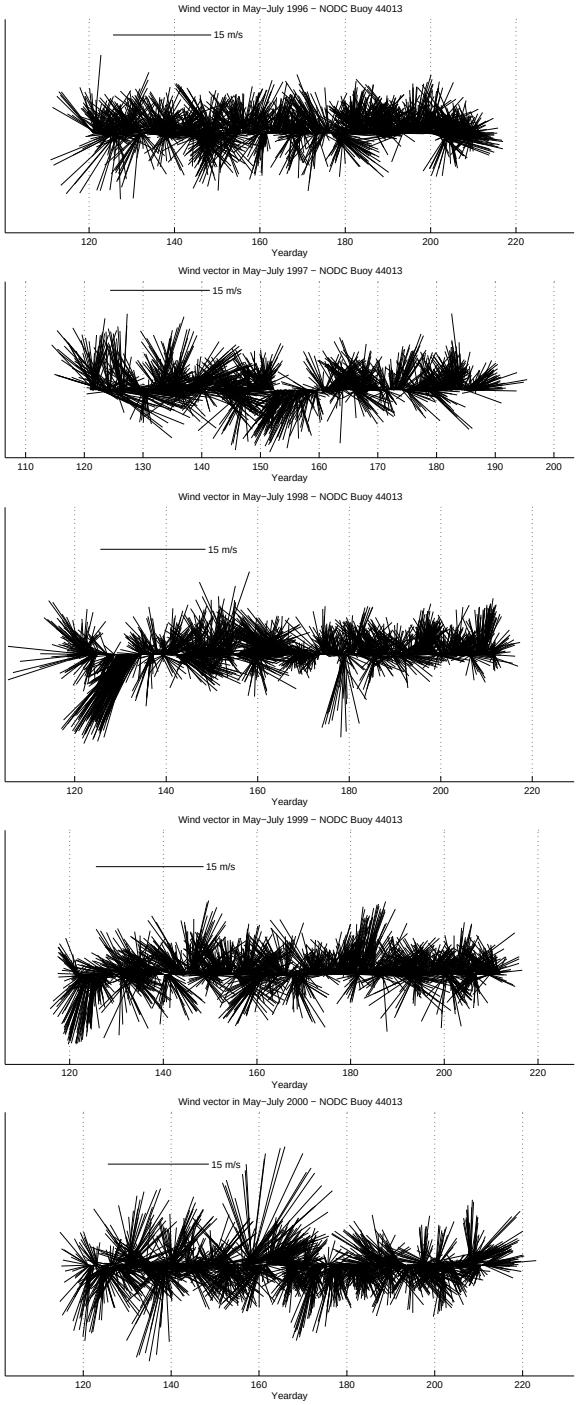

Figure A.3: Wind Vectors at MassBay Buoy: May-July, 1996-2000

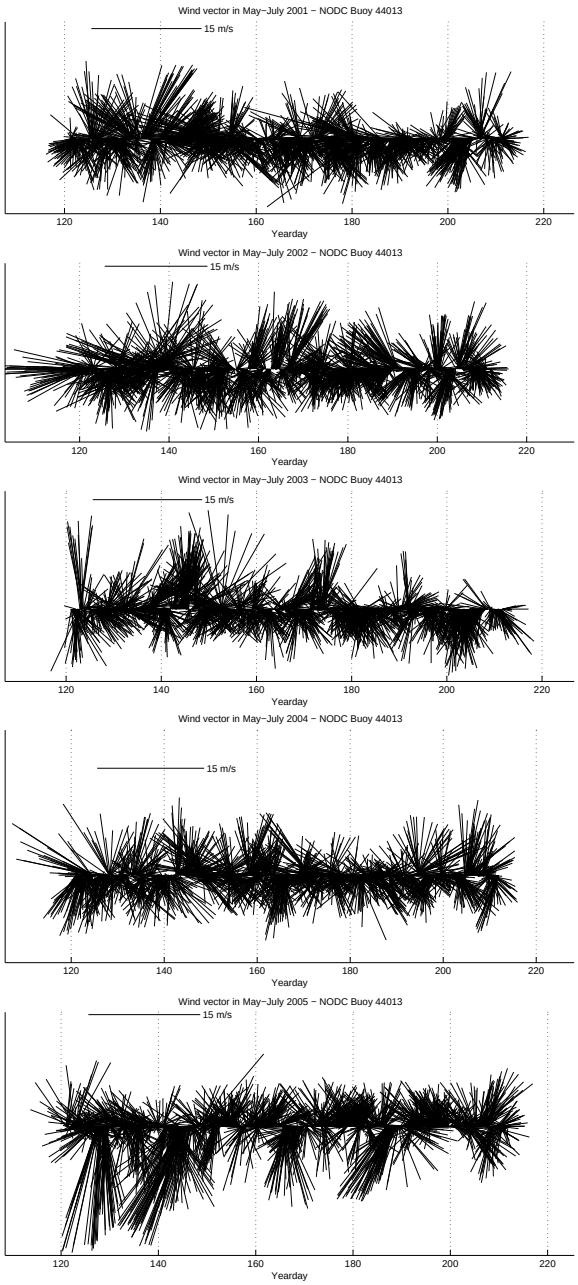

Figure A.4: Wind Vectors at MassBay Buoy: May-July, 2001-2005